Model-driven segmentation of X-ray left ventricular angiograms

Oost, C.R.

Model-Driven Segmentation of X-Ray Left Ventricular Angiograms

Colophon

About the cover
The sequence of images on the cover shows half a cardiac cycle of the left ventricle in an X-ray left ventricular angiographic acquisition. The utmost left image represents the left ventricle in the end diastolic phase. When following the string of images in a counter-clockwise fashion, the contraction of the left ventricle over time is depicted, ending at the end systolic phase. In both the end diastolic and the end systolic image frame a yellow contour line is drawn. These contours are the results of the automated methodology, as presented in this thesis. After visual inspection, the analyzing expert cardiologist ratified both contours without further manual editing. The combination of all images together represents a typical shape of the projected left ventricle as seen in a single-plane 30° right anterior oblique view acquisition.

About the quotes
The Japanese quotes (and their English translations) that are used on the title pages of each chapter aim to deliver in short the scope of the chapter. What these quotes have in common is that they all use the Japanese character 心 (‘kokoro’), signifying (among other possible meanings) ‘heart’.

Model-driven segmentation of X-ray left ventricular angiograms
Oost, Cornelis Roel

Printed by Ponsen & Looijen b.v., The Netherlands
ISBN 978-90-9023398-7

Model-Driven Segmentation of X-Ray Left Ventricular Angiograms

Proefschrift

ter verkrijging van

de graad van Doctor aan de Universiteit Leiden,

op gezag van Rector Magnificus prof. mr. P.F. van der Heijden,

volgens besluit van het College voor Promoties

te verdedigen op dinsdag 30 september 2008

klokke 15.00 uur

door

Cornelis Roel Oost
geboren te Rutten
in 1976

Promotiecommissie

promotor:	Prof. dr. ir. J.H.C. Reiber
co-promotor:	Dr. ir. B.P.F. Lelieveldt
referent:	Dr. A. Wahle University of Iowa, Iowa, USA
overige leden:	Prof. dr. A. de Roos
	Prof. dr. C. von Birgelen Universiteit Twente, Enschede

The research described in chapters 2, 3 and 5 was financially supported by the Dutch Technology Foundation STW (grant LGN 4508).

Financial support for the publication of this thesis was kindly provided by:

- Stichting Beeldverwerking Leiden
- Foundation Imago Oegstgeest
- Medis medical imaging systems bv

Financial support by the Netherlands Heart Foundation for the publication of this thesis is gratefully acknowledged.

Contents

一心に
‘devotedly’

Chapter 1

Introduction

1.1 Background

Worldwide millions of people suffer from cardiovascular diseases [1;2], which have been the number one cause of death in the western world for decades. Possible defects in the cardiac system can be either blood flow related, electrically induced, or they can be caused by congenital defects of the cardiac anatomy. However, most cardiac defects eventually result in a reduced cardiac function, leading to a reduced blood flow through the body or worse.

The human heart consists of four chambers, the right atrium, the left atrium, the right ventricle and the left ventricle (Figure 1.1). In a healthy subject, deoxygenated blood enters the right atrium and oxygenated blood enters the left atrium from the lungs. When the atria are filled, they contract and the atrio-ventricular valves open, filling both the right and the left ventricle. Subsequently, the atrioventricular valves close, both ventricles contract and the semi-lunar valves open. This way the right ventricle pumps deoxygenated blood to the lungs while the left ventricle pumps oxygenated blood throughout the body.

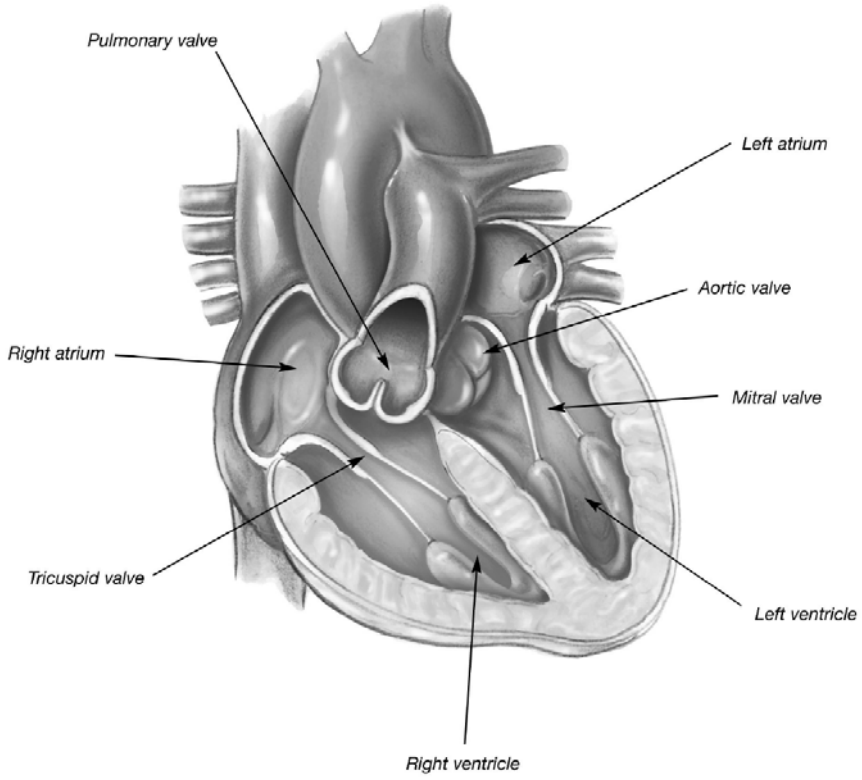

Figure 1.1: A cross section of the human heart (© Edwards Lifesciences, Irvine, California, used with permission).

The process of blood circulation is a delicate rhythmic alternation of contraction and relaxation of the four heart chambers that is regulated by an electrical system, of which the sino-atrial (SA) node is the pacing element. This area of specialized tissue located near the right atrium produces a continuous sequence of electrical pulses, of which the frequency adapts to the metabolic demands of the body. This electrical discharge of the SA-node propagates over the right and the left atria, resulting in a contraction of these chambers, injecting the blood from the atria into the ventricles. The electrical signal then passes through the atrio-ventricular (AV) node to the bundle of His, the right and left bundle and eventually to the Purkinje fibers. This system of electrically conducting fibers causes both the ventricles to contract in a controlled fashion, pumping the blood to the lungs and body.

A variety of cardiovascular diseases exist, which can be roughly categorized as follows. In Ischemic Heart Disease parts of the heart muscle (myocardium) receive a limited supply of blood, resulting in a reduction of cardiac function. One of the main reasons for Ischemic Heart Disease is a narrowing of one or more of the coronary arteries, which supply the myocardium from blood. Such an obstruction can be caused either by an accumulation of plaque in the vessel or by an embolism: a blockage of the vessel by a blood clot. Myocardial Ischemia can eventually lead to the death of myocardial tissue (myocardial infarction).
Arrhythmia is a combinatory term for defects in the electrical cardiac system. Arrhythmia can either be caused by a reduced conductivity, arrhythmical pulse generation by the SA-node, or by ectopic triggers.
Valvular dysfunction can lead to a reduced inflow of blood in a heart chamber or regurgitation through the valve. Common causes of valvular dysfunction are valvular stenoses, valvular inflammation or a congenital valvular defect.
Congestive Heart Failure is a disease that is primarily caused by hypertension, which if left untreated, may cause an irreversible remodeling of the heart due to the increased blood pressure, which in turn reduces cardiac output. It can also be triggered by a (combination of) the aforementioned disorders.

Eventually, most cardiac diseases result in a reduced cardiac function. The large amount of people suffering from cardiac disease stresses the importance of cardiac function diagnostics. Therefore, over time several cardiac imaging methods have been developed that enable the assessment of cardiac function, all with different characteristics. Echocardiography is non-invasive and can give a quick indication of global cardiac function. The image quality however remains relatively poor. Positron Emission Tomography (PET) and Single Photon Emission Computed Tomography (SPECT) are nuclear imaging modalities, in which a radioactive tracer provides information on myocardial perfusion or glucose metabolism in the myocardium (PET), albeit with a relatively low resolution. On the other hand, Magnetic Resonance Imaging (MRI) and Multi Slice Computed Tomography (MSCT) have rapidly evolved over the last decade and are considered to be the modalities of the future. MSCT enables the simultaneous assessment of coronary and ventricular function, and has a high spatial and temporal resolution and a short acquisition time. The main drawback of MSCT is the X-ray radiation dose to which the patient is exposed to. MRI also has a high spatial and temporal

resolution, it does not involve radiation and it has a wide range of possible scan protocols to be applied in order to assess valvular function and ventricular function. The prolonged acquisition time is the major disadvantage of using MRI for functional cardiac imaging. Nonetheless, MSCT and MRI provide a highly intuitive 4 dimensional (3D + time) visualization of the heart.

X-ray LV angiography is also a widely used technique to assess cardiac function. Although this modality gives a 2D or bi-plane visualization of the heart, in the majority of hospitals worldwide a catheterization laboratory (cathlab) with X-ray LV angiography equipment (Figure 1.2) is available. During each cardiac catheterization procedure, the LV angiogram is acquired, providing essential information to the interventional cardiologist, since it enables the analysis of regional and global cardiac function. Drawbacks of X-ray LV angiography are the invasive procedure, the use of contrast dye and, similar to MSCT, the radiation dose to which the patient is exposed. However, due to the availability and a superior spatial and temporal resolution with respect to the MSCT and MRI systems available in the average hospital, X-ray LV angiography is still considered to be an important clinical standard.

The focus of the work presented in this thesis mainly lies on the analysis of X-ray LV angiography, although some chapters also address MRI based studies. The emphasis of the latter studies was mainly on elaborating on conceptual methodology.

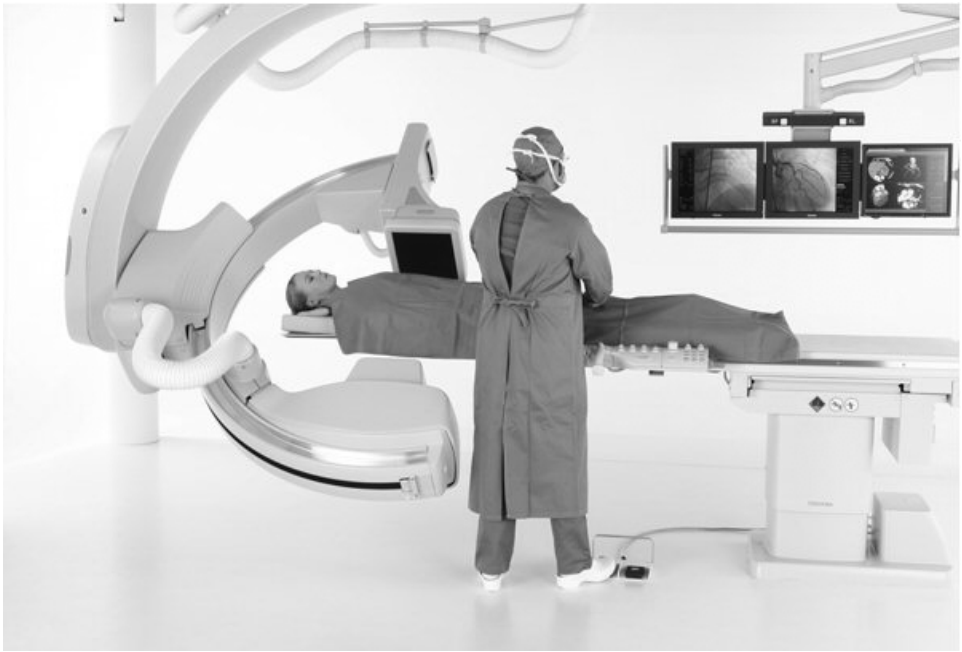

Figure 1.2: A cardiovascular X-ray Angiography Imaging Device: The Toshiba CC-i (© Toshiba Cooperation).

1.2 X-ray LV Angiography

1.2.1 X-ray LV Angiography Acquisition

X-ray LV angiography is a catheterization procedure, in which an X-ray opaque contrast dye is injected into the left ventricle through a catheter. This catheter is inserted in the patient's groin, is forwarded through the vascular system of the patient and eventually enters the left ventricle through the aorta. The image acquisition can be performed from two different angles (bi-plane) or from one fixed angle (single-plane). A bi-plane acquisition normally combines the antero-posterior view and the lateral view or the 30° right anterior oblique view and the 60° left anterior oblique view. Although bi-plane image sequences intrinsically provide more information, single-plane acquisitions (generally obtained in the 30° right anterior oblique view) are considered to be the clinical standard.
The amount of injected X-ray opaque contrast dye should be minimized to diminish possible adverse reactions in the patient. When the so-called bolus of contrast fluid arrives at the left ventricle, it fills the ventricle in approximately two or three cardiac cycles. The injection of the contrast agent somewhat irritates the myocardium, causing one or two irregular cardiac contractions (extra-systole). After 8 to 12 cardiac cycles (i.e. approximately 10 seconds) the contrast fluid has been washed out of the left ventricle. The time-window in which the left ventricle is visualized therefore is limited: normally the second or third cardiac cycle after the injection of the contrast dye is considered to provide an optimal visualization, because the distribution of the contrast fluid is maximally homogeneous and possible extra-systole have subsided. From this optimally visualized cardiac cycle two frames are selected for analysis: the end diastolic (ED) image frame, in which the LV volume is maximal, and the first subsequent end systolic (ES) image frame, in which the LV is maximally contracted. An example of a pair of properly acquired ED and ES LV angiogram is shown in Figure 1.3.

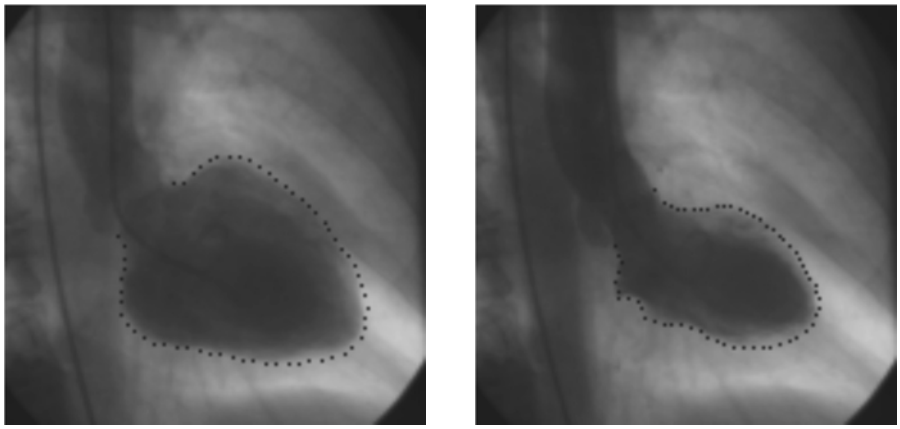

Figure 1.3: ED (left) and ES (right) frame of a properly acquired X-ray angiogram. Black dotted lines denote manually drawn expert contours.

1.2.2 X-ray LV Angiography Image Processing Challenges

The output of an X-ray LV angiography acquisition is an image sequence of approximately 100 to 200 image frames. The clinical information that can be extracted from it is twofold:

- The ejection fraction, defined as the difference between the ED and ES volumes divided by the ED volume.
- The regional myocardial wall motion characteristics.

The acquisition quality of an X-ray LV angiogram can vary a lot, due to the experience of the operator and the physical condition of the patient. For patients it is difficult to comply with the requirement of holding their breath during the acquisition, which is necessary to prevent the diaphragm from overlapping with the posterior wall of the left ventricle. Furthermore, the visualization of the anterior wall can be occluded by a rib. Such overlapping anatomical structures complicate the image interpretation and patient study analysis. Figure 1.4a displays an example of an acquisition in which the LV and the diaphragm are overlapping. Figure 1.4b shows a similar impediment for image interpretation: the shutter of the imaging device, responsible for prevention of over-exposure, can produce a substantial shadow in the image, as expressed in this example as a diagonal dark band.
Poor contrast can be caused by under- or over-exposure of the image sequence, as can be seen in Figure 1.4c. This specific example can be regarded a worst case scenario. Besides under-exposure of the image, the diaphragm and the left ventricle are overlapping and a shutter induced shadow can be observed. Additionally, poor contrast can be caused by the selection of the frames that are to be analyzed by the expert cardiologist. When, for example, the filling of the LV is not optimal because the patient is suffering from dilated cardiomyopathy, or the patient shows a more than average amount of extra-systole after the injection of the contrast fluid, there will be no optimal cardiac cycle to analyze.
During the catheterization procedure, the placement of the catheter tip is of significant importance. The optimal position is in the vicinity of the valve plane, i.e. in the vicinity of the mitral valve (the valve between the left atrium and the left ventricle) and the aortic valve (the valve between the left ventricle and the aorta). When the contrast dye is released it immediately mixes with the incoming blood flow through the mitral valve. Placing the catheter tip near the apex increases the risk of an uneven distribution of the contrast dye, as can be seen in Figure 1.4d.

In current clinical practice there are two ways to interpret an X-ray LV angiographic image sequence. An experienced cardiologist can make a quick estimation of the ejection fraction, just by visual inspection of the image data. In a more thorough analysis the endocardial edge of the left ventricle is delineated manually in the optimally visualized ED and ES frames, using a dedicated software package. Surface areas are calculated from these contour curves and a specialized equation, the area-length method [3] is employed to determine the ED and ES

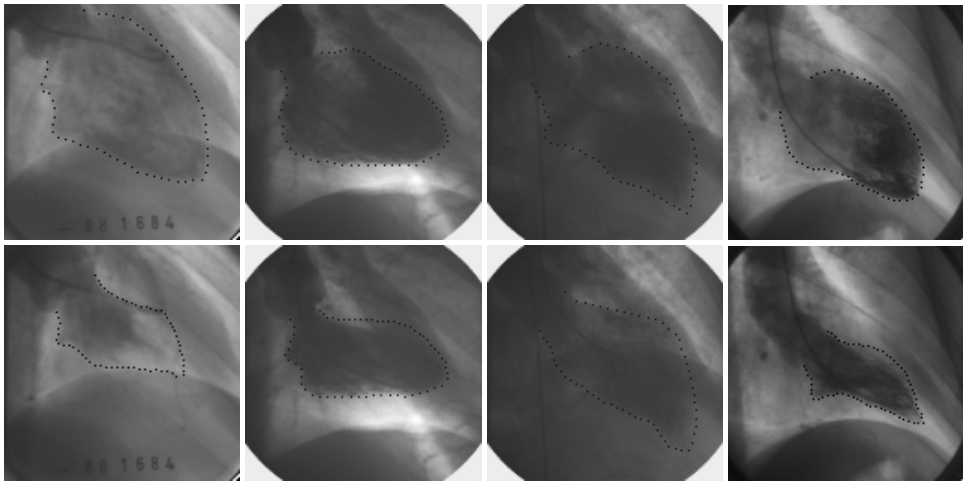

Figure 1.4: Poor X-ray LV angiogram acquisitions. Upper row displays ED frames, lower row displays ES frames, black dotted lines denote manually traced contours. From left to right: diaphragm overlap, shutter shadow, poor contrast and uneven distribution of contrast agent (mainly observed near the mitral valve in the ED image).

volumes. Subsequently the ejection fraction (EF), defined as the difference between the ED and ES volumes divided by the ED volume, is calculated and regional wall motion can be assessed using a variety of different models [4-6]. Figure 1.5 presents a typical result of such a wall motion model.
Both approaches have serious shortcomings. Visual inspection depends highly on the training of the clinical expert. Moreover, the training culture can differ between different hospitals. Visual inspection is therefore not always reproducible, which leads to a non-standardized diagnosis and which complicates follow-up studies of patients. Manual contouring on the other hand, brings along a high workload. It is time consuming and is prone to inter- and intra-observer variabilities.
Consequently, the need for an automated methodology to assess global cardiac function from X-ray LV angiograms is apparent. It is also clear that, to ensure reproducible results, this automated methodology should provide contours that can be translated into clinical significance: the ejection fraction and the wall motion models.

1.3 Prior Literature on Automated X-ray LV Analysis

For more than three decades attempts have been made to facilitate the delineation of endocardial left ventricular contours in X-ray angiograms [7-18]. The fact that so many researchers have tried to solve this problem underscores the complexity of the problem. Mainly the automatic delineation of the ES image is notoriously difficult. In a properly acquired angiogram one can expect a proper filling and distribution of the contrast dye in the ED frame, making it rather intuitive to decide

on the location of the endocardial border. This does not necessarily hold for the ES image frame, even in a perfectly acquired image sequence. Due to the cardiac contraction, the majority of the mixture of blood and contrast dye is squeezed out of the ventricle, complicating the definition of the endocardial boundary. This specifically holds in the vicinity of trabeculations and papillary muscles (i.e. the muscles restricting the movement of the mitral valve). The amount of contrast fluid in between these structures is generally low, hampering local border detection.

It is generally acknowledged that to achieve an automatic delineation of left ventricular contours, using low level image processing techniques alone do not suffice. Hence the majority of proposed techniques in literature incorporated some level of a priori information, mainly regarding the shape of the left ventricle.

Early examples of automated LV contour delineation methods in angiograms used a priori information regarding general edge characteristics. Chow and Kaneko [7], for example, implemented a dynamic threshold algorithm. Clayton *et al.* [8] determined the left ventricular border positions by calculating edge probabilities. Pope *et al.* [12] applied Dynamic Programming to delineate the left ventricle. Slager *et al.* and Reiber *et al.* [9-11] used a dynamic thresholding based interactive technique that enabled real time (i.e. at video speed being 12.5 to 15 frames/s) processing of a cardiac cinefilm; the thresholds were adapted on a video line-by-line basis. The implemented system, the Contouromat, has been used in many clinical research studies, among others by Hooghoudt *et al.* [19-21].
Tehrani *et al.* [14] proposed one of the first approaches in which a priori information of the shape of the ventricle was used. A statistical model, describing the shape variation of a cardiac left ventricle, was employed to connect fractions of possible LV boundaries, obtained by a low level edge detector. These candidate fractions of the endocardial boundary were either rejected or accepted by a means of a blackboard architecture and the statistical model. Eventually a selection of fractions remained to form a complete LV delineation.
Lilly *et al.* [15] used a similar approach. First a series of low level image processing algorithms (regional intensity information, edge information, and multiple regional thresholding) was used to construct a set of candidate LV edge points. Subsequently Dynamic Programming was applied to fit a contour through these points. Template matching using a template library, derived from manually traced LV contours, incorporated the required a priori information, neutralizing contour irregularities and contour drift due to insufficient image information.
De Figueiredo and Leitão [16] proposed an algorithm based on maximum a priori probability in a Bayesian framework in combination with Markov random field contour modeling. Contrary to the previously described methods, both shape and image intensity information is incorporated in this approach. However, the method was only tested on digital subtraction angiography (DSA), in which an image acquired before the injection of the contrast fluid is subtracted from all following images to suppress the image background. In a clinical setting, optimal background removal is extremely difficult, mainly due to motion artifacts. For many patients it is difficult to hold their breath during the examination, resulting in respiratory motion. Cardiac motion artifacts could be neutralized by ECG gated acquisitions.

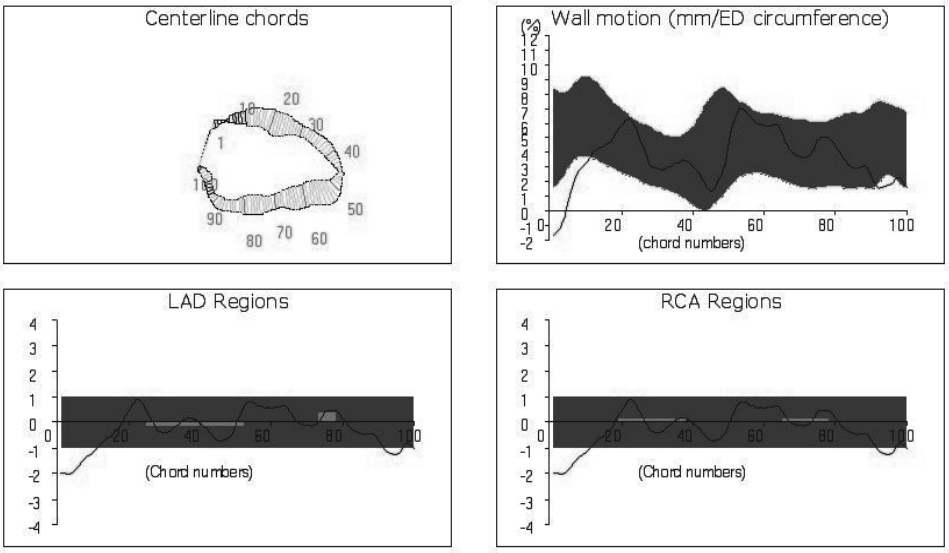

Figure 1.5: Example results from the centerline wall motion model. Top left: ED and ES contour overlay and construction of 100 chords connecting them. Top right: wall motion per chord. Bottom left: wall motion specified for the Left Anterior Descending regions. Bottom right: wall motion specified for the Right Coronary Artery regions.

Nonetheless, using ECG gating for selecting the proper frames for subtraction from the ED and ES images is hampered by arrhythmia caused by the release of the contrast agent or catheter contact with the endocardial wall.
McDonald and Sheehan [17] introduced a method using boosted decision trees for pixel classification based on feature images. Similar to [16], both shape and image intensity information are exploited. This approach mimicked the drawing behavior of the expert cardiologist scrolling through the neighboring time frames around the frame of interest. A clinical expert uses this information to grasp additional information of the contraction dynamics of the left ventricle. The feature images used in McDonald and Sheehan's algorithm were constructed from geometry features and gray-level statistics of such a sequence of images around the ED and ES frames. For initialization of the algorithm, three anatomical landmark points (the endpoints of the aortic valve and the apex) needed to be positioned manually.
Suzuki *et al.* [18] proposed a methodology applying two different edge detection mechanisms: a standard edge detection based on low-pass filtering and edge enhancement and a modified multilayer neural network. The neural network edge detector was trained on manually drawn LV contours and is able to identify less pronounced subjective edges. This approach does not utilize image intensity information and, as in [16], has been applied on DSA images only. After placing the endpoints of the aortic valve manually, the contours are traced automatically.

None of the aforementioned methods has proven to produce left ventricular contours that are of a sufficiently high degree of accuracy and robustness that is acceptable in clinical practice. Only a few of these methods have been introduced in daily clinical practice; van der Zwet *et al.* [13] proposed a method that was

incorporated in a clinical package in the first half of the 1990's. This approach combined a pyramidal segmentation algorithm, neural networks and Dynamic Programming. One general conclusion that can be drawn from this listing of prior work is that automatic delineation of the cardiac left ventricle in X-ray angiograms cannot be achieved without the use of a priori information, describing the shape and appearance of the ventricle. In this work we explore the application of statistical models of shape and appearance to incorporate a priori information into an automatic segmentation scheme for X-ray LV angiograms.

1.4 Statistical Models for Image Segmentation

In the past decade, much progress has been made in the field of automated medical image segmentation. Especially the statistical shape modeling methods introduced by Cootes [22-26] have received widespread attention. Most statistical shape modeling methods consist of two parts: a Point Distribution Model (PDM) that captures object shape and shape variations from a set of examples, and an intensity model that is used for fitting the model to image data. A Point Distribution Model [22] describes the training contours by sampling them with an equal number of corresponding landmark points. After Procrustes alignment [27] of the training shapes to eliminate pose and scale differences, the variations in the shapes are computed using Principal Component Analysis (PCA), an eigenvector decomposition method. A shape similar to the objects in the training set can be generated as a linear combination of the average shape and the modes of variation.

An Active Shape Model (ASM) [23;24] extends the PDM with a model fitting algorithm to segment the object in a target image. Through every point of the PDM a scanline is placed, perpendicular to the contour. Edge information is gathered along these scanlines and used to propose new positions for the contour points. The newly hypothesized shape is expressed as a linear combination of the PDM average and eigenvariations and if any of the modes of variation exceeds a statistical limit (normally 2 or 3 standard deviations), the newly hypothesized shape is constrained to this parameter limit. This way, the generated segmentation hypothesis is constrained to statistically plausible shapes. ASMs have proven their merit in medical image segmentation by combining speed with segmentation robustness. Among many others, examples exist of segmentation algorithms in 2D [28], 2D+time [29] and 3D [30-32].

While in ASMs only the local image intensities along scanlines are used, an Active Appearance Model (AAM) uses an entire image patch to model global image intensity characteristics [25;26]. For every training object an image patch is derived from the object contour. These patches are resampled and aligned and a PCA is applied on the intensities, resulting in an average image intensity representation and a set of eigenvariations. Subsequently, the shape model and the intensity model are concatenated to form a statistical representation of combined shape and intensity. Finally all model and pose parameters are individually perturbed with a

set of known magnitudes, to create a set of pre-computed parameter gradients that can be employed to estimate parameter updates during model matching.
Employing an AAM to segment an object of interest in a target image consists of initializing the model in the vicinity of the object, followed by an iterative matching. The root-mean-square difference between the model and the pixel intensities of the underlying image is minimized with respect to the model and pose parameters using pre-computed parameter gradients. Convergence is achieved when the error does not decrease significantly for a number of iterations. The synthesized model shape represents an approximation of the actual object contour in the image.
Similar to ASMs, the AAM updates are constrained to a certain statistical limit, normally around 2 or 3 standard deviations. Because the parameter gradients that are used to direct the parameter updates are determined individually, every single parameter adjustment attempts to maximally neutralize the difference between the model patch and the underlying image. Hence, parameter updates possibly are overestimated and a statistical constraint is needed.
AAMs implicitly model the relationship between the expert drawn contours and the underlying image features. Hence, AAMs are considered to outperform other approaches, such as ASMs or deformable models because they can cope with images containing fuzzy or spurious edge information.

Application of Active Appearance Models in medical image segmentation are ample and diverse in their extensions. Cootes *et al.* first applied them to knee cartilage segmentation in MRI [25] and later used AAMs for the automatic detection of brain structures in MRI [33]. Another 2D approach was presented by Roberts *et al.* [34], employing a sequence of Active Appearance sub-Models to vertebra segmentation. Beichel *et al.* [35] proposed a robust AAM and applied it to segmentation of hand bones and the segmentation of the diaphragm. In this method the residue, yielded from the subtraction of the model intensities from the image intensities, is used to construct an optimal set of model parameter updates. The first 3D Active Appearance Model, applied to cardiac MRI, was presented by Mitchell *et al.* [36]. Furthermore, Mitchell *et al.* proposed a hybrid AAM/ASM to improve local border delineation in cardiac MRI segmentation [37]. Bosch *et al.* created the Active Appearance Motion Model, modeling a full cardiac cycle of the left ventricle in echocardiography [38]. Another echocardiographic application is presented by Hansegård *et al.* [39], segmenting triplane echocardiograms by a Dynamic Programming constrained AAM. Üzümcü *et al.* explored an AAM in which the shape modeling was performed by using Independent Component Analysis instead of Principal Component Analysis [40]. Finally, Stegmann *et al.* applied an AAM for the registration of cardiac MRI perfusion sequences [41].
This wide range of applications proves the value of AAMs in medical image segmentation. Also for segmentation of the left ventricle in X-ray angiograms, AAMs are expected to perform adequately.

However, some limitations of Active Appearance Models in general and to their application to X-ray LV angiograms specifically can be identified. These shortcomings and their possible solutions will be explored in this thesis, to accomplish a proper segmentation of the left ventricle in X-ray LV angiograms.

1.4.1 Limitations of Active Appearance Models

During matching of an AAM to the underlying image information, the model parameters are iteratively updated. The decision on whether such a new model representation is an improvement or not is based on an error criterion that is defined as the sum of squared differences between the image pixel values and the corresponding model intensity values. Since the error criterion is a global parameter, an AAM does not necessarily emphasize strong local edge information. This can be an advantage when fuzzy or spurious edge information is available in the image. Nonetheless, locally accurate border detection is not guaranteed and in the specific case of X-ray angiography an additional effort is required. Furthermore, as Figure 1.6 illustrates, the error criterion has proven to be unstable when applying an AAM in X-ray LV angiography. Hence, the need for improving the robustness of the algorithm is apparent.

A second limitation is the possible over-constraining towards the training data during statistical model fitting. This can be expressed by a suboptimal local border definition. As reported by Bosch *et al.* [38], an AAM has a tendency to find a "too normal" shape. Furthermore, statistical models of shape (and intensity) are highly dependent on the composition of the training data. For every application it remains difficult to estimate the amount of training data needed and the composition of the characteristics of the training examples.

1.5 Scope of this Thesis

As discussed previously, the interpretation of the ED image in X-ray LV angiography is relatively intuitive, while the ES image is notoriously problematic to segment. However, the ED and ES image frames represent the same left ventricle and the same uptake and washout characteristics of the injected contrast dye. Hence, a high degree of similarity in shape and image intensity information can be observed. This information should be exploited and integrated in the Active Appearance Model.

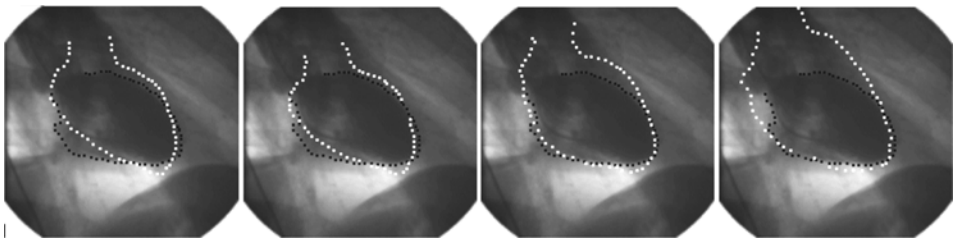

Figure 1.6: An example of spurious error criterion behavior. Black dotted lines denote manually traced reference contours, white dotted lines represent intermediate results obtained by the Active Appearance Model. From Left to right, the error criterion decreases, signifying a supposedly improved model segmentation.

Despite the successful application of AAMs in medical image segmentation, applying them in X-ray LV angiograms remains challenging, due to the limitations described in the previous section. This thesis investigates the application of Active Appearance Models in X-ray LV angiography, to generate an automatic segmentation of the left ventricle in both the ED and the ES phase. The goal of the research described in this thesis is therefore:

- to investigate ways to integrate all available shape and image intensity information in the AAM framework, by exploiting redundancies and similarities between the ED and ES frames.
- to increase the robustness of AAMs with respect to the unstable behavior of the error criterion.
- to investigate the influence of the size and composition of the model training data set on AAM segmentation performance.
- to address the issue of over-constraining towards the training data and investigate ways to improve local LV border delineation.
- to demonstrate the applicability of the resulting algorithm in daily clinical practice, producing clinically acceptable results, reducing the workload of the expert cardiologist and reducing inter- and intra-variabilities in clinical diagnostics.

1.6 Thesis Outline

The remainder of this thesis is structured as follows.

In Chapter 2 an exploratory investigation is reported on the merit of a combined modeling of the ED and ES image frames in an Active Appearance Model framework. For every training example, one shape vector was constructed, concatenating the manually drawn ED and ES contours. Similarly, for all training examples, an image intensity vector was constructed, combining information from both frames. This representation formed the basis of the presented Multi-View Active Appearance Model. In addition, a first step forwards was made towards improving local border delineation. After global segmentation of the left ventricle in ED and ES by the Multi-View AAM, a specialized AAM was employed, focusing on the model description of the LV border. In this specialized model, the intensity information of the center of the ventricle was ignored. Only the intensities in a rim around the LV border were modeled, covering specifically the edge of the ventricle and it's direct surroundings.

The methodology of the Multi-View Active Appearance Model is similar to the Active Appearance Motion Model by Bosch *et al.* [38] in which a full cardiac cycle

was modeled. However, Chapter 3 explored whether this approach could still provide acceptable results when either the amount of data is very sparse in the time domain (only modeling the ED and ES frame in X-ray LV angiography, instead of a full cardiac cycle), or when the shape and intensity features are significantly different for all views. For this latter experiment a Multi-View AAM was constructed to simultaneously model the short-axis view, the two chamber view and the four chamber view of a cardiac MRI acquisition. For both experiments, similarly as in Chapter 2, shape and intensity information of multiple views was modeled in a combined fashion, while the model pose parameters were modeled separately for all views.

Chapter 4 discusses the influence of the composition of the training set that is used in constructing an Active Appearance Model. Due to the problem description, the research goals and the availability of data, this study was performed on a cardiac MRI data set. Three aspects were investigated. First, the optimal size of the training data set, was assessed. In other words, how many training examples are required to obtain a proper statistical description of the population. Second, the ratio between patient study examples and samples from healthy volunteers in the training set was examined. The influence of this ratio on the segmentation results was measured. And third, the influence of the scanner that is used for acquisition was investigated. When segmenting a patient study, acquired with a scanner produced by a specific manufacturer, the segmentation results between applying a scanner specific AAM and an AAM constructed on data from multiple scanners was compared.

In Chapter 5 a new approach to improve local border delineation is presented. To overcome over-constraining of the segmentation result by the model, a dedicated Dynamic Programming is proposed. In this post-processing step, the search area was constrained by the final segmentation result of the Active Appearance Model. Furthermore, the contraction dynamics of the cardiac left ventricle were captured in the Dynamic Programming scheme, by constructing a cost matrix on both the underlying (ED or ES) image information and the information of a subtraction image, created by subtracting the ED frame from the ES frame. A new model matching scheme, the Controlled Gradient Descent, was introduced to improve the robustness of the AAM. In this approach only one or a few model parameters were updated per AAM matching iteration. This way a more smooth and gradual convergence towards the object of interest was expected. In addition, a thorough technical validation was performed, investigating the overall segmentation performance and investigating the merit of all novel elements separately versus their merit when they are applied in a synergetic fashion. Finally, Chapter 5 explored the limits of automation, by comparing a fully automatic X-ray LV angiogram segmentation method with a version of the algorithm in which the user needed to initialize the model by placing three landmark points manually.

Chapter 6 transfers the created methodology into clinical practice. A study on the impact on the clinical workflow was performed, investigating whether the produced contours are of clinically acceptable quality, whether the presented method is capable of reducing the average patient analysis time and the workload of the

cardiologist, and whether the inter- and intra-observer variabilities can be reduced. To assess all this, two expert cardiologists were asked to analyze a data set of 30 patient studies in two ways: First by drawing endocardial contours in ED and ES manually and second by using the automated delineation method, which was incorporated in a dedicated software package. Naturally, in the latter procedure, the expert cardiologists were allowed to edit regions of the automatically determined contours, when they considered them to be sub-optimal. Hence, three types of contours were generated: manual contours, automatic contours and edited automatic contours. These contours were mutually compared with respect to the accuracy of LV delineation. In addition, timings of manual and automatic procedures were compared.

Chapter 7 provides a general discussion and conclusions of the work presented in this thesis.

References

[1] American Heart Association, Heart disease and stroke statistics - 2008 update. Circulation, Dallas, Texas, U.S. Online available: *http://circ.ahajournals.org*

[2] British Heart Foundation Health Promotion Research Group, European cardiovascular disease statistics - 2008 edition. Univ. of Oxford, Oxford, U.K. Online available: *http://www.heartstats.org*

[3] H. Sandler and H. T. Dodge, "The use of single plane angiocardiograms for the calculation of left ventricular volume in man," *American Heart Journal*, vol. 75, no. 3, pp. 325-334, 1968.

[4] C. J. Slager, T. E. H. Hooghoudt, P. W. Serruys, J. C. H. Schuurbiers, J. H. C. Reiber, G. T. Meester, P. D. Verdouw, and P. G. Hugenholtz, "Quantitative assessment of regional left ventricular motion using endocardial landmarks," *Journal of the American College of Cardiology*, vol. 7, no. 2, pp. 317-326, 1986.

[5] E. L. Bolson, S. Kliman, F. Sheehan, and H. T. Dodge, "Left ventricular segmental wall motion: a new method using local direction information," *Computers in Cardiology*, pp. 245-248, 1980.

[6] J. K. Doss, L. D. Hillis, G. Curry, S. E. Lewis, G. J. Dehmer, R. W. Parkey, J. H. Mitchell, and J. T. Willerson, "A new model for the assessment of regional ventricular wall motion," *Radiology*, vol. 143, no. 3, pp. 763-770, 1982.

[7] C. K. Chow and T. Kaneko, "Automatic boundary detection of left ventricle from cineangiograms," *Computers and Biomedical Research*, vol. 5, no. 4, pp. 388-410, 1972.

[8] P. D. Clayton, L. D. Harris, S. R. Rumel, and H. R. Warner, “Left ventricular videometry,” *Computers and Biomedical Research*, vol. 7, no. 4, pp. 369-379, 1974.

[9] C. J. Slager, J. H. C. Reiber, J. C. H. Schuurbiers, and G. T. Meester, “Automated detection of left ventricular contour. Concept and application,” in Heintzen, P. H. and Bursch, J. H. (eds.) *Roentgen-Video-Techniques for dynamic studies of structure and function of the heart and circulation.* Stuttgart: Georg Thieme Publishers, 1978, pp. 158-167.

[10] C. J. Slager, J. H. C. Reiber, J. C. H. Schuurbiers, and G. T. Meester, “Contouromat – A hard-wired left ventricular angio processing system. I. Design and application,” *Computers and Biomedical Research*, vol. 11, no. 5, pp. 491-502, 1978.

[11] J. H. C. Reiber, C. J. Slager, J. C. H. Schuurbiers, and G. T. Meester, “Contouromat – A hard-wired left ventricular angio processing system. II. Performance evaluation,” *Computers and Biomedical Research*, vol. 11, no. 5, pp. 503-523, 1978.

[12] D. L. Pope, D. L. Parker, P. D. Clayton, and D. E. Gustafson, “Left ventricular border recognition using a dynamic search algorithm,” *Radiology*, vol. 155, no. 2, pp. 513-518, 1985.

[13] P. N. J. van der Zwet, G. Koning, and J. H. C. Reiber, “Left ventricular contour detection: a fully automated approach,” *Computers in Cardiology*, pp. 359-362, 1992.

[14] S. Tehrani, T. E. Weymouth, and G. B. J. Mancini, “Model generation and partial matching of left ventricular boundaries,” *Proceedings of SPIE Medical Imaging*, vol. 1445, pp. 434-445, 1991.

[15] P. Lilly, J. Jenkins, and P. Bourdillon, “Automatic contour definition on left ventriculograms by image evidence and a multiple template-based model,” *IEEE Transactions on Medical Imaging*, vol. 8, no. 2, pp. 173-185, 1989.

[16] M. A. T. de Figueiredo and J. M. N. Leitão, “Bayesian estimation of ventricular contours in angiographic images,” *IEEE Transactions on Medical Imaging*, vol. 11, no. 3, pp. 416-429, 1992.

[17] J. A. McDonald and F. H. Sheehan, “Ventriculogram segmentation using boosted decision trees,” *Proceedings of SPIE Medical Imaging*, vol. 5370, pp. 1804-1814, 2004.

[18] K. Suzuki, I. Horiba, N. Sugie, and M. Nanki, “Extraction of left ventricular contours from left ventriculograms by means of a neural edge detector,” *IEEE Transactions on Medical Imaging*, vol. 23, no. 3, pp. 330-339, 2004.

[19] T. E. H. Hooghoudt, C.J. Slager, J.H.C. Reiber, P.W. Serruys, J.C.H. Schuurbiers, and G.T. Meester, "Regional contribution to global ejection fraction used to assess the applicability of a new all motion model to the detection of regional wall motion in patients with asynergy," *PhD thesis, Erasmus University Rotterdam*, 1980.

[20] T. E. H. Hooghoudt, P. W. Serruys, J. H. C. Reiber, C. J. Slager, M. van den Brand, and P. G. Hugenholtz, "The effect of recanalization of the occluded coronary artery in acute myocardial infarction on left ventricular function," *European Heart Journal*, vol. 3, no. 5, pp. 416-421, 1982.

[21] P. W. Serruys, T. E. H. Hooghoudt, J. H. C. Reiber, C. Slager, R. W. Brower, and P. G. Hugenholtz, "Influence of intracoronary nifedipine on left ventricular function, coronary vasomotility, and myocardial oxygen consumption," *British Heart Journal*, vol. 49, no. 5, pp. 427-441, 1983.

[22] T. F. Cootes, C. J. Taylor, D. H. Cooper, and J. Graham. "Training models of shape from sets of examples," *Proceedings of the British Machine Vision Conference*, Berlin: Springer Verlag, 1992, pp. 9-18.

[23] T. F. Cootes and C. J. Taylor, "Active shape models - 'smart snakes'," *Proceedings of the British Machine Vision Conference*, Berlin: Springer Verlag, 1992, pp. 266-275.

[24] T. F. Cootes, C. J. Taylor, D. H. Cooper, and J. Graham, "Active shape models - their training and application," *Computer Vision and Image Understanding*, vol. 61, no. 1, pp. 38-59, 1995.

[25] T. F. Cootes, G. J. Edwards, and C. J. Taylor, "Active appearance models," *Proceedings of the European Conference on Computer Vision*, H. Burkhardt and B. Neumann, Eds., vol. 2, Berlin: Springer Verlag, 1998, pp. 484-498.

[26] T. F. Cootes and C. J. Taylor, "Statistical models of appearance for computer vision," Online available:
http://personalpages.manchester.ac.uk/staff/timothy.f.cootes/Models/app_models.pdf

[27] J. C. Gower, "Generalized procrustes analysis," *Psychometrika*, vol. 40, no. 1, pp. 33-51, 1975.

[28] B. van Ginneken, A. F. Frangi, J. J. Staal, B. M. ter Haar Romeny, and M. A. Viergever, "Active shape model segmentation with optimal features," *IEEE Transactions on Medical Imaging*, vol. 21, no. 8, pp. 924-933, 2002.

[29] G. Hamarneh and T. Gustavsson, "Deformable spatio-temporal shape models: extending active shape models to 2D+time," *Image and Vision Computing*, vol. 22, no. 6, pp. 461-470, 2004.

[30] M. de Bruijne, B. van Ginneken, M. A. Viergever, and W. J. Niessen, "Adapting active shape models for 3D segmentation of tubular structures in medical images," *Proceedings of Information Processing in Medical Imaging*, vol. 2732, Berlin: Springer Verlag, 2003, pp. 136-147.

[31] H. C. van Assen, M. G. Danilouchkine, F. Behloul, H. J. Lamb, R. J. van der Geest, J. H. C. Reiber, and B. P. F. Lelieveldt, "Cardiac LV segmentation using a 3D active shape model driven by fuzzy inference," *Proceedings of Medical Image Computing and Computer-Assisted Intervention*, vol. 2876, Berlin: Springer Verlag, 2003, pp. 533-540.

[32] H. C. van Assen, M. G. Danilouchkine, A. F. Frangi, S. Ordas, J. J. M. Westenberg, J. H. C. Reiber, and B. P. F. Lelieveldt, "SPASM: a 3D-ASM for segmentation of sparse and arbitrarily oriented cardiac MRI data," *Medical Image Analysis*, vol. 10, no. 2, pp. 286-303, 2006.

[33] T. F. Cootes, C. Beeston, G. J. Edwards, and C. J. Taylor, "A unified framework for atlas matching using active appearance models," *Proceedings of Information Processing in Medical Imaging*, vol. 1613, Berlin: Springer Verlag, 1999, pp. 322-333.

[34] M. G. Roberts, T. F. Cootes, and J. E. Adams, "Linking sequences of active appearance sub-models via constraints: an application in automated vertebral morphometry," *Proceedings of the British Machine Vision Conference*, Berlin: Springer Verlag, 2003, pp. 349-358.

[35] R. Beichel, H. Bischof, F. Leberl, and M. Sonka, "Robust active appearance models and their application to medical image analysis," *IEEE Transactions on Medical Imaging*, vol. 24, no. 9, pp. 1151-1169, 2005.

[36] S. C. Mitchell, J. G. Bosch, B. P. F. Lelieveldt, R. J. Van der Geest, J. H. Reiber, and M. Sonka, "3-D active appearance models: segmentation of cardiac MR and ultrasound images," *IEEE Transactions on Medical Imaging*, vol. 21, no. 9, pp. 1167-1178, 2002.

[37] S. C. Mitchell, B. P. F. Lelieveldt, R. J. Van der Geest, H. G. Bosch, J. H. C. Reiber, and M. Sonka, "Multistage hybrid active appearance model matching: segmentation of left and right ventricles in cardiac MR images," *IEEE Transactions on Medical Imaging*, vol. 20, no. 5, pp. 415-423, 2001.

[38] J. G. Bosch, S. C. Mitchell, B. P. F. Lelieveldt, F. Nijland, O. Kamp, M. Sonka, and J. H. C. Reiber, "Automatic segmentation of echocardiographic sequences by active appearance motion models," *IEEE Transactions on Medical Imaging*, vol. 21, no. 11, pp. 1374-1383, 2002.

[39] J. Hansegård, S. Urheim, K. Lunde, and S. I. Rabben, "Constrained active appearance models for segmentation of triplane echocardiograms," *IEEE Transactions on Medical Imaging*, vol. 26, no. 10, pp. 1391-1400, 2007.

[40] M. Üzümcü, A. F. Frangi, M. Sonka, J. H. C. Reiber, and B. P. F. Lelieveldt, "ICA vs. PCA active appearance models: application to cardiac MR segmentation," *Proceedings of Medical Image Computing and Computer-Assisted Intervention*, vol. 2876, Berlin: Springer Verlag, 2003, pp. 451-458.

[41] M. B. Stegmann, H. Olafsdottir, and H. B. W. Larsson, "Unsupervised motion-compensation of multi-slice cardiac perfusion MRI," *Medical Image Analysis*, vol. 9, no. 4, pp.394-410, 2005.

心眼を開く
'gain insight'

Chapter 2

Left Ventricle Contour Detection in X-Ray Angiograms using Multi-View Active Appearance Models

This chapter was adapted from:
Left Ventricle Contour Detection in X-Ray Angiograms using Multi-View Active Appearance Models
E. Oost, B.P.F. Lelieveldt, G. Koning, M. Sonka, and J.H.C. Reiber
In: Proceedings of SPIE Medical Imaging, M. Sonka and J.M. Fitzpatrick Eds., vol. 5032, pp. 394-404, 2003.

Abstract

Automatic Left Ventricle (LV) border detection in X-ray angiograms for the quantitative assessment of cardiac function has proven to be a highly challenging task. The main difficulty is segmenting the End Systolic (ES) phase, in which much of the contrast dye has been squeezed out of the LV due to contraction, resulting in poor LV definition. 2D Active Appearance Models (AAMs) have shown utility for segmenting End Diastolic (ED) angiograms, but do not perform satisfactory in individual ES angiograms. In this work, we present a new Multi-View AAM in which we exploit the existing correlation in shape and texture between ED and ES phase to steer the segmentation of both frames simultaneously. Model scale, orientation and position remain independent, whereas appearance statistics are coupled. In addition, an AAM is presented in which the gray-value information of the inner part of the LV is not taken into account. This so-called boundary AAM is applied mainly to enhance local boundary localization performance. Both models are applied in a combined manner and are validated quantitatively. In 61 out of 70 experiments good convergence for both ED and ES segmentation was achieved, with average border positioning errors of 1.86 mm (ED) and 1.93 mm (ES).

2.1 Introduction

Left Ventricle (LV) angiography is a widely used modality for assessing left ventricular function. Because the heart itself is not visible in X-ray images, patients undergo a catheterization procedure, in which the left ventricle is filled with an X-ray opaque contrast dye. During this procedure 150 to 200 images are acquired in the right anterior oblique view, at a typical rate of 25 to 50 images per second. This generally covers 7 to 9 cardiac cycles. From this image sequence the second or third cardiac cycle is selected. Irregular muscle contractions due to the injection of the contrast agent are expected to have faded at this stage, while the contrast agent distribution within the left ventricle is expected to be optimal. The End Diastolic (ED) and End Systolic (ES) image frames from this cardiac cycle are the starting point for the quantification of left ventricular function. In both the ED and the ES image, a contour line is drawn around the left ventricle. Subsequently a surface area of the projected left ventricle is calculated for both phases, followed by an estimation of the ED and ES volumes, for which we used the volume estimation method proposed by Sandler and Dodge [1]. The ejection fraction is determined from both calculated volumes.

Currently, software packages are available that assist the cardiologists in drawing the contours around the left ventricle manually. But drawing these contours by hand is a difficult and time-consuming task. The poor image quality and varying distribution of the contrast agent complicate the drawing of correct contours. Also, manual contour drawing intrinsically introduces significant inter-observer and intra-observer variability.

Recognizing these difficulties, the need for a reliable and reproducible automatic method for segmenting the left ventricle becomes apparent. Automatic contour

detection in X-ray angiograms is a challenging task for which a reliable technique has not been developed yet to the point of robust clinical application. Several knowledge-based approaches have been proposed over the last two decades, starting with regular edge detection followed by a procedure to merge the separately found LV edges by means of a statistical shape model [2], or approaches using Dynamic Programming and template matching [3].

Until now, the most promising results were obtained in segmenting the ED image, while results in ES segmentation remained poor. Because much of the contrast agent is pumped out of the LV during contraction, the ES image quality and LV definition in general is rather poor, hampering the automatic segmentation of the ventricle. In this chapter, we overcome this by using additional knowledge: for an individual patient, the left ventricular shape and appearance in end diastolic images and end systolic images are highly correlated, although the position and orientation of the ventricle can change significantly due to cardiac motion and contraction. The emphasis of this research lies in the improvement of the ES segmentation results, by using this correlation between the ED phase and the ES phase, resulting in an overall improved automatic assessment of cardiac function.

The methodology is an extension on the Active Appearance Models (AAMs), introduced by Cootes *et al.* [4,5], which in recent years have proven to be highly successful in automatic object segmentation in medical images. AAMs, derived from the earlier introduced Active Shape Models (ASMs), are statistical models describing the shape and the appearance of an object. For both shape and gray-values, an average and a series of eigenvectors is computed, from which the "modes of variation" of the model are determined. When matching the model to an unseen image, it searches the LV contours by minimizing the error between the model and the image, within the boundaries of statistically plausible deformations, as defined by the model.

Direct application of AAMs to ED LV angiograms already shows great potential for automatic segmentation and thus towards automatic quantitative evaluation of LV function. However, segmenting ES images using general Active Appearance Models still does not result in satisfactory results, because of the poor ventricle definition in ES. To exploit the correlation between the LV shape in ED (usually with a better image contrast) and ES, we have developed the Multi-View AAM, which models multiple views of an object. By training the model on the available shape and texture information of both ED and ES simultaneously, the existing correlation between the two phases is preserved and used to steer the segmentation. The idea presented here resembles Cootes' Coupled View AAMs for tracking faces and estimating head pose [6], but differs greatly in both the training and matching procedure.

In addition, Active Appearance Models have proven to be less accurate then Active Shape Models [7], when it comes to precise border localization. Because global appearance is modeled, accurate border characteristics are less pronounced and image intensity in the middle of the ventricle may negatively influence boundary localization performance. Therefore, we have developed a matching refinement step, where an AAM is applied in which the gray-value information of the inner part of the LV is not taken into account. This "boundary AAM" is also applied in a Multi-View manner: appearance optimization is coupled, while pose is refined for

each frame independently. The principal difference between the boundary AAM and the classic Active Shape Model is the simultaneous optimization of shape and local appearance using a single criterion function, whereas in ASMs, shape and local appearance are optimized independently.
To summarize the novel aspects of this work:

- We have developed the Multi-View Active Appearance Model, allowing to exploit existing correlations between different views of the same object.

- We have introduced a refinement matching procedure, consisting of a boundary model that only takes gray-value information near the suspected LV border into account.

2.2 Active Appearance Models

An Active Appearance Model is a statistical description of appearance of an image in terms of object shape and texture. Applying AAMs consists of two parts: training and matching. Both the construction of the AAM and the matching procedure are briefly introduced in this section. An elaborate explanation can be found in [5].

2.2.1 Active Appearance Model Training

An AAM is trained on a series of representative images, all containing the specific object to segment, in our case X-ray LV angiograms. For each image in the training

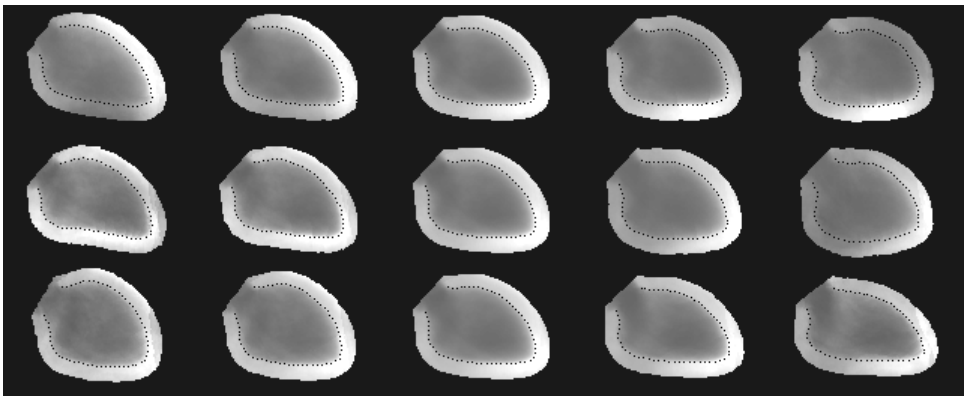

Figure 2.1: The first three modes of variation for a left ventricle AAM, end diastolic phase. From top to bottom, the rows represent mode 1, 2 and 3, respectively. From left to right the columns represent a standard deviation of minus two sigma, minus one sigma, zero, plus one sigma and plus two sigma. In this example the first mode of variation describes the shape variation in elongation while the texture emphasis changes from the lower part of the ventricles embedding to the upper part. The second mode of variation mainly describes the shape variation in the bottom part of the ventricle and the brightness in the valve area. The third mode of variation is a combination of elongation and skewing variations.

set, an expert segments the object of interest manually, the drawn contour is sampled in n points and defined (for 2D) as a vector of 2n elements, identifying image coordinates. This vector is defined as

$$\mathrm{x} = (x_1, y_1, x_2, y_2, x_3, y_3, ..., x_n, y_n)^T \tag{2.1}$$

Before statistical models of shape and texture are computed, all sample point vectors are aligned using Procrustes Analysis. By applying Principal Component Analysis (PCA) on the sample covariance matrix, a statistical shape model can be built. The eigenvectors and eigenvalues are calculated and the eigenvectors are ordered following descending eigenvalues. Arranging the eigenvectors in this manner enables elimination of less significant eigenvectors, resulting in a statistical model based on the most dominant eigenvectors. The statistical shape model can be formulated as

$$\mathrm{x} \approx \bar{\mathrm{x}} + P_s b_s \tag{2.2}$$

where any shape vector x in the training set can be approximated by a linear combination of the mean shape $\bar{x}$, and the eigenvectors in P_s, which are weighted by the shape coefficients in parameter vector b_s.
Creating the texture model consists of the following steps. First, a convex hull is constructed from every sample point vector, from which an image patch is sampled. For every training image this image patch is warped onto the mean shape, creating a shape free patch, from which the texture vectors g are extracted. Usually the area of this image patch is dilated to a certain extent, in order to incorporate gray-value information of the direct object surroundings in the model. The elements of a texture vector g represent the pixel intensities in the image patch. All texture vectors are normalized to zero average and unit variance and a PCA is performed on the sample covariance matrix, resulting in the statistical texture model. Analogous to the shape model, each texture sample g is approximated by

$$\mathrm{g} \approx \bar{\mathrm{g}} + P_g b_g \tag{2.3}$$

with mean texture vector $\bar{\mathrm{g}}$, texture eigenvector matrix P_g and the set of texture parameters b_g.
From the shape and texture models, an Active Appearance Model is created by concatenating the shape parameter vector and the texture parameter vector, derived from equations (2.2) and (2.3):

$$b = \begin{pmatrix} W b_s \\ b_g \end{pmatrix} = \begin{pmatrix} W P_s^T (\mathrm{x} - \bar{\mathrm{x}}) \\ P_g^T (\mathrm{g} - \bar{\mathrm{g}}) \end{pmatrix} \tag{2.4}$$

W denotes a weight factor coupling the shape and texture coefficients. After a final Principal Component Analysis over the set of appearance vectors b the resulting Active Appearance Model can be written as

$$b = Qc \tag{2.5}$$

in which Q is the matrix containing the eigenvectors and c denotes the appearance parameters. The modes of variation of the AAM display the characteristic variations in shape and gray-value of the model. Figure 2.1 shows the first three modes of variation of an AAM trained on end diastolic LV angiograms.
The last part of training the AAM is to estimate the parameter update steps required to drive the model matching iterations. These are computed from the residual images $\delta g_0 = g_s - g_m$, where g_s denotes the target image, and g_m the model synthesized image. By applying parameter perturbations on the model, pose and texture parameters for model samples with known parameters, gradient matrices R_c, R_p and R_t can be estimated for the model, pose and texture respectively. In our approach, we followed Cootes' direct gradient approach, as recommended in [8].

2.2.2 Active Appearance Model Matching

When matching the model to an unseen image, the model searches the LV contours by minimizing the relative mean square error between the model and the image, within the boundaries of statistically plausible deformations of the model. Based on the model image patch, the image to segment, the current estimate of the model parameters c_0 and the parameter derivatives for the model, texture and pose parameters (matrices R_c, R_t & R_p respectively), Cootes describes an iterative matching algorithm, consisting of the following steps [5]:

1) Calculate the difference-vector between the image and model patch $\delta g_0 = g_s - g_m$

2) Calculate the root mean square (RMS) error of the difference-vector $E_0 = |\delta g_0|^2$

3) Determine the predicted model parameter updates $\delta c = R_c \delta g_0$, pose update $\delta p = R_p \delta g_0$ and texture update $\delta t = R_t \delta g_0$

4) Set k = 1 and determine a new estimate for the model parameters $c_1 = c_0 - k\delta c$, pose parameters $p_1 = p_0 - k\delta p$ and texture parameters $t_1 = t_0 - k\delta t$

5) Calculate a new model based on c_1, p_1 & t_1

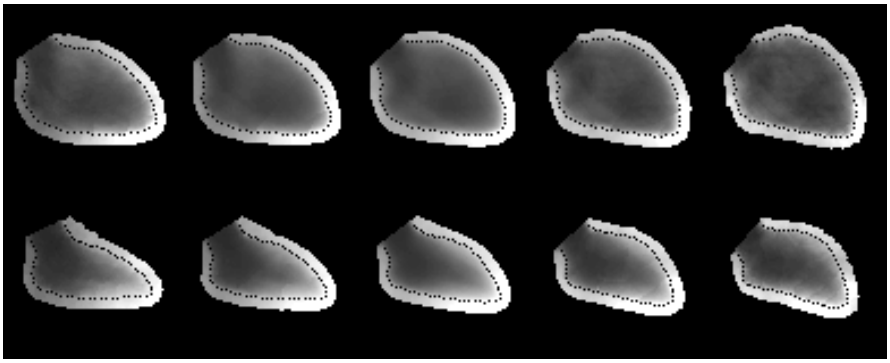

Figure 2.2: First mode of variation for a left ventricle Multi-View AAM for X-ray LV angiography. Upper row denotes ED, lower row denotes ES. The correlation in shape between ED and ES is clearly visible. Also the texture variation, describing mainly the local contrast between the LV and it's embedding around the mitral valve, shows clear similarities for ED and ES.

6) Determine a new difference-vector and calculate its RMS error E_1

7) If $E_1 < E_0$, select c_1, p_1 & t_1 as the new parameter vectors, else try $k = 1.5$, $k = 0.5$, $k = 0.25$ etc. and go to step 4

The stop criterion of this algorithm is determined by a fixed number of passes through step 7.

2.2.3 Medical Applications of Active Appearance Models

Several examples exist regarding the application of Active Appearance Models in medical image segmentation. Cootes has demonstrated the application of 2D AAMs on finding structures in brain MR images [9], and knee cartilage in MR images [5]. In 2D cardiac MR images, Mitchell *et al.* applied AAMs to segment the left and right ventricle [10]. Thodberg [11] applied a 2D AAM to reconstruct bones in hand radiographs. Bosch *et al.* successfully used 2D + time AAMs in order to segment endocardial borders in echocardiography [12]. Beichel *et al.* describe a semi 3D AAM extension applied to segmentation of the diaphragm dome in 3D CT data [13]. Mitchell *et al.* describe a full 3D AAM extension, and apply it to 3D cardiac MR data and 2D + time echocardiograms [14]. Research on utilizing AAMs in other modalities is ongoing, but for X-ray LV angiography, no trials have been reported yet.
Active Appearance Models have shown to outperform other segmentation approaches in MRI and echocardiography and are also believed to outperform other methods in LV angiography because of the following advantages:

- Because in many cases the image quality of left ventricular angiograms is poor, it is required to use a priori knowledge about intensity characteristics. Active Appearance models make good use of all available gray-value

information. By supplying it with a sufficiently varied set of LV images, the AAM is adapted to the image appearances that can be expected. This also means that, when supplied with sufficient examples in the training set, AAMs are capable of recognizing pathological shape variations and texture variations caused by acquisition artifacts.

- The left ventricular border does not necessarily coincide with the strongest edges in the image. Because an Active Appearance Model is a statistical description of shape *and* appearance, it is able to copy the drawing characteristics of the cardiologist(s) that drew the contours in the training images. This implies that the model does not necessarily follow the strongest edges, but is adaptive to observer preferences.

2.3 New AAM Extensions

2.3.1 Multi-View Active Appearance Models

The most challenging aspect of automatic border detection in LV angiography is segmenting the left ventricle in the end systolic phase. Due to contraction of the papillary muscles, contrast fluid is squeezed out of the LV in the ES phase, seriously hampering the ES LV visualization. Since manual segmentation of ES images is already highly subjective, automatic segmentation of individual ES images appears to be very difficult. In manual segmentation, the cardiologist reviews the images in cine-mode, instinctively coupling the shape characteristics and texture information of the ventricle and its embedding in ED phase and in ES phase. This observation is our main motivation to pursue simultaneous segmentation of both phases. The Multi-View Active Appearance Model presented here is designed to exploit this existing correlation between ED and ES LV appearance and therefore potentially produces better segmentation results in ES images.
In the Multi-View Active Appearance model, the LV shape is modeled by aligning the training shapes for ED and ES separately, and concatenating the aligned shape vectors for each view. In this application, a shape vector is defined as:

$$\mathrm{x} = \left(x_{1ED}, y_{1ED}, x_{2ED}, y_{2ED}, ..., x_{nED}, y_{nED}, x_{1ES}, y_{1ES}, x_{2ES}, y_{2ES}, ..., x_{nES}, y_{nES}\right)^T \qquad (2.6)$$

For the intensity vectors, the same applies: all intensity vectors are separately normalized to zero mean and unit variance, and subsequently concatenated:

$$\mathrm{g} = \left(i_{1ED}, i_{2ED}, i_{3ED}, ..., i_{nED}, i_{1ES}, i_{2ES}, i_{3ES}, ..., i_{nES}\right)^T \qquad (2.7)$$

Analogous to the single frame AAM, a PCA is applied to the concatenated sample covariance matrices for shape and appearance, and subsequently a combined

model is computed. In the combined model, the shape and appearance of both views are strongly interrelated, as is illustrated in Figure 2.2.
Estimation of the gradient matrices for computing parameter updates during image matching is performed by applying perturbations on the model, pose and texture parameters. Because of the correlations between views in the model, a parameter disturbance in the model parameters yields difference images in both views simultaneously. The pose parameters however, are perturbed for each view separately, hence the model is trained to accommodate for trivial differences in object pose in each view, whereas the shape and intensity gradients are trained for all views.

In the matching procedure, the pose transformation for each view is also performed separately, whereas the model coefficients intrinsically influence multiple frames at a time. Hence, the allowed shape and intensity deformations are coupled for all frames, whereas pose parameter vectors for each view are optimized independently. This is a significant difference as compared to the coupled view AAM by Cootes *et al.*, where separately trained 2D models are matched to each separate view, and subsequently the appearance model constraints are imposed from a combined appearance model [6].

2.3.2 Boundary Active Appearance Models

Because global appearance is modeled in AAMs, accurate border characteristics are less pronounced, causing possible deterioration of boundary localization performance. Therefore we have developed a boundary Active Appearance Model, which, besides shape information, takes only gray-value information in the vicinity of the detected border into account. By eliminating the gray-value information of the inner part of the ventricle, we aim to improve the border detection accuracy. Figure 2.3 shows the first 3 modes of variation for a boundary AAM.

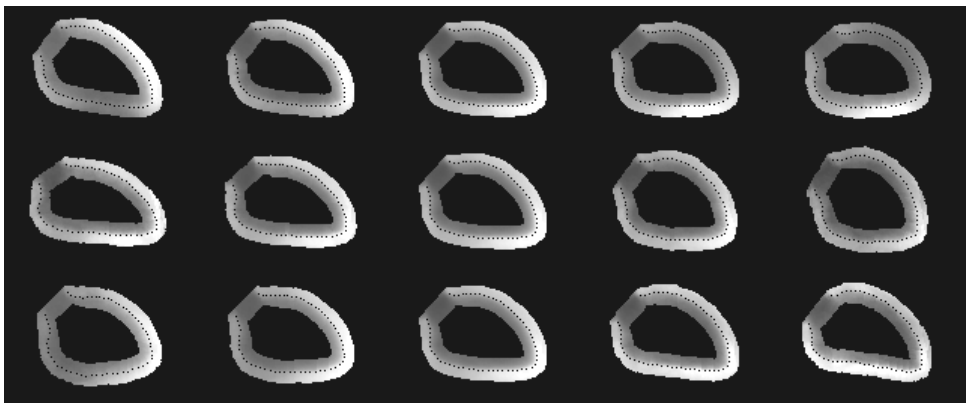

Figure 2.3: First three modes of variation for a left ventricle boundary AAM, end diastolic phase. From top to bottom, the rows represent mode 1, 2 and 3, respectively. From left to right the columns represent a standard deviation of minus two, minus one, zero, plus one and plus two sigma.

The boundary AAM approach presented here resembles the original ASM formulation, however it differs in the fact that more intensity information in the vicinity of the boundary is utilized: this way, the relation between the manually drawn contour and the underlying image intensity patch is preserved. Also, the boundary AAM matching intrinsically relies on the simultaneous optimization of shape and appearance using a single criterion function, as in ASMs this is performed separately. Applying Active Shape Models for border positioning refinement is not likely to improve results, because of the poor LV border definition, especially in the ES image.

2.4 Experiments and Results

2.4.1 Experimental Setup

To test the clinical efficacy of the Multi-View and boundary AAM, 70 ED-ES pairs of representative LV angiograms from infarct patients were collected. Apart from high quality images with good LV definition in both ED and ES, images were selected, in which frequently appearing acquisition artifacts were present (poor LV contrast, inhomogeneous distribution of the contrast agent, presence of an overlap of the diaphragm with the LV). Figure 2.4 displays a few examples of images that were used in our models. An expert manually defined contours in both frames, and point correspondence was defined based on three prominent landmarks: both aorta valve points and the apex. Every contour was equidistantly resampled to 60 points. 14 leave-five-out models were trained on 65 out of 70 ED-ES image pairs, leaving out 5 sets for testing purposes. To speed up the training and matching process and to reduce model dimensionality, all images were subsampled with a factor 4.

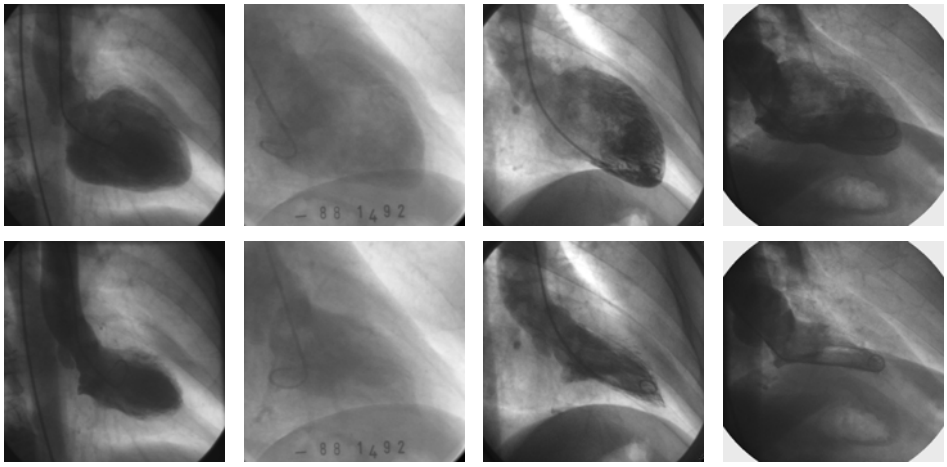

Figure 2.4: LV example images for ED (upper row) and ES (lower row). From left to right: well defined LV, poor contrast, inhomogeneous distribution of the contrast agent (most apparent in ED) and presence of an overlap of the diaphragm with the LV.

In this validation, we aimed to minimize user interaction, therefore all model matching experiments were initialized from a fixed position in the image (the image center), assuming that there is sufficient overlap between the model and the true location of the LV. To minimize the risk of convergence to local minima, sequential application of several AAMs was performed, where the amount of preserved AAM variation was increased from 80% to 99%. For the first model matching, a coupling between the pose and scale parameters in ED and ES was enforced. In subsequent matches, this constraint was released, and pose and scale were allowed to vary for each frame separately.
In addition, the added value of the boundary AAM was investigated by executing an additional model run with the boundary AAM after the regular Multi-View model and comparing their performances.

2.4.2 Evaluation Method

A matching experiment was considered a success when the distance of more than two thirds of the total number of contour points was within 5 pixels of the manual contour. Because there was no calibration factor available for every image, we used a calibration factor of 0.25 mm per pixel, which is representative for most LV angio acquisition systems. In the four-times-subsampled 512 x 512 images that we used, an error of 5 pixels corresponds with 5 mm. Failed matches were repeated with manually set initial position, and cases still yielding matching failure were reported and excluded from further quantitative analysis. These matching failures were divided into three classes: failure in only ED, failure in only ES and failure in both frames. On the successful matches, a statistical analysis was performed, in which the following metrics were used to compare the automatically generated contours with the manual reference contours:

- the border positioning errors (point-to-curve) for the ED and ES contours separately.
- the error in the surface area enclosed by the contours for the ED and ES frames separately.
- the error in estimated ED and ES volumes, as obtained with the Sandler and Dodge volume estimation method [1].
- the error in calculated ejection fraction.

Equation (2.8) describes the volume estimation according to Sandler and Dodge, based on the projected surface Area A and the distance L_A from the upper aortic valve point to the apex:

$$V = \frac{8A^2}{3\pi L_A} \tag{2.8}$$

2.4.3 Results

When matching the LV with a fixed initial position, 57 out of 70 cases (81%) showed convergence. In 4 cases a failure in the calculated ED contour occurred, in 4 other cases the computed ES contour was unsatisfactory and in 5 other cases there was failure in determining both the ED and the ES contour. These 13 failures in LV delineation were matched again, but this time the initialization of the model was done manually. This way 9 failures remained (resulting in a success rate of 87%), 2 in ED, 4 in ES and 3 in ED and ES. Border positioning errors for the 61 successful segmentations are summarized in Table 2.1. For the ED matching results, 72% of the calculated LV contour points was positioned within 2 mm from the expert contour, another 22% was positioned between 2 and 5 mm from the expert contour and the remaining 6% were more than 5 mm away from the expert contour. For the ES matching results, the distribution was 67% (error < 2 mm), 27% (2 mm < error < 5 mm) and 6% (error > 5 mm).

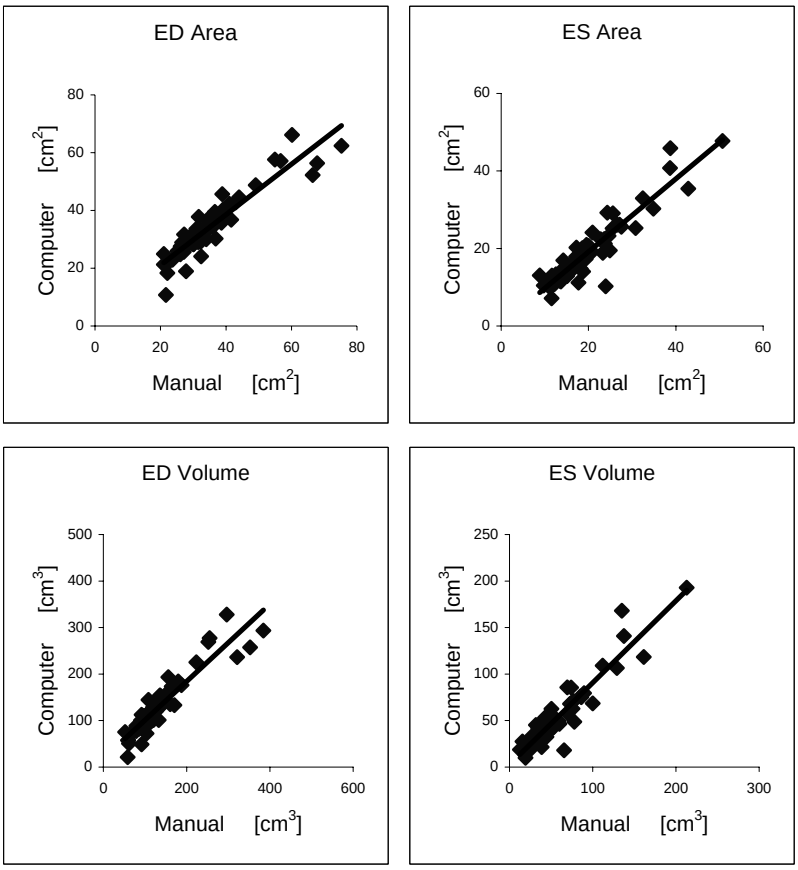

Figure 2.5: Comparison of manual and model results for ED Area (r = 0.93; y = 0.87x + 3.57 [cm^2]), ES Area (r = 0.93; y = 0.94x + 0.31 [cm^2]), ED Volume (r = 0.93; y = 0.83x + 17.74 [cm^3]) and ES Volume (r = 0.94; y = 0.88x + 2.62 [cm^3]).

	Average positioning error [mm]	Average upper valve error [mm]	Average lower valve error [mm]	Average apex error [mm]
ED	1.86 ± 2.45	4.47 ± 3.23	4.60 ± 4.06	4.54 ± 4.63
ES	1.93 ± 2.11	4.46 ± 2.90	3.68 ± 2.67	6.50 ± 5.11

Table 2.1: LV border positioning error and errors in the location of upper valve, lower valve and apex. Errors are expressed as unsigned average ± standard deviation.

	Average positioning error [mm]	Average upper valve error [mm]	Average lower valve error [mm]	Average apex error [mm]
ED	1.87 ± 2.50	4.47 ± 3.25	4.70 ± 4.22	4.39 ± 4.34
ES	1.97 ± 2.17	4.56 ± 3.24	3.64 ± 2.62	6.44 ± 5.26

Table 2.2: LV border positioning error and errors in the location of upper valve, lower valve and apex, after application of the boundary AAM. Results denote unsigned average ± standard deviation.

Good correlation has been achieved in comparing the areas and volumes calculated from expert contours and the areas and volumes calculated from the model-determined contours (Figure 2.5). Comparing the calculated ejection fraction for expert contours and model contours, the average signed error was −0.26% with a standard deviation of 14.89%. Still large errors occur, varying from -82% to +33%. Figure 2.6 shows examples of a good matching result and a rejected matching result.

The results for the boundary AAM, also based on the 61 cases of successful segmentation, are summarized in Table 2.2. The average signed error between calculated ejection fractions for expert contours and model contours is 0.24% with a standard deviation of 13.22%. Minimum and maximum errors still can be very large ranging from −71% to +32%. The performance of the boundary AAM is comparable to the results mentioned above: the average boundary positioning errors did not differ statistically significantly as compared to the Multi-View AAM alone. Figure 2.7 displays the potential refinement achievement of the boundary AAM.

2.5 Discussion

The reported method shows promising results in automatic segmentation of left ventricles in X-ray angiograms. The method uses coupled statistical information on

shape and image intensities in the ED and ES images. The matching procedure is based on expert-drawn LV contours and copies human drawing behavior. Although the method has not yet evolved to clinical applicability and especially has difficulties with the segmentation of the LV in poor-quality images, it is the first method that performs well in a large variety of LV shapes in X-ray angiograms for both ED and ES, even when using a fixed initialization in the image center.

We divided the 70 image pairs that were used in this study into four categories: good contrast (28 cases), poor contrast (30 cases), overlap between LV and diaphragm (4 cases) and both poor contrast and overlap (8 cases). When using a fixed initialization, in 57 out of 70 experiments (81%), successful segmentation was achieved, without requiring user interaction. 13 matching failures occurred from which 1 image pair was found to have good contrast, 8 belonged to the poor contrast subset, 1 image pair had an overlap between LV and diaphragm and 3 image pairs both had an overlap and poor contrast. After repeating the 13 failures with manual initialization, 9 cases of failure remained (success rate = 87%), in which 6 image pairs with poor contrast and 3 image pairs with both poor contrast and an overlap between LV and diaphragm.

Figures 2.6a, 2.6b, 2.6e and 2.6f show a representative example of a successful segmentation. From a fixed starting position in the image center, with a scaling that corresponds to the average LV size in the training set, the model finds the correct LV location and deforms within statistically plausible limits to match the underlying LV contours as close as possible. For this specific example, the average border positioning errors are 1.20 ± 1.07 mm and 1.00 ± 0.97 mm for ED and ES

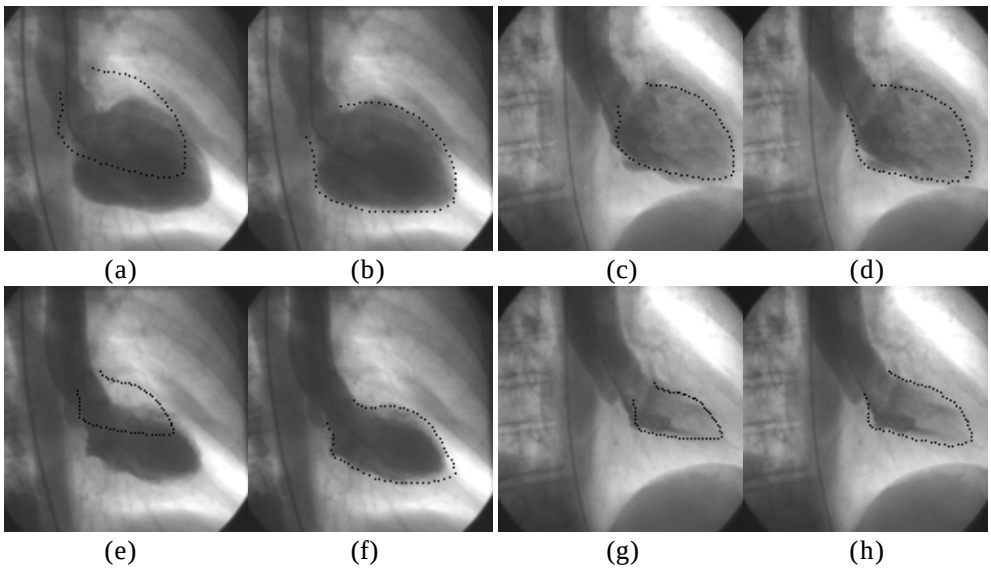

Figure 2.6: Examples of a good matching result (b and f) and a rejected matching result (d and h) for both ED (upper row) and ES (lower row). a and e show fixed initializations in the center of the image, c and g show manual initialization.

respectively. A critical remark that can be made about these successful segmentation results concerns the errors in valve positions in the ED frame and the error in the apex position in the ES frame, which can have a large effect on the volume estimation that is based on the distance between upper valve and apex [1].
Figures 2.6c, 2.6d, 2.6g and 2.6h show a representative example of a failed segmentation. In this case the ED contour was unsatisfactorily detected; the entire region between upper valve and apex should have been drawn wider. This is clearly the result of poor image contrast in this region. Hence, most failures can be assigned to poor contrast conditions and overlap between LV and diaphragm. In the latter case the LV contour will, either locally or entirely, drift away from the true location of the LV.

The success rate of our method suggests that it is capable to cope with a variety of LV shapes. Image pairs with large infarcted areas around the apex however were a minor category in the training set and therefore resulted in a failure in segmentation. When considering the 61 cases of successful segmentation, the average point-to-curve border positioning error was 1.86 ± 2.45 mm for ED images and 1.93 ± 2.11 mm for ES images, which for automatic LV angiographic segmentation is a good performance. Especially the results for ES images are excellent compared to previously explored X ray LV angio segmentation methods [2,3]
The regression lines in Figure 2.5 are based on the 61 occurrences of successful convergence and show a good correlation between surface area and volume computation based on manually drawn contours and based on model-generated contours. Correlation coefficients are 0.93 for ED area, ES Area and ED Volume and 0.94 for ES Volumes, which demonstrates that automatic ES segmentation can accomplish the same level of performance as automatic ED segmentation performance. The error in calculated ejection fraction is −0.26% with a standard deviation of 14.89 %. For both calculated volumes and for the ejection fraction, the systematic errors are close to zero. The accompanying high standard deviations on the other hand show that large errors may still occur, and an improvement is still required to meet clinically demanded error margins.

The three landmark points that are used for calculation of LV volume (upper valve point, lower valve point and apex) have a considerably higher average positioning error than the average border positioning error over the entire contour. Because these three points are of high influence on the calculation of LV volume, future research must aim on decreasing border positioning errors of these three points.

The main difficulty in interpreting the obtained results is that there is no ‘gold standard’, describing the characteristics of a well-drawn LV contour. In clinical practice different medical doctors will have different signatures in drawing contours and therefore an automatic technique is only clinically reliable when the difference in performance between the automatic technique and a medical expert is comparable to the difference in performance between several medical experts. In order to achieve this for Active Appearance Models one may use multiple contours from several different medical experts in model training.

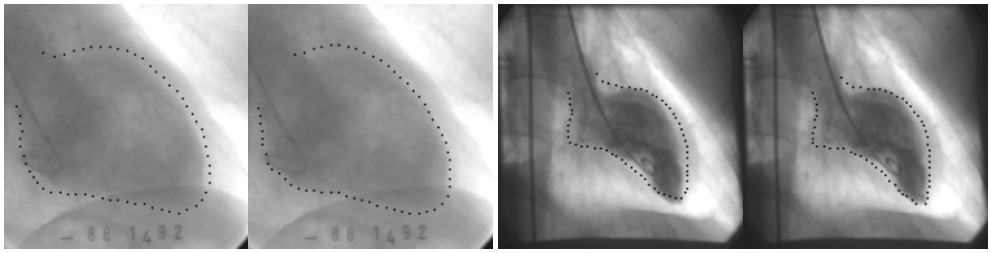

(a) (b) (c) (d)

Figure 2.7: Boundary AAM performance examples for ED (a = AAM result, b = boundary AAM result) and ES (c = AAM result, d = boundary AAM result).

The performance criterion of 67% of the calculated contour points to be within 5 millimeters of the actual LV border has not yet been compared with figures for inter-observer variability. This standard is likely to be insufficient in clinical practice, although inter-observer variability can also amount to high values, especially in the difficult images, where observers tend to disagree. Therefore, in the current stage of development of an automatic method for LV segmentation in X-ray angiograms it is legitimate to use this classification to define convergence to an acceptable contour.

The boundary AAM that was introduced for refinement of the segmentation results shows results comparable with the regular Multi-View AAM. However, overlooking all 61 cases, only 41 ED segmentations (67%) and 34 ES (56%) segmentations showed improvement after the boundary AAM. Figure 2.7 shows the potential capacity of the boundary AAM. In Figure 2.7a and 2.7b the segmentation of the lower part of the LV in ED phase has clearly improved and the location of the upper valve is more accurate. Figure 2.7c and 2.7d show improvements in the ES segmentation after application of the boundary AAM, especially expressed in a better segmentation of the apex region.

References

[1] H. Sandler and H. T. Dodge, “The Use of Single Plane Angiocardiograms for the Calculation of Left Ventricular Volume in Man”, *American Heart Journal*, vol. 75, no.3, pp. 325-34, 1968.

[2] S. Tehrani, T. E. Weymouth, and G. B. J. Mancini, “Model generation and partial matching of left ventricular boundaries,” *Proceedings of SPIE Medical Imaging*, vol. 1445, pp. 434-445, 1991.

[3] P. Lilly, J. Jenkins, and P. Bourdillon, “Automatic contour definition on left ventriculograms by image evidence and a multiple template-based model,” *IEEE Transactions on Medical Imaging*, vol. 8, no. 2, pp. 173-185, 1989.

[4] T. F. Cootes, G. J. Edwards, and C. J. Taylor, “Active appearance models,” *Proceedings of the European Conference on Computer Vision*, H. Burkhardt and B. Neumann, Eds., vol. 2, Berlin: Springer Verlag, 1998, pp. 484-498.

[5] T. F. Cootes and C. J. Taylor, “Statistical models of appearance for computer vision,” Online available: *http://personalpages.manchester.ac.uk/staff/timothy.f.cootes/Models/app_models.pdf*

[6] T.F. Cootes, G.V. Wheeler, K.N. Walker, C.J. Taylor, “View-based active appearance models,” *Image and Vision Computing*, vol. 20, no. 9-10, pp. 657-664, 2002.

[7] T.F. Cootes, G. J. Edwards and C. J. Taylor, “Comparing Active Shape Models with Active Appearance Models,” *Proceedings of British Machine Vision Conference*, T.Pridmore and D.Elliman, Eds., vol. 1, pp. 173-182, 1999.

[8] T.F.Cootes, P.Kittipanya-ngam, “Comparing Variations on the Active Appearance Model Algorithm,” *Proceedings of British Machine Vision Confererence*, vol.2, pp. 837-846, 2002.

[9] T. F. Cootes, C. Beeston, G. J. Edwards, and C. J. Taylor, “A Unified Framework for Atlas Matching Using Active Appearance Models,” *Proceedings of Information Processing in Medical Imaging*, Kuba, Samal and Todd-Pokropek, Eds, vol. 1613, pp. 322-333, 1999.

[10] S. C. Mitchell, B. P. F. Lelieveldt, R. J. Van der Geest, H. G. Bosch, J. H. C. Reiber, and M. Sonka, “Multistage hybrid active appearance model matching: segmentation of left and right ventricles in cardiac MR images,” *IEEE Transactions on Medical Imaging*, vol. 20, no. 5, pp. 415-423, 2001.

[11] H.H. Thodberg, “Hands on Experience with Active Appearance Models,” *Proceedings of SPIE Medical Imaging*, vol. 4684, pp. 495-506, 2002.

[12] J. G. Bosch, S. C. Mitchell, B. P. F. Lelieveldt, F. Nijland, O. Kamp, M. Sonka, and J. H. C. Reiber, “Automatic segmentation of echocardiographic sequences by active appearance motion models,” *IEEE Transactions on Medical Imaging*, vol. 21, no. 11, pp. 1374-1383, 2002.

[13] R. Beichel, G. Gotschuli, E. Sorantin, F. Leberl, M. Sonka, “Diaphragm Dome Surface Segmentation in CT Data Sets: A 3D Active Appearance Model Approach,” *Proceedings of SPIE Medical Imaging*, vol. 4684, pp. 475-484, 2002.

[14] S.C. Mitchell, J.G. Bosch, B.P.F. Lelieveldt, R.J. van der Geest, J.H.C. Reiber, M. Sonka, “3D Active Appearance Models: Segmentation of Cardiac MR and Ultrasound images,” *IEEE Transactions on Medical Imaging*, vol. 21, no. 9, pp. 1167-1178, 2002.

改心
'improvement'

Chapter 3

Multi-View Active Appearance Models: Application to X-Ray LV Angiography and Cardiac MRI

This chapter was adapted from:
Multi-View Active Appearance Models: Application to X-Ray LV Angiography and Cardiac MRI
C.R. Oost, B.P.F. Lelieveldt, M. Üzümcü, H. Lamb, J.H.C. Reiber, and M. Sonka
In: Proceedings of IPMI 2003, C.J. Taylor and J.A. Noble Eds., vol. 2732, pp. 234-245, 2003.

Abstract

This chapter describes a Multi-View Active Appearance Model (AAM) for coherent segmentation of multiple cardiac views. Cootes' AAM framework was adapted by considering shapes and intensities from multiple views as single shape and intensity samples, while eliminating trivial difference in object pose in different views. This way, the coherence in organ shape and intensities between different views is modeled, and utilized during image search. The method is validated in two substantially different and novel applications: segmentation of combined end-diastolic and end-systolic X-ray left ventricular angiograms, and simultaneous segmentation of a combination of four chamber, two chamber and short-axis cardiac MR views.

3.1 Introduction

In cardiac imaging, typically multiple acquisitions are acquired within one patient examination following fixed imaging protocols, where images may depict different geometrical or functional features of the heart. For instance, in cardiac MR imaging, the short-axis, long-axis, perfusion, rest-stress and delayed enhancement images provide complementary information about different aspects of geometry and function of the same heart. Also, in bi-plane X-ray left ventricular (LV) angiography, different views are acquired of the LV, which are the left anterior oblique 60° and right anterior oblique 30°, showing the left ventricle from different projection angles. Different time frames from an angiographic or echographic image sequence are other examples of such interrelated views.

To quantify cardiac function and morphology from such image sets, a (preferably automatic) segmentation of the heart is required. However, typically, automatic segmentation methods focus on one subpart of a patient examination. Segmentation is achieved for one view at a time, and the different parts of a patient examination are treated separately. As a result, not all available information is used to achieve a segmentation result, since additional shape information of the same organ may be available from a different view. The goal of this work was to develop a segmentation method that exploits existing shape and intensity redundancies and correlations between different parts of a patient examination. Potentially, this increases robustness, and enforces segmentation consistency between views, therefore yielding a better segmentation.

To realize this, we have developed the Multi-View Active Appearance Model (AAM): an extension of Cootes' AAM framework [1-5] that captures the coherence and correlation between multiple parts of a patient examination. Model training and matching are performed on multiple 2D views simultaneously, combining information from all views to yield a segmentation result. To investigate the clinical potential, we validate the Multi-View AAM in two substantially different, largely unsolved segmentation problems: automatic definition of the LV contours in pairs

of X-ray LV angiograms in ED and ES phase, and second, simultaneous LV contour detection in a combination of short-axis, four and two chamber cardiac MR views.

3.2 Background

An Active Appearance Model is a statistical model of object shape and texture. The construction of the AAM and the matching procedure are briefly introduced in this section. A detailed description can be found in [3].

3.2.1 AAM Training

An AAM is trained on a series of representative images, in which an expert manually segmented the object of interest. Contours are resampled in n corresponding points, and, for the 2D case, expressed as a vector of $2n$ elements:

$$\mathrm{x} = \left(x_1, y_1, x_2, y_2, x_3, y_3, ..., x_n, y_n\right)^T \tag{3.1}$$

After Procrustes alignment of the shape vectors to eliminate trivial pose differences, a shape model is built by applying Principal Component Analysis (PCA) on the sample covariance matrix. Arranging the eigenvectors according to descending eigenvalues enables elimination of less significant eigenvectors.

Similarly, a texture model is created by warping the training images onto the mean shape and creating a shape free patch, from which pixel intensity vectors g are extracted. Texture vectors are normalized to zero average and unit variance and PCA is performed on the sample covariance matrix, resulting in the statistical texture model. Using the shape and texture models, the sample shapes x and textures g can be approximated from the respective models:

$$\mathrm{x} \approx \bar{\mathrm{x}} + P_s b_s \quad \text{and} \quad \mathrm{g} \approx \bar{\mathrm{g}} + P_g b_g \tag{3.2}$$

where $\bar{\mathrm{g}}$ and $\bar{\mathrm{x}}$ represent the average texture and shape vectors, P_g and P_s the texture and shape eigenvector matrices, and b_g and b_s the texture and shape parameters characterizing each training sample.

From the shape and texture models, an AAM is created by concatenating the shape and texture parameter vectors:

$$b = \begin{pmatrix} W b_s \\ b_g \end{pmatrix} = \begin{pmatrix} W P_s^T \left(\mathrm{x} - \bar{\mathrm{x}}\right) \\ P_g^T \left(\mathrm{g} - \bar{\mathrm{g}}\right) \end{pmatrix} \tag{3.3}$$

W denotes a weight factor coupling the shape and texture coefficients.

After a final PCA over the set of appearance vectors *b* the resulting AAM can be written as:

$$b = Qc \tag{3.4}$$

in which *Q* is the matrix containing the eigenvectors and *c* denotes the appearance parameters for the combined model.

Matching the model to an unseen image involves minimizing the root mean square error between the model generated image and the target image, within the boundaries of statistically plausible model limits. To drive the model matching iterations the parameter update steps are computed from the residual images $\delta g_0 = g_s - g_m$, where g_s denotes the target image, and g_m the model synthesized image. By applying known parameter perturbations on model, pose and texture, gradient matrices R_c, R_p and R_t can be estimated for model, pose and texture respectively. In our approach, we adopted the direct gradient method by Cootes *et al.* [5].

3.2.2 AAM Matching

From the current estimate of the model parameters c_0 and the parameter derivatives for the model, texture and pose parameters (matrices R_c, R_t & R_p respectively), Cootes describes an iterative matching algorithm, consisting of the following steps [2]:

1) Calculate the residual between target image and model patch $\delta g_0 = g_s - g_m$

2) Calculate the RMS error from the difference-vector $E_0 = |\delta g_0|^2$

3) Using the pre-computed gradient matrices, determine the model parameter update $\delta c = R_c \delta g_0$, pose update $\delta p = R_p \delta g_0$ and texture update $\delta t = R_t \delta g_0$

4) Set k = 1 and determine a new estimate for the model parameters $c_1 = c_0 - k\delta c$, pose parameters $p_1 = p_0 - k\delta p$ and texture parameters $t_1 = t_0 - k\delta t$

5) Calculate a new model based on c_1, p_1 & t_1

6) Determine a new difference-vector and calculate its RMS error E_1,

7) If $E_1 < E_0$, select c_1, p_1 & t_1 as the new parameter vectors, else try k = 1.5, k = 0.5, k = 0.25 etc. and go to step 4

Repeat until convergence (either using a fixed number of iterations, or until no improvement is achieved).

3.2.3 Medical Applications of AAMs

Since introduction, several successful medical applications of AAMs in medical image segmentation have been presented. Initially, Cootes has demonstrated the application of 2D AAMs on finding structures in brain MR images [2], and knee cartilage in MR images [3]. In 2D cardiac MR images, Mitchell *et al.* successfully applied AAMs to segment the left and right ventricle [6]. Thodberg [7] applied a 2D AAM to reconstruct bones in hand radiographs. Bosch *et al.* applied a 2D + time AAM to segment endocardial borders in echocardiography [8], introducing a correction method to compensate for non-Gaussian intensity distributions in echocardiographic images. Beichel *et al.* described a semi-3D AAM extension applied to the segmentation of the diaphragm dome in 3D CT data [9]. Mitchell *et al*. described a full 3D AAM extension, and applied it to 3D cardiac MR data and 2D + time echocardiograms [10].
In many of the applications mentioned here, Active Appearance Models have been shown to outperform other segmentation approaches for two reasons:

- They combine correlated intensity and shape knowledge, thus maximally integrating a priori knowledge, resulting in highly robust performance.

- They model the relationship between expert contours and underlying image data, and are therefore capable of reproducing expert contour drawing behavior.

3.3 Multi-View Active Appearance Models

The Multi-View AAM presented here is designed to exploit the existing correlation between different views of the same object. It is derived from Cootes' work on coupled view AAMs [4], where a frontal and a side view of a face are segmented simultaneously by building separate models for each view, and a combined model for both views. During matching, segmentation is performed using single view models, however shape constraints are applied from a combined model. The approach presented here differs in that the organ shape is modeled simultaneously for all views from the start, contrary to only imposing model constraints from a combined model.

The Multi-View model is constructed by aligning the training shapes for different views separately, and concatenating the aligned shape vectors x_i for each of the N views. A shape vector for N frames is defined as:

$$\mathrm{x} = \left(x_1^{\,T}, x_2^{\,T}, \ldots x_N^{\,T}\right)^T \tag{3.5}$$

By applying a PCA on the sample covariance matrix of the combined shapes, a shape model is computed for all frames simultaneously. The principal model components represent shape variations, which are intrinsically coupled for all views.

For the intensity model, the same applies: an image patch is warped on the average shape for view *i* and sampled into an intensity vector g_i, the intensity vectors for each single frame are normalized to zero mean and unit variance, and concatenated:

$$g = \left(g_1^T, g_2^T, \ldots, g_N^T\right)^T \tag{3.6}$$

Analogous to the single frame AAM, a PCA is applied to the sample covariance matrices of the concatenated intensity sample vectors, and subsequently each training sample is expressed as a set of shape- and appearance coefficients. A combined model is computed from the combined shape-intensity sample vectors. In the combined model, the shape and appearance of both views are strongly interrelated, as is illustrated in Figure 3.1.

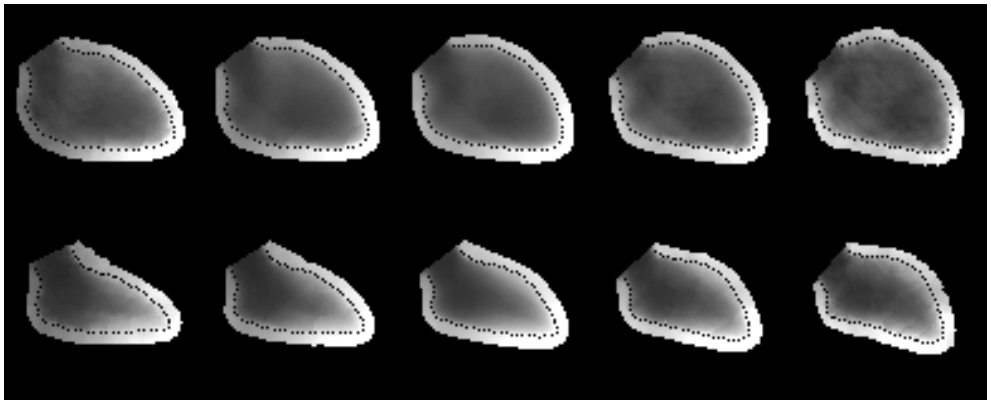

Figure 3.1: First mode of variation for a left ventricle Multi-View AAM, constructed from 70 ED-ES X-ray LV angiograms. Upper row = ED, lower row = ES. The correlation in shape between ED and ES is clearly visible. Also the texture variation, describing mainly the local contrast between the LV and it's embedding around the mitral valve, shows clear similarities for ED and ES.

Estimation of the gradient matrices for computing parameter updates during image matching is performed by applying perturbations on the model, pose, and texture parameters, and measuring their effect on the residual images. Because of the correlations between views in the model, a disturbance in an individual model parameter yields residual images in all views simultaneously. The pose parameters however, are perturbed for each view separately: the model is trained to accommodate for trivial differences in object pose in each view, whereas the shape and intensity gradients are correlated for all views.

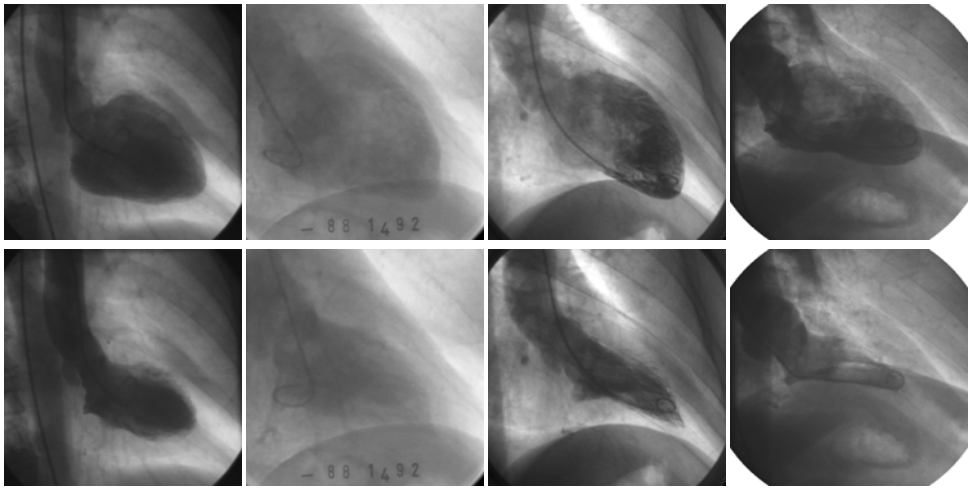

Figure 3.2: X-ray LV angiography example images for ED (upper row) and ES (lower row). From left to right: well defined LV, poor contrast, inhomogeneous distribution of the contrast agent (most apparent in ED) and presence of a diaphragm overlapping the LV.

In the matching procedure, the pose transformation for each view is also applied separately, whereas the model coefficients intrinsically influence multiple frames at a time. Hence, the allowed shape and intensity deformations are coupled for all frames, whereas pose parameter vectors for each view are optimized independently. This is a significant difference as compared to the coupled view AAMs by Cootes *et al.*, where separately trained 2D models are matched to each separate view, and subsequently only the appearance constraints are imposed from a combined appearance model [4].

3.4 Experimental Validation

To determine the clinical utility of the Multi-View AAMs, we investigated two issues:

- To what extent can information from different frames improve overall segmentation performance. To address this, we have tested the Multi-View AAM on X-ray left ventricular angiography images in the ED and ES phase. Though other segmentation methods for LV angiograms have been reported [11,12], these images are notoriously difficult to segment, especially the ES phase. This is mainly due to the fact that in ES a large amount of the contrast agent has already been ejected, therefore border definition of the ventricle is rather poor. For this modality, we expect that the better LV shape definition in ED frames improves the segmentation of ES frames.

- The potential of the Multi-View AAM to segment substantially different geometrical shapes in multiple views. To evaluate this, we selected a combination of cardiac MR short-axis and long-axis views. To our knowledge, this is the first report of an automatic contour detection for endo- and epicardial contours in long-axis cardiac MR views.

3.4.1 X-Ray LV Angiography

The effectiveness of the Multi-View AAM was tested on ED-ES pairs of clinically representative LV angiograms from 70 infarct patients, 140 images in total. Apart from high quality images with good LV definition in both ED and ES, images were selected, in which frequently appearing acquisition artifacts were present (poor LV contrast, inhomogeneous distribution of the contrast agent, presence of a diaphragm overlapping the LV). Figure 3.2 shows representative examples.
An expert manually defined contours in both frames, and point correspondence was defined based on three prominent landmarks: both aortic valve points and the apex. Every contour was equidistantly resampled to 60 points. 14 leave-five-out models were trained on 65 out of 70 ED-ES image pairs, leaving out 5 sets for testing purposes. To speed up the training and matching process and to reduce model dimensionality, all images were subsampled by a factor of 4.

3.4.2 Cardiac MRI

To assess the performance of the Multi-View AAM method for simultaneous segmentation of several different cardiac views with a different geometric definition, the method was evaluated on a commonly acquired combination of cardiac MR views. Usually, during acquisition of a routine cardiac MR patient exam, a two chamber view, a four chamber view and a short-axis stack are acquired following strictly defined acquisition protocols, allowing an optimal depiction of LV anatomy. Following this protocol, image data was acquired from 29 patients with various cardiac pathologies.
The Multi-View AAM was constructed based on the ED two chamber view, the ED four chamber view and the ED mid-ventricular short-axis slice. Endo- and epicardial contours were drawn manually by an expert observer in all views. To maximize the amount of evaluation data, validation and training was performed using a leave-one-out approach. The initial position for the model matching was manually set by indicating the apex and base in the long-axis views, and the LV midpoint in the short-axis views.

3.4.3 Evaluation Method

Matching results for each patient study were first qualitatively scored to three categories: matching success for all views, failure in one view and failure in more than one view. Failures were reported and excluded from quantitative evaluation.

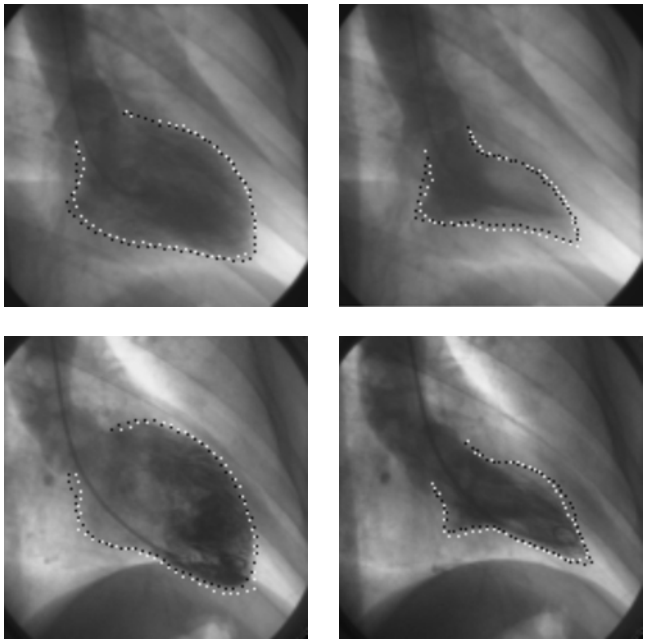

Figure 3.3: Two successful matches for ED (left) and ES (right). Black dotted lines denote the manual contours, white dotted lines represent the model contours. Note that even with inhomogeneous contrast agent distribution (ES image top, ED image below), contours are accurately determined.

On the successful matches, quantitative comparison with expert contours was performed on:

- point-to-curve border positioning errors for the contours as compared to the manually defined expert contours, calculated separately for each view.
- endocardial contour area for each frame separately.
- for the LV angio application, area ejection fraction.

Linear regression was used to determine relationships between manually traced and computer determined values. A two-tailed paired samples t-test was applied to area measurements from automatic and manual contours to investigate systematic errors. A p-value smaller than 0.05 was considered significant.

3.4.4 Results

For the LV angiographic study, the Multi-View AAM yielded borders that agreed closely with the expert defined outlines in both ED and ES in 56 out of 70 patients. In 10 cases, partial failure was observed, where the contour in one frame clearly failed. In 4 cases, neither ED nor ES contours were correctly detected. In total, 122

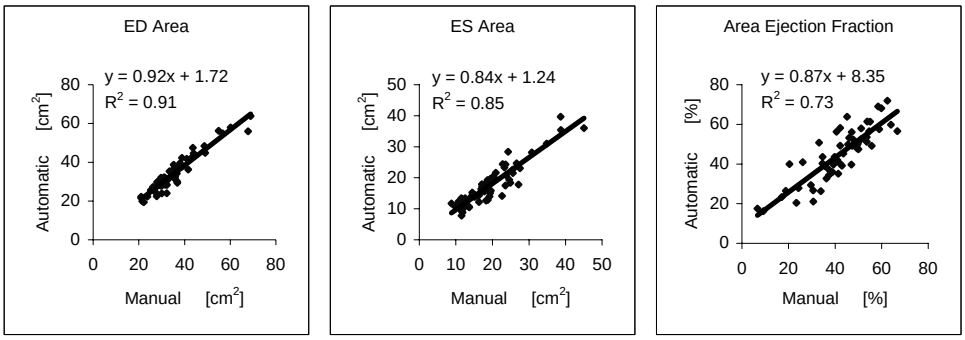

Figure 3.4: Area regression plots for ED (left) and ES (middle) and area ejection fraction (right).

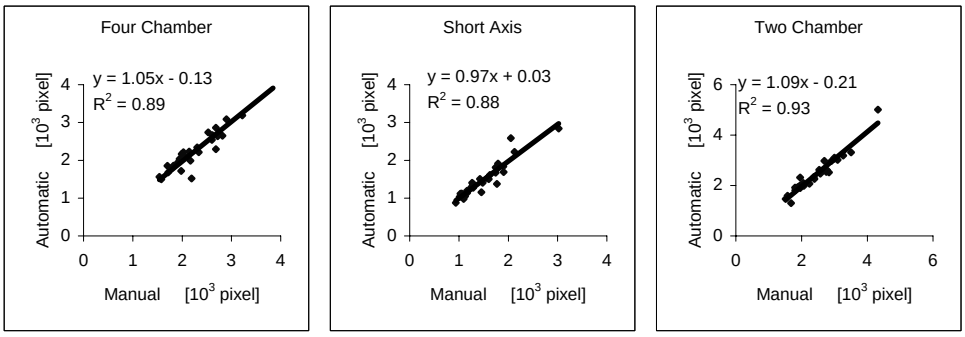

Figure 3.5: Area regression plots for four chamber (left), short-axis (middle) and two chamber (right) cardiac MR views.

	Border positioning errors [pixels]
MRI 2 Chamber	1.7 ± 0.8
MRI 4 Chamber	1.5 ± 0.7
MRI Short axis	1.4 ± 0.7
LV angio ED	6.5 ± 2.8
LV angio ES	8.0 ± 3.7

Table 3.1: Point-to-curve border positioning errors in pixels for the cardiac MR and LV angiography validation studies.

out of 140 images (87%) were successfully segmented, whereas in the other 18 images, manual interaction was required.

In general, for the successful matches, contours showed an excellent agreement with the manually defined contours, even in compelling images with artifacts such as LV-diaphragm overlap, and partial filling. In Figure 3.3, two representative examples of automatically detected contours are given. Border position errors were generally small, and are given in Table 3.1. Area and ejection fraction regressions are given in Figure 3.4. In both ED and ES phases, area errors were slightly, but statistically significantly underestimated ($p<0.001$, relative error for ED 3.5%, for ES 9.4%). The area ejection fraction was slightly overestimated (relative error 7%, $p=0.003$).

The cardiac MR validation yielded 27 successful matches out of 29, and in 2 cases partial failure was observed, where the model drifted away from the LV boundaries in one of the three views. No total failures occurred. Examples of automatically detected contours in the cardiac MR views are given in Figure 3.6. For the contours from successful matches (87 out of 89 images in total, 98%), area correlations between manually and automatically detected contours are given in Figure 3.5, and border positioning errors in Table 3.1. In a paired samples t-test, differences between manually and automatically determined endocardial contour areas were found statistically insignificant for all three views ($p>0.7$ for all views).

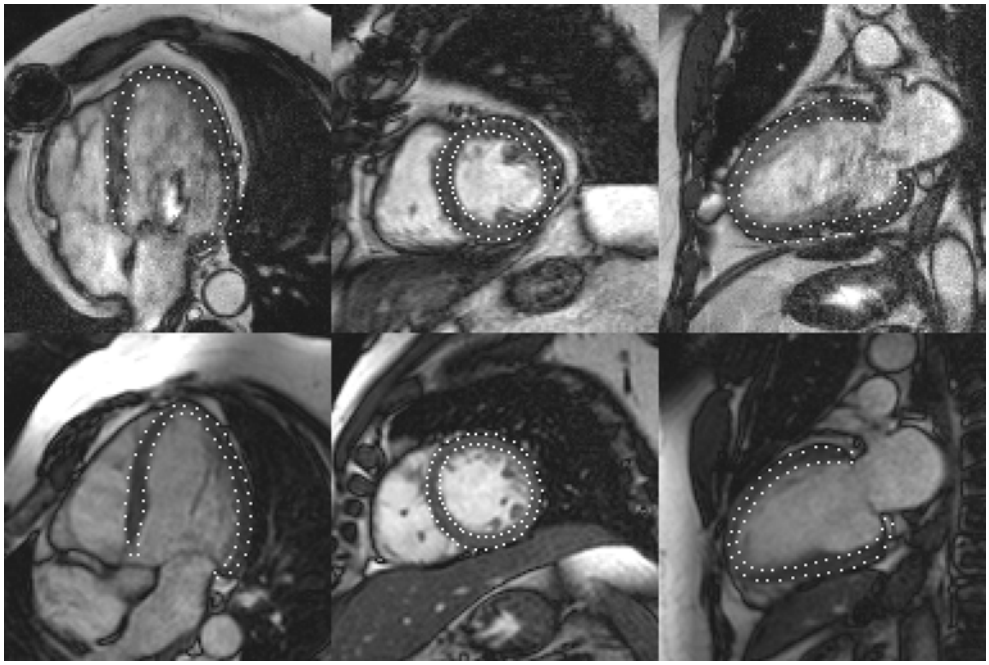

Figure 3.6: Automatically detected contours (white dotted lines) for two patients (top and bottom row) in a four chamber (left), short-axis (middle) and two chamber view.

3.5 Discussion and Conclusions

In general, the presented Multi-View AAM yielded good results in two challenging clinical segmentation problems. Contours were detected with a minimal user interaction to initially position the model, and showed high agreement with manually defined contours. Especially in ES LV angiograms, segmentation results were very good compared to other segmentation methods reported for this modality [11,12]. This good performance in ES images can mainly be attributed to the coupling of information from both ED and ES.

In LV angiography, a success rate of 87% was achieved. Matching failure mainly occurred in cases where contrast was extremely low, when there was a significant overlap between the LV and the diaphragm or in cases of large dilated areas near the apex, as is illustrated in Figure 3.7.

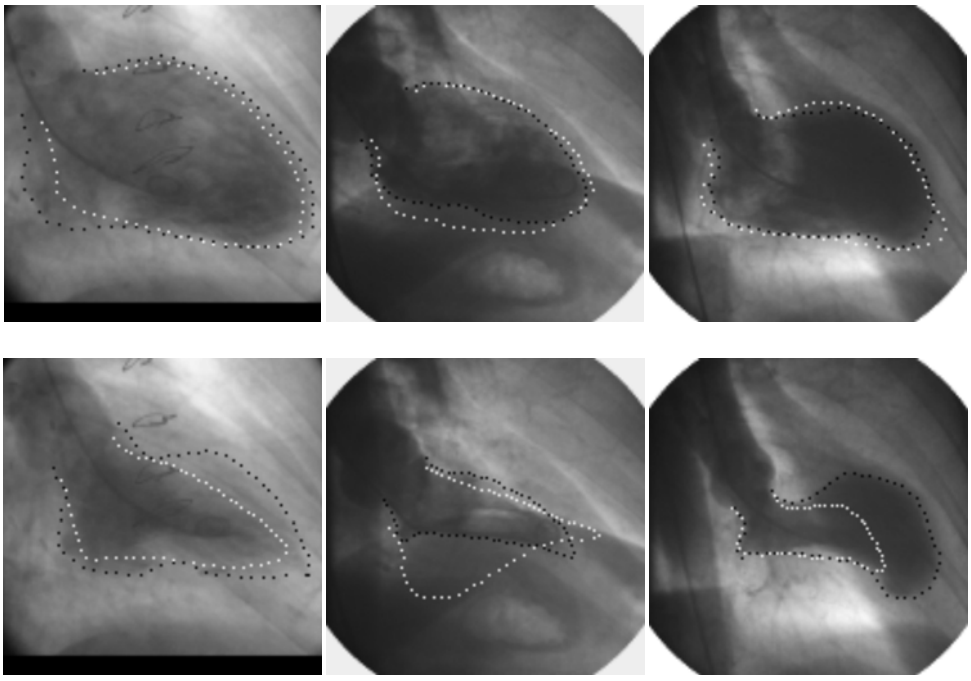

Figure 3.7: Examples of segmentation failures for ED (upper row) and ES (lower row), due to poor contrast (left), overlap between LV and diaphragm (middle) and large dilated areas near the apex (right). The black dotted lines denote the manual contours, the white dotted lines represent the model contours.

Comparison between manually and automatically derived area measurements showed a good correlation, though a slight underestimation of LV area in both ED and ES was present. This underestimation is mainly caused by the lack of dynamic information: a manual observer draws the contours in ED and ES after reviewing

the whole dynamic sequence, whereas automatically generated borders are only based on ED and ES views. When manually examining an entire image run, this motion is used to decide on the border location of the ventricle, especially in "problem areas"; therefore the manual borders are generally drawn slightly wider around the ventricle than visually apparent in only ED and ES. Also, since interpretation and contour drawing in LV angiograms is highly subjective, an assessment of intra- and inter-observer variation inherent to manual contour drawing is ongoing, to compare the accuracy and reproducibility of the automated method for different experts.

The cardiac MR study showed a significantly higher success rate than the LV angiography study: in 98% of the images, a successful match was achieved. This can mainly be attributed to the better definition of the ventricle in cardiac MR views. Though acquisition related artifacts were present in some patient studies (surface coil intensity gradients), overall LV endo- and epicardial contour definition is significantly stronger in the cardiac MR study. Area calculations, which serve as a basis for LV volume estimates, did not differ statistically significantly between manual and automatic analysis. Also for this application, border positioning errors were small (comparable to errors reported in [6]), and well within clinically acceptable margins.

In this study we have tested the Multi-View AAM robustness and performance from a manually set initial position, yielding good results. However, we foresee a further increase in robustness by also coupling the scale of the object in all views, since this is correlated as well between views. This is a topic of current research. Moreover, future research will focus on analysis of Multi-View AAM shape parameters to distinguish between pathologies. We expect the coupling of shape information from different parts of a patient examination to enhance pathology identification. For cardiac MR, methods to automatically position the initial models based on a geometrical thorax template model [13] will be investigated.

In summary, we conclude that the Multi-View AAM presented here combines a high robustness with clinically acceptable accuracy. It demonstrated good automatic segmentation results for two substantially different and novel clinical applications. A cardiac MR case study showed the utility to simultaneously segment different geometrical shapes, and a case study on X-ray LV angiography proving that poor ventricle definition in one view (ES) can be resolved by information from a corresponding (ED) view.

References

[1] T. F. Cootes, G. J. Edwards, and C. J. Taylor, "Active appearance models," *Proceedings of the European Conference on Computer Vision*, H. Burkhardt and B. Neumann, Eds., vol. 2, Berlin: Springer Verlag, 1998, pp. 484-498.

[2] T. F. Cootes, C. Beeston, G. J. Edwards, and C. J. Taylor, “A Unified Framework for Atlas Matching Using Active Appearance Models,” *Proceedings of Information Processing in Medical Imaging*, Kuba, Samal and Todd-Pokropek, Eds, vol. 1613, pp. 322-333, 1999.

[3] T. F. Cootes and C. J. Taylor, “Statistical models of appearance for computer vision,” Online available: *http://personalpages.manchester.ac.uk/staff/timothy.f.cootes/Models/app_models.pdf*

[4] T.F. Cootes, G.V. Wheeler, K.N. Walker, C.J. Taylor, “View-based active appearance models,” *Image and Vision Computing*, vol. 20, no. 9-10, pp. 657-664, 2002.

[5] T.F.Cootes, P.Kittipanya-ngam, “Comparing Variations on the Active Appearance Model Algorithm,” *Proceedings of British Machine Vision Confererence*, vol.2, pp. 837-846, 2002.

[6] S. C. Mitchell, B. P. F. Lelieveldt, R. J. Van der Geest, H. G. Bosch, J. H. C. Reiber, and M. Sonka, “Multistage hybrid active appearance model matching: segmentation of left and right ventricles in cardiac MR images,” *IEEE Transactions on Medical Imaging*, vol. 20, no. 5, pp. 415-423, 2001.

[7] H.H. Thodberg, “Hands on Experience with Active Appearance Models,” *Proceedings of SPIE Medical Imaging*, vol. 4684, pp. 495-506, 2002.

[8] J. G. Bosch, S. C. Mitchell, B. P. F. Lelieveldt, F. Nijland, O. Kamp, M. Sonka, and J. H. C. Reiber, “Automatic segmentation of echocardiographic sequences by active appearance motion models,” *IEEE Transactions on Medical Imaging*, vol. 21, no. 11, pp. 1374-1383, 2002.

[9] R. Beichel, G. Gotschuli, E. Sorantin, F. Leberl, M. Sonka, “Diaphragm Dome Surface Segmentation in CT Data Sets: A 3D Active Appearance Model Approach,” *Proceedings of SPIE Medical Imaging*, vol. 4684, pp. 475-484, 2002.

[10] S.C. Mitchell, J.G. Bosch, B.P.F. Lelieveldt, R.J. van der Geest, J.H.C. Reiber, M. Sonka, “3D Active Appearance Models: Segmentation of Cardiac MR and Ultrasound images,” *IEEE Transactions on Medical Imaging*, vol. 21, no. 9, pp. 1167-1178, 2002.

[11] S. Tehrani, T. E. Weymouth, and G. B. J. Mancini, “Model generation and partial matching of left ventricular boundaries,” *Proceedings of SPIE Medical Imaging*, vol. 1445, pp. 434-445, 1991.

[12] P. Lilly, J. Jenkins, and P. Bourdillon, “Automatic contour definition on left ventriculograms by image evidence and a multiple template-based model,” *IEEE Transactions on Medical Imaging*, vol. 8, no. 2, pp. 173-185, 1989.

[13] B. P. F. Lelieveldt, M. Sonka, L. Bolinger, T. D. Scholz, H. W. M. Kayser, R. J. van der Geest, and J. H. C. Reiber, “Anatomical Modeling with Fuzzy Implicit Surface Templates: Application to Automated Localization of the Heart and Lungs in Thoracic MR Volumes.” *Computer Vision and Image Understanding*, vol. 80, pp. 1-20, 2000.

好奇心
'curiosity'

Chapter 4

The Effect of the Composition of the Training Set

This chapter was adapted from:
Automated Contour Detection in Cardiac MRI Using Active Appearance Models: The Effect of the Composition of the Training Set
E. Angelié, E.R. Oost, D. Hendriksen, B.P.F. Lelieveldt, R.J. van der Geest, and J.H.C. Reiber
Investigative Radiology, vol. 42, no. 10, pp. 697-703, 2007.

Abstract

This chapter aims to define the characteristics of an optimal training set for the automated segmentation of short-axis left ventricular magnetic resonance (MR) images in clinical practice, using an Active Appearance Model (AAM). We investigated the segmentation accuracy by varying the size and composition of the training set (i.e., the ratio between pathologic and normal ventricle images, and the vendor dependence). The accuracy was assessed using the degree of similarity and the difference in ejection fraction between automatically detected and manually drawn contours. Including more images in the training set results in a better accuracy of the detected contours, with optimum results achieved when including 200 to 250 images. Using AAM-based contour detection with a mixed model of 80% normal and 20% pathologic cases provides good segmentation accuracy in clinical routine. Finally, this work shows that it is essential to define different AAM models for images from different MRI systems. A model defined on a sufficient number of images with the correct distribution of image characteristics achieves good results in clinical routine.

4.1 Introduction

Cardiac magnetic resonance (MR) imaging is playing an increasingly important role in anatomic and functional assessment of the cardiovascular system. An accurate delineation of the endocardial (endo) and epicardial (epi) boundaries is important to quantify left ventricular (LV) function. Manual segmentation requires expert knowledge and is a time-consuming procedure, which limits the routine clinical use of cardiovascular MR. Moreover, manual segmentation is observer-dependent and therefore is associated with considerable inter- and intra-observer variability [1]. Various automated contour detection techniques have been developed to overcome the disadvantages of manual contour drawing, but clinically available systems still require too much user-interaction.

An automated contour detection method should incorporate a priori knowledge, including information about the cardiac shape as well as information about the image characteristics, which depend on the pulse sequence and the MR hardware used (MR vendors, coils, etc). The widely recognized effectiveness of statistical models stems from their ability to segment images of anatomic structures by exploiting constraints derived from the image data together with a priori knowledge about the location, size, and shape of the structures of interest. These constraints are derived from training data using manually drawn contours. Active Appearance Models have been introduced as a powerful technique for modeling images of anatomic objects and has been successfully used in a variety of automated medical image segmentation applications [2-4].

The AAM segmentation procedure consists of 2 different phases, a training phase and a matching phase:

- For training an AAM, a data set of manually annotated example images is used in which all expert drawn contours should have the same point distribution. Using principal component analysis (PCA) a statistical model is constructed, representing the observed shape variations in the training data. After extracting a shape-free pixel intensity patch for all example images, PCA is applied on these texture vectors, resulting in a model describing the observed pixel intensity variations. Concatenation of both statistical models and another PCA results in an AAM. Additionally, this model learns the relationship between model parameters and the residual errors, induced by known perturbations on single model parameters.

- The matching (detection) phase attempts to find the best fit of the model to the data in a new image. Matching to an image involves finding the model and pose parameters, which minimize the difference between the image and a synthesized model example, projected onto the image.

An elaborate description of model training and matching can be found in [2] and [5]. Despite promising preliminary results in cardiovascular MR [6-9], the validation and definition of optimal settings of such an algorithm are still very challenging. Whereas in the cardiac MR case, large variations in shape characteristics are seen due to the spectrum of pathologies [10], the assessment of the current segmentation techniques remains still narrowed on image data sets obtained from healthy subjects and/or small populations of images [1,5,8,11]. Moreover, in clinical practice a wide range of acquisition protocols coexists, resulting in MR images with large texture variations [12,13]. The evaluation of AAM-based techniques has not yet provided conclusions on the definition of the optimal constitution of the training set. For instance, it has not been studied whether image data from multiple pathologies should be used to define a model, or whether image data from different vendors should be included in a single model, or vendor-specific models should be used.

Therefore, the purpose of this study was to define the composition of the training data set, from which an AAM is constructed that performs optimally in clinical practice. This model should provide good segmentation results for images acquired by scanners of any vendor, it should be able to cope with the entire range of relevant pathologies as seen in short-axis MR examinations, and it should be able to deal with possible poor image quality, induced either by acquisition or by pathology. Three different questions were addressed in this work:

- What is the optimal number of images to be included in the training set?

- What is the optimal mixture of images from healthy and pathologic cases in the training set?

- Is it necessary to construct separate models for different vendors, or is it sufficient to construct a model based on data from multiple vendors?

4.2 Materials and Methods

4.2.1 Study Population

Clinical short-axis MR imaging studies were obtained from 8 institutions using MR equipment from 3 different MR vendors. All examinations were performed using a steady-state free-precession (SSFP, 256 x 256 field of view) imaging protocol on a 1.5 Tesla MR system. The inclusion of data from different institutions guarantees sufficient wide range of variation in imaging protocols and patient population. MR images of 207 LV short-axis examinations (105 from vendor 1, 35 from vendor 2, and 67 from vendor 3) formed the database we used in this study. To differentiate between normal and pathologic cases, we used the criteria proposed by Rominger *et al.* [14], defining an ejection fraction (EF) between 54% and 75% combined with an LV mass between 79 and 137 gram, as normal [15]. The histograms presented in Figure 4.1 illustrate the distribution of EF and LV mass of the population studied. Following these criteria, 98 subjects were considered normal and 109 pathologic.

4.2.2 Slice Labeling and Manual Contour Tracking

Endocardial and epicardial contours were manually traced in the end-diastolic (ED) and end-systolic (ES) phases excluding papillary muscle and trabeculations from the myocardial wall. A reference point was placed in each image at the posterior junction of the right ventricle free wall with the septum, which was used to establish registration between images. For the AAM experiments the images at the most basal and most apical slice level were excluded to avoid extreme shape and texture variations in the AAM model.

4.2.3 Assessment of the Segmentation Quality

To evaluate the quality of the AAM image segmentation, 2 different metrics were used: the degree of similarity and the EF calculation. The degree of similarity is defined as the percentage of points that is similar between 2 contours [16]:

$$S = \frac{\sum_{n=0}^{N} p_n(d)}{N} \quad where\ p_n(d) = \begin{cases} 1 & if \quad d \le T \\ 0 & if \quad d > T \end{cases} \tag{4.1}$$

where d is the distance between each pair of corresponding points on the manually drawn contour and the automatically detected contour, N is the number of sample points per contour (N = 25 for the presented experiments), and T is a distance threshold [17]. Pairs of corresponding points are assumed to be similar if the distance does not exceed a certain threshold value T (For the presented experiments T was set to T = 2 mm).

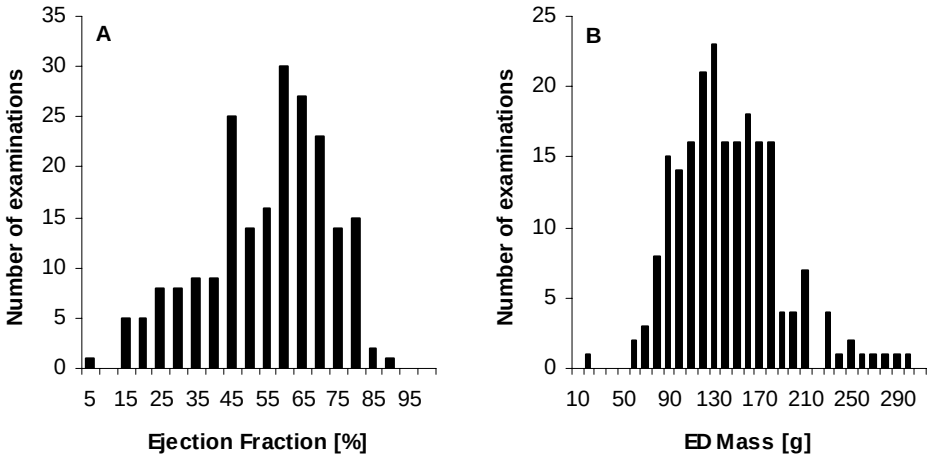

Figure 4.1: Histograms related to the population of MR examinations included in this study. Figure A displays the ejection fraction distribution in the study population. Figure B displays the distribution of ED mass within the study population. These 2 graphs illustrate that the study population contains sufficiently different image characteristics to give a proper representation of the data seen in clinical routine.

The ejection fraction is an important clinical parameter. Evaluation of the difference between the manually derived EF and the automatically derived EF should indicate the clinical relevance of the contour detection using AAMs [18].

4.2.4 Inter-Observer Study

To rate the quality and clinical relevance of the automatic segmentation results obtained by the AAM, we produced inter-observer variability measures based on manual image analysis for comparison. Two observers independently segmented 24 randomly chosen MR examinations manually (50% pathologic and 50% normal, distributed equally between different vendors). The difference in EF and in degree of similarity were computed using only the contours in the ED and ES phase, and slices comprising the section between apex and base. These differences were used as a gold standard in the following studies, presenting the results in a more clinical context.

4.2.5 Optimal Number of Training Images

This study aims at the assessment of the minimal number of data needed to train a model to give good segmentation results. The 2D AAM algorithm used a model shape defined on 25 points equidistantly sampled for both the epicardial and endocardial contours. Ninety-nine percent of variation in shape, texture, and appearance were kept in the defined models to guarantee a proper description of

the variation observed in the training data set [4]. A stepwise increase (from 23 to 298) of the number of randomly chosen training data from a set of normal examinations from a single type of MR scanner was used to define different models that were used to automatically segment an independent set of 194 images with similar characteristics. We analyzed the measurements using a regression analysis.

4.2.6 Impact of the Normal versus Pathologic Ratio

In clinical practice, shape characteristics vary mainly with the pathologies. Therefore, in this study we analyzed the impact on the accuracy of the segmentation when varying the distribution between pathologic (P) and normal (N) examinations in the training data. A fixed number of 180 images were included in the training set, which approximates the number that was defined by the outcome of the previous experiment. Three experiments were realized. The first one consisted of defining a model on a 50% N – 50% P distribution training data. The accuracy of segmentation using such a model was tested on 3 different matching sets (one described with a 50% N – 50% P distribution, the other with a 80% N – 20% P distribution, and the last with a 20% N – 80% P distribution). The second and third experiments consisted of repeating the first experiment with models defined on a 80% N – 20% P and 20% N – 80% P distribution training set, respectively.

4.2.7 Impact of the Distribution of Acquisition Systems

The main cause of texture variation can be attributed to the MR system or to the pulse sequence used [19,20]. Therefore, we also studied the impact on the segmentation accuracy of including images from different vendors in the training set. We created 4 different models: 3 were vendor specific and 1 was created on a mixed population. We performed the automatic segmentation on different sets of images corresponding to different vendors. The “mixed model” was trained on a population of images where all 3 vendors were equally represented. Based on the limited availability of MR images, the models were trained on a set of 76 images defined using 50% N and 50% P examinations and matched on an independent set of 76 images showing the same image characteristics.

4.3 Results

4.3.1 Inter-Observer Study

The inter-observer variability in EF, based on manual contour tracing, was 4.5% ± 2.8%, which is in agreement with previously published results [21]. The degree of similarity between contours drawn by the 2 experts is summarized in Table 4.1. These values will be used as reference values for the degree of similarity and EF.

	ED epi	ED endo	ES epi	ES endo
Degree of Similarity	84 %	84 %	81 %	74 %

Table 4.1: Inter-observer variability in the degree of similarity between two observers.

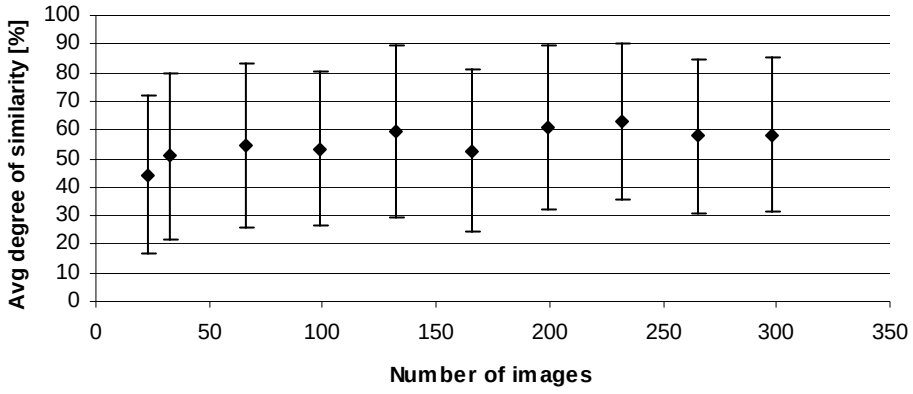

Figure 4.2: Influence of the number of images included in the training on the averaged degree of similarity (Averaged over results for the ED and ES phases, for the endo and epicardial contours).

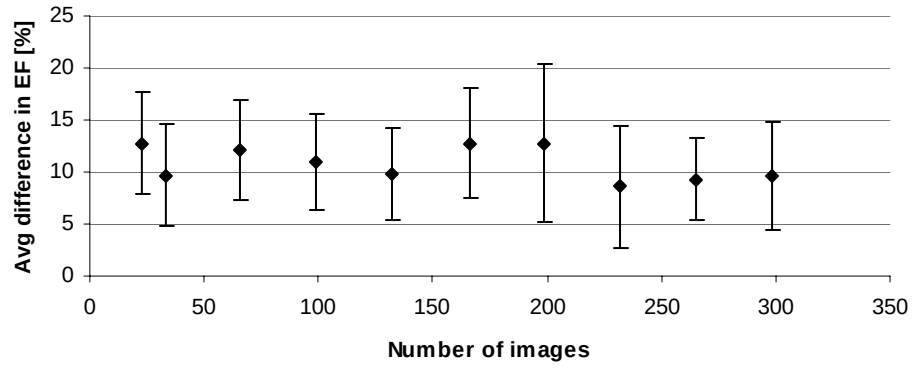

Figure 4.3: Average difference between and standard deviation of the EF calculated using the automatically and manually drawn contours versus the number of images in the training set.

4.3.2 Optimal Number of Training Images

Figures 4.2 and 4.3 illustrate how the quality of AAM contour detection is influenced by the number of images included in the training set. As expected, the

degree of similarity significantly increases with an increasing number of images in the training set ($P < 0.05$ in all the regressions except the variation in ED endocardial contours). The best estimation from Figures 4.2 and 4.3 of the minimal number of images to be included in the training set was around 200 to 250 images. This was supported by the data given in Table 4.2, which shows optimal values for ED at 199 training images and for ES at 232 training images, while including more training images results in only marginally different values. Table 4.2 also points out that the accuracy of the endo contour segmentation is better than the one of the epi contour segmentation and that the quality of the automated segmentation is better for ED than for ES images. In agreement with these observations, Figure 4.3 shows a slight but non-significant ($P = 0.72$) decrease in the deviation in EF with the increase in the number of images in the training set.

	ED Phase		ES Phase		Average
nr of images	endo	epi	endo	epi	
23	74.26	51.03	35.69	16.53	44.38
33	67.59	56.35	44.32	34.75	50.75
66	72.64	62.35	46.22	36.68	54.47
99	71.99	59.14	45.02	36.52	53.17
132	76.91	66.43	50.45	44.56	59.59
166	70.42	60.26	43.92	36.35	52.74
199	79.88	71.35	50.59	42.12	60.99
232	78.05	70.99	55.05	47.54	62.91
265	70.71	63.05	51.75	45.7	57.80
298	76.59	67.6	47.59	41.09	58.22

Table 4.2: Influence of number of images included in the training set on the degree of similarity for the endocardial and epicardial contours in the ED and ES phases.

4.3.3 Impact of the Normal versus Pathologic Ratio

Figures 4.4 and 4.5 display the impact of using a model defined on a set of images for the automatic segmentation of images with different characteristics. Figure 4.4 shows that the highest segmentation accuracy is obtained using the 80% N – 20% P model regardless of the segmentation population. The overall best average degree of similarity was observed when applying the 80% N – 20% P model to 80% N – 20% P data. Similarly, Figure 4.5 shows that the minimum difference between EF is obtained when using a model that describe a mixed population of 80% normals and 20% patient studies.

4.3.4 Impact of the Distribution of Acquisition Systems

Tables 4.3 and 4.4 illustrate the impact of using models from different scanners on the accuracy of the segmentation. In particular, this study demonstrates that the highest accuracy of segmentation (70% in the ED phase and 50% in the ES phase) is obtained using a model defined on a population with the same texture characteristics as the matching population of image. In terms of segmentation performance, a mixed model resulted in lower accuracies (maximally 54% in ED phase and 41% in ES phase). These observations were convincing for vendor 1 and vendor 2 data, however, considerably lower degrees of similarity were found for vendor 3 data, in which rather poor image quality was observed.

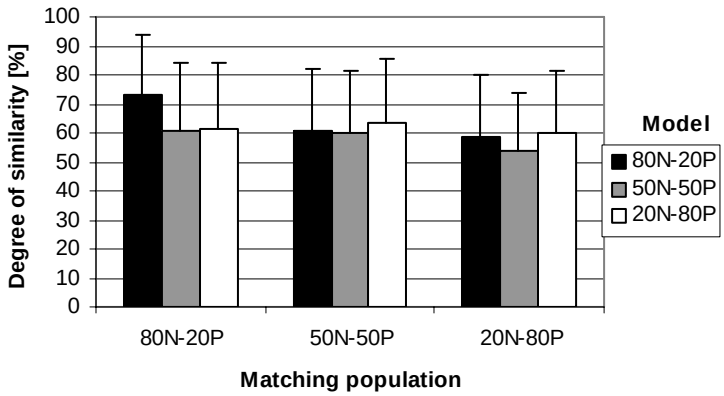

Figure 4.4: Average degree of similarity between automated segmentation results and manually defined gold standard (ED and ES phase, endocardial and epicardial contour) when using different models on different matching populations.

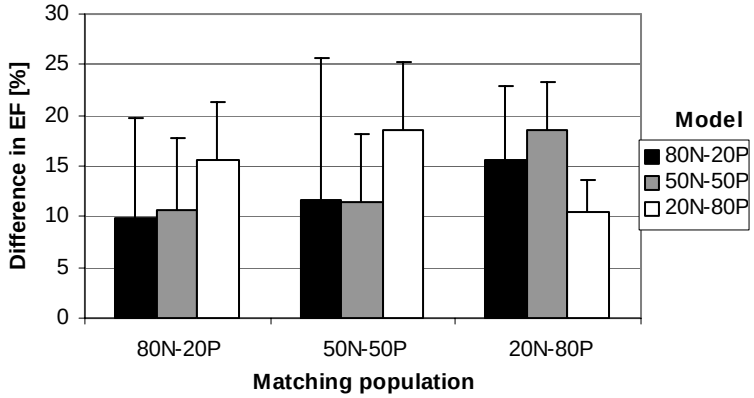

Figure 4.5: Average difference in ejection fraction between automatically detected and manually drawn contours when using different models on different matching populations.

ED degree of similarity	Matching population		
Model	Vendor-1	Vendor-2	Vendor-3
Vendor-1	70±27	57±28	43±28
Vendor-2	60±28	58±33	39±31
Vendor-3	52±22	44±21	34±26
Mixed	54±29	50±29	50±29
Vendor - Mixed	16%	8%	-16%

Table 4.3: Average degree of similarity (%) and standard deviation observed in the segmentation of the ED phase using models trained on images from different vendors. The segmentation accuracy is lower when vendor 3 images/model are concerned.

ES degree of similarity	Matching population		
Model	Vendor-1	Vendor-2	Vendor-3
Vendor-1	50±31	34±30	22±32
Vendor-2	43±29	42±33	21±31
Vendor-3	40±31	26±30	15±30
Mixed	41±30	32±30	27±27
Vendor - Mixed	9%	10%	-12%

Table 4.4: Average degree of similarity (%) and standard deviation observed in the segmentation of the ES phase using models trained on images from different vendors. The segmentation accuracy is lower when vendor 3 images/model are concerned.

4.4 Discussion

Domain knowledge about the geometrical properties of cardiac structures is an important feature for segmentation in medical images. So far, a strong focus was put on the development of new segmentation methods using statistical models. By fitting a model to image data, cardiac surface positions can be predicted with a high accuracy [6,8,20,22,23]. Potentially such a model can be used to automate a large range of diagnostic and therapeutic applications in cardiac medicine [24]. For the application of such a model in the context of automatic segmentation of cardiac image data, practical issues need to be addressed. The goal of this study was to analyze whether AAM-based segmentation could be used in clinical routine. For this, we analyzed the impact of the definition of the training set on the accuracy of the automatic segmentation.

4.4.1 Optimal Number of Training Images

When comparing a model that was trained on 23 images with a model that was trained on approximately tenfold more data, an improvement of the degree of similarity of 6% and 20% could be observed for ED endo en ED epi (both at n=199), respectively. Similar experiments resulted in an increase of the degree of similarity of 19% for ES endo and 31% for ES epi (both at n=232), respectively. This indicates that increasing the number of data included in the training set improves the AAM contour detection. Given that including even more images (n > 199 for ED, n > 232 for ES) does not substantially improve or deteriorate the degree of similarity, a minimal amount of training data should be determined at approximately 200 to 250 images. This is supported by the results for the difference in ejection fraction (Figure 4.3), showing the best results for the three models with the highest amount of training images (n=232, n=265 and n=298).

In addition, the accuracy measured with the degree of similarity in the endo contour detection is higher than in the epi contour detection. This could be explained by the intensity gradient between external tissue and the myocardial wall being weaker than the gradient between the blood pool and the myocardial wall. Thus, the border of the endo contour has a clearer definition, and as a consequence is delineated more robustly than the epi border. The promising endo contour detection results suggest that the presence of papillary muscles or trabeculations does not affect the performance of the AAM. This was supported by visual inspection. Furthermore, the non-significant variation in the degree of similarity measured in the endo contour detection showed that the endo contour detection is less dependent on the number of images included in the training set than the epi contour detection.

The measurement in this study displayed significant increase in the degree of similarity with the number of images defining the model and non-significant decrease in the difference in EF between automatically detected and ground truth contours. From this, we conclude that including numerous images in the training set to define the AAM's model does not matter when the clinical study focuses only on EF measurements, whereas it does have a big impact when analyzing border displacement measurements (wall thickness measurement).

The design of analyzing the optimal number of images to be included in an AAM had some limitations. To facilitate the process of training a model, we narrowed the analysis to only examination of healthy ventricles in the training set. Thus, we limited the variation in LV shape, and possibly artificially reduced the minimally required number of images. This experiment stressed that an AAM model can be described using at least 200 to 250 images from normal examinations, and we expect that more images should be included in the training set for covering all shape change variations in routine clinical practice.

4.4.2 Impact of the Normal versus Pathologic Ratio

A difference in degree of similarity up to 15% was noticed when matching a model describing a particular shape variation on images with different characteristics, and

matching a model defined on the same image characteristics. This experiment stressed the importance of using a suitable model for a population of images used. The accuracy seemed to be reduced when using an equally mixed model.
Although there is a significant improvement of the accuracy of the contour detection when optimizing the population distribution in the training set, the difference in EF measurements (10%) still remained high compared with the inter-observer variability (4.5%). The results show a noticeable discrepancy between EF calculated from detected contours and from reference contours, which can be the consequence of either an average poor detection or the presence of few contour outliers. In fact, the EF is sensitive to a single contour detection failure for a single image, whereas the degree of similarity measurement still remains high. The high degree of similarity of the corresponding contours (~70%) associated with a standard deviation (~20%) leads to the conclusion that the presence of few outliers or detection failure did not affect the degree of similarity because of the larger number of samples included in this measure compared with the EF quantification quantity (the degree of similarity relies on the number of contour data, whereas the EF relies on the number of examinations).
Regarding short-axis MR segmentation, using a model of 80% normals and 20% patients appeared to be the best choice.

4.4.3 Impact of the Distribution of Acquisition Systems

Several inherent problems appear in cardiac MR image segmentation. The change in image contrast [20], the non-uniform nature of the MR signal intensity introduced by noise, physiological factors, and non-uniform radio frequency fields [19] are major challenges when designing and implementing a reliable automated contour detection algorithm.
It was observed that the data from vendor 3 was of relatively poor image quality, mainly due to radio frequency pulse inhomogeneity artifacts. It is expected that Active Appearance Models in which vendor 3 training data was incorporated, were possibly deteriorated. When mutually comparing the results for vendor 1 and vendor 2, it is proven that vendor specific models provide better results than when, for example, a vendor 2 model is used to analyze vendor 1 data, or vice versa. Differences in performance can amount to 10% degree of similarity.
Given the poor image quality of the vendor 3 data, it is difficult to assess the performance of the mixed model. However, averaging the values in the bottom rows of Tables 4.3 and 4.4, results in a positive score for the vendor specific Active Appearance Model results. These findings, combined with the results of the mutual comparison of vendor 1 and vendor 2, shows the need for the application of vendor specific AAMs in clinical practice. In general, poor quality images should evidently not be incorporated in the training data set of an Active Appearance Model.
Due to the availability of image data, this study was designed on only 76 MR images as a training set. Therefore, the overall performance in terms of degree of similarity values is lower than the values reported in the other two experiments. These findings are in correspondence with the results presented in section 4.3.2 and discussed in section 4.4.1.

4.5 Conclusions

It was demonstrated that AAM-based contour detection can be used in cardiac MR imaging studies in clinical practice. Defining an appropriate training set of at least 200 to 250 data sets is a crucial step towards obtaining high quality results of the AAM-based segmentation. Furthermore, the best training set distribution of images from normal and pathologic ventricles seems to be 80–20%. Finally, in case MR scanners from multiple vendors are used, it is essential to define different models for each of the vendors. The inclusion of low quality images in the training set should be avoided.

References

[1] C. Corsi, C. Lamberti, A. Sarti, G. Saracino, T. Shiota, and J. D. Thomas, "A semi-automatic method for left ventricle volume estimate: an in vivo validation study," *Computers in Cardiology*, vol. 28, pp. 109-112, 2001.

[2] T. F. Cootes, G. J. Edwards, and C. J. Taylor, "Active appearance models," *Proceedings of the European Conference on Computer Vision*, H. Burkhardt and B. Neumann, Eds., vol. 2, Berlin: Springer Verlag, 1998, pp. 484-498.

[3] E. Oost, G. Koning, M. Sonka, P. V. Oemrawsingh, J. H. C. Reiber, and B.P.F. Lelieveldt, "Automated contour detection in X-ray left ventricular angiograms using multiview active appearance models and dynamic programming," *IEEE Transactions on Medical Imaging*. vol. 25, no. 9, pp. 1158-1170, 2006.

[4] T. F. Cootes and C. J. Taylor, "Anatomical statistical models and their role in feature extraction," *British Journal of Radiology*. vol. 77, pp. 133-139, 2004.

[5] M. B. Stegmann, B.K. Ersboll, and R. Larsen, "FAME—a flexible appearance modeling environment," *IEEE Transactions on Medical Imaging*, vol. 22, no. 10, pp. 1319-1331, 2003.

[6] M. Üzümcü, R. J. van der Geest, M. Sonka, H. J. Lamb, J. H. C. Reiber, and B. P. F. Lelieveldt, "Multiview active appearancemodels for simultaneous segmentation of cardiac 2-and 4-chamber long-axis magnetic resonance images," *Investigative Radiology*, vol. 40, no. 4, pp. 195-203, 2005.

[7] M. Üzümcü, R. J. van der Geest, C. Swingen, J. H. C. Reiber, and B. P. F. Lelieveldt, "Time continuous tracking and segmentation of cardiovascular magnetic resonance images using multidimensional dynamic programming," *Investigative Radiology*, vol. 41, no. 1, pp. 52-62, 2006.

[8] R. J. van der Geest, B. P. F. Lelieveldt, E. Angelié, M. Danilouchkine, C. Swingen, M. Sonka, and J. H. C. Reiber, "Evaluation of a new method for automated detection of left ventricular boundaries in time serie of magnetic resonance images using active appearance motion model," *Journal of Cardiovascular Magnetic Resonance*, vol. 6, no. 3, pp. 609-617, 2004.

[9] S. C. Mitchell, B. P. F. Lelieveldt, R. J. Van der Geest, H. G. Bosch, J. H. C. Reiber, and M. Sonka, "Multistage hybrid active appearance model matching: segmentation of left and right ventricles in cardiac MR images," *IEEE Transactions on Medical Imaging*, vol. 20, no. 5, pp. 415-423, 2001.

[10] M. F. Santarelli, V. Positano, C. Michelassi, M. Lombardi, and L. Landini, "Automated cardiac MR image segmentation: theory and measurement evaluation," *Medical Engineering and Physics*, vol. 25, no. 2, pp. 149-159, 2003.

[11] R. Beichel, H. Bischof, F. Leberl, and M. Sonka, "Robust active appearance models and their application to medical image analysis," *IEEE Transactions on Medical Imaging*, vol. 24, no. 9, pp. 1151-1169, 2005.

[12] H. J. Michaely, K. Nael, S. O. Schoenberg, G. Laub, M. F. Reiser, J. P. Finn, and S. G. Ruehm, "Analysis of cardiac function— comparison between 1.5 Tesla and 3.0 Tesla cardiac cine magnetic resonance imaging: preliminary experience," *Investigative Radiology*, vol. 41, no. 2, pp.133-140, 2006

[13] M. Fenchel, V. S. Deshpande, K. Nael, J. P. Finn, S. Miller, S. Ruehm, and G. Laub, "Cardiac cine imaging at 3Tesla: initial experience with a 32-element body-array coil," *Investigative Radiology*, vol. 41, no. 8, pp.601-608, 2006.

[14] M. B. Rominger, G. F. Bachmann, W. Pabst, and W. S. Rau, "Right ventricular volumes and ejection fraction with fast cine MR imaging in breath-hold technique: applicability, normal values from 52 volunteers, and evaluation of 325 adult cardiac patients," *Journal of Magnetic Resonance Imaging*, vol. 10, no. 6, pp. 908-918, 1999.

[15] L. E. Hudsmith, S. E. Petersen, D. J. Tyler, J. M. Francis, A. S. H. Cheng, K. Clarke, J. B. Selvanayagam, M. D. Robson, and S. Neubauer, "Determination of cardiac volumes and mass with FLASH and SSFP cina sequences at 1.5 vs. 3 Tesla: a validation study," *Journal of Magnetic Resonance Imaging*, vol. 24, no. 2, pp. 312-318, 2006.

[16] E. Angelié, J. J. M. Westenberg, R. J. van der Geest, M. Danilouchkine, G. Koning, and J. H. C. Reiber, "How to define the quality of a segmentation: application for the assessment of left ventricular function from short-axis cardiac MR data sets," [abstract] *EuroCMR*, 2002.

[17] P. R. Detmer, G. Bashein, R. W. Martin, “Matched filter identification of left-ventricular endocardial borders in transesophageal echograms,” *IEEE Transactions on Medical Imaging*, vol. 9, no. 4, pp. 396-404, 1990.

[18] C. M. Swingen, R. T. Seethamraju, M. Jerosh-Herold, “Feedback-assisted three-dimensional reconstruction of the left ventricle with MRI,” *Journal of Magnetic Resonance Imaging*, vol. 17, no. 5, pp. 528-537, 2003.

[19] L. P. Clarke, R. P. Velthuizen, M. A. Camacho, J. J. Heine, M. Vaidyanathan, L. O. Hall, R. W. Thatcher, and M. L. Silbiger, “MRI segmentation: methods and applications,” *Magnetic Resonance Imaging*, vol. 13, no. 3, pp. 343-368, 2004.

[20] I. M. Scott, T. F. Cootes, and C. J. Taylor, “Improving appearance model matching using local image structure,” *Proceedings of Information Processing in Medical Imaging*, C. J. Taylor and J. A. Noble Eds., vol. 2732, pp. 258-269, 2003.

[21] R. J. M. van Geuns, T. Baks, E. H. B. M. Gronenschild, J. M. M. Aben, P. A. Wielopolski, F. Cademartiri, and P. J. de Feyter, “Automatic quantitative left ventricular analysis of cine MR images by using three-dimensional information for contour detection,” *Radiology*. vol. 240, pp. 215-221, 2006

[22] X. P. Zhu, C. E. Hutchinson, J. M. Hawnaur, T. F. Cootes, C. J. Taylor, and I. Isherwood, “Magnetic resonance image synthesis using a flexible model,” *British Journal of Radiology*, vol. 67, no. 802, pp.976-982, 1994.

[23] Z. Zhou, J. You, P. A. Heng, and D. Xia, “Cardiac MR image segmentation and left ventricle surface reconstruction based on level set method,” *Studies in Health Technology and Informatics*, vol. 111, pp. 629-632, 2005.

[24] C. Lorenz and J. von Berg, “A comprehensive shape model of the heart,” *Medical Image Analysis*, vol. 10, no. 4, pp, 657-670, 2006.

中心思想
'the central idea'

Chapter 5

Automated Contour Detection in X-Ray Left Ventricular Angiograms Using Multi-View Active Appearance Models and Dynamic Programming

This chapter was adapted from:
Automated Contour Detection in X-Ray Left Ventricular Angiograms Using Multi-View Active Appearance Models and Dynamic Programming
E. Oost, G. Koning, M. Sonka, P.V. Oemrawsingh, J.H.C. Reiber, and B.P.F. Lelieveldt
IEEE Transactions on Medical Imaging, vol. 25, no. 9, pp. 1158-1171, 2006.

Abstract

This chapter describes a new approach to the automated segmentation of X-ray left ventricular (LV) angiograms, based on Active Appearance Models (AAMs) and Dynamic Programming. A coupling of shape and texture information between the end-diastolic (ED) and end-systolic (ES) frame was achieved by constructing a Multi-View AAM. Over-constraining of the model was compensated for by employing Dynamic Programming, integrating both intensity and motion features in the cost function. Two applications are compared; a semi-automatic method with manual model initialization, and a fully automatic algorithm. The first proved to be highly robust and accurate, demonstrating high clinical relevance. Based on experiments involving 70 patient data sets, the algorithm's success rate was 100% for ED and 99% for ES, with average unsigned border positioning errors of 0.68 mm for ED and 1.45 mm for ES. Calculated volumes were accurate and unbiased. The fully automatic algorithm, with intrinsically less user interaction was less robust, but showed a high potential, mostly due to a Controlled Gradient Descent in updating the model parameters. The success rate of the fully automatic method was 91% for ED and 83% for ES, with average unsigned border positioning errors of 0.79 mm for ED and 1.55 mm for ES.

5.1 Introduction

X-ray left ventricular (LV) angiography is a widely applied modality for the assessment of cardiac function. To visualize the heart with this modality, patients undergo a catheterization procedure in which the LV is filled with an X-ray opaque contrast dye. Acquisition can be made in bi-plane (combining the antero-posterior view and the lateral view or combining the 30° right anterior oblique view and the 60° left anterior oblique view) or in single-plane (generally 30° right anterior oblique view). Average acquisition time is around 8 to 10 seconds, covering 7 to 9 cardiac cycles. In the second or third cardiac cycle after the injection of the contrast fluid, irregular cardiac contractions generally have subsided and the distribution of the contrast dye within the LV is considered to be optimal. Hence, one of these cycles is selected for analysis of cardiac function by choosing the image frame in which the LV is fully filled (ED) and the first next image frame in which the ventricle is maximally contracted (ES). In both frames endocardial contours are drawn around the LV manually and used to determine surface areas of the projected LV, from which the ventricular volume in ED and ES can be estimated [1]. In addition, relevant clinical parameters such as regional wall motion and ejection fraction (EF) can be determined.

Currently, several packages are available that assist the cardiologists in manually drawing contours in LV angiograms. However, due to frequently occurring poor image quality, an expert examines an X-ray image sequence not only by considering the ED and ES image frame. To decide on the correct boundary locations neighboring frames around ED and ES are inspected. This way,

knowledge about contraction dynamics is used to improve the segmentation accuracy. This makes drawing contours by hand difficult, time-consuming and prone to inter- and intra-observer variability. The goal of the work presented here is to automate the contour detection process to reduce the cardiologist's workload and diminish inter- and intra-observer variability. Because of the aforementioned difficulties of interpreting X-ray angiograms, low level image processing tools have not shown to be sufficiently robust and integration of a priori knowledge is a necessity. Therefore, we aim to integrate the same priors that an expert uses in segmenting the left ventricle, i.e. shape, texture and contraction dynamics priors.

Several knowledge-based approaches for automated segmentation of the left ventricle have been reported, however none of these have been incorporated in daily clinical practice. Tehrani *et al.* [2], for example, combined fractions of possible LV edges, obtained by low level image processing, by means of blackboard architecture and statistical shape models, to come to a full LV delineation. Lilly *et al.* [3] used Dynamic Programming to fit a contour through a set of proposed candidate points, based on regional intensity information, edge information and multiple regional thresholding algorithms. Contour irregularities and contour drift due to insufficient image information were neutralized by template matching using a template library derived from manually traced contours. Figueiredo and Leitão [4] proposed an approach using maximum a priori probability in a Bayesian framework in combination with Markov random field contour modeling. However, this method was applied only on digital subtraction angiography (DSA), in which an image acquired before the injection of the contrast agent is subtracted from all following images, to remove the background of the images and only retaining the object of interest.
Recently McDonald and Sheehan [5] introduced a method using boosted decision trees for pixel classification based on feature images, containing geometry features and gray-level statistics of a sequence of images around the ED and ES frames. By using information from images around ED and ES, LV contraction dynamics is integrated in these feature images. This semi-automatic method requires 3 anatomical landmark points (the endpoints of the aortic valve and the apex) to be positioned manually.
Suzuki *et al.* [6] proposed a combination of edge detection by a modified multilayer neural network and a standard edge detection based on low-pass filtering and edge enhancement. The first method is able to localize less pronounced subjective edges and is trained on manually drawn LV contours, the latter detects rough edges in the images. After placing the two aortic valve points manually, the contours are traced automatically based on both edge detection methods. As in [4] this approach has been applied on DSA images only.

5.1.1 Contribution of this Work

Recent work [5-8] has shown the need for a priori knowledge of shape, image intensities and contraction induced motion in automated segmentation of LV angiograms. The majority of previously reported methods used only shape

knowledge, or was applied to DSA in which most of the intensity information is removed. Only the approach proposed by McDonald and Sheehan [5] uses knowledge about shape and image intensities and motion due to cardiac contraction.

The contribution of this work is fourfold:

- Multi-View AAMs are developed in which statistical information of different views of the same object is modeled simultaneously. The existing correlation in shape and texture between ED and ES is exploited. The more reliable LV information present in the ED images supports the segmentation of the frequently poorly defined LV in the ES images.

- To prevent the model from locking in on local minima, we propose a novel, Controlled Gradient Descent optimization, in which a limited number of model parameters is updated at a time. This greatly improves convergence robustness.

- Motion-based Dynamic Programming is applied to compensate for over-constraining by the model and thus to attain better local border delineation. The cost function is constructed from both image features and features from a subtraction image (ES minus ED). The latter incorporates contraction motion information in the algorithm.

- An elaborate evaluation of clinical efficiency of the algorithm is described based on 70 ED-ES image pairs. To our knowledge, this is the largest evaluation of an automated segmentation method for clinically realistic X-ray LV angiograms.

5.2 Background

Active Appearance Models, introduced by Cootes [9,10], are highly suitable to integrate knowledge in segmentation problems. AAMs are statistical models describing an object's shape and image texture. For both shape and gray-values, an average and a series of eigenvectors is computed, from which the modes of variation of the model are determined. When matching the model to an unseen image, the object contours are localized by minimizing the error between the model and the image, within the boundaries of statistically plausible deformations of the model.

Examples of successful application of AAMs in automatic segmentation in medical images, whether in 2D, 2D + time, 3D or 3D + time, are ample for a range of imaging modalities. An elaborate overview can be found in [11]. The general construction of an AAM and the conventional matching procedure are briefly introduced in this section. A detailed description can be found in [12].

5.2.1 AAM Training

An AAM is trained on a series of representative images, in which an expert manually segmented the object of interest. Contours are resampled in n corresponding points, and (for 2D) expressed as a vector of $2n$ elements:

$$\mathrm{x} = \left(x_1, y_1, x_2, y_2, x_3, y_3, \ldots, x_n, y_n\right)^T \tag{5.1}$$

After Procrustes alignment [13] of the shape vectors to eliminate pose differences, a shape model is built by applying Principal Component Analysis (PCA) on the sample covariance matrix. Arranging the eigenvectors according to descending eigenvalues enables elimination of less significant eigenvectors.

The texture model is created by warping the intensities of the object of interest from the training images onto the mean shape. This way, an image patch is created, which is normalized for the shape of the individual samples; from this patch, pixel intensity vectors g are extracted. Typically, a thin strip around the object is included in the patch, to acquire information of pixel intensities outside the object's boundaries. Texture vectors are normalized to zero average and unit variance and PCA is performed on the sample covariance matrix, resulting in the statistical texture model.

To reduce model size, AAM models are generally constructed using only the eigenvectors corresponding to the largest n eigenvalues, capturing for example 98 % of the available variation. Using shape and texture models, the sample shapes x and textures g can be approximated from the respective models:

$$\mathrm{x} \approx \bar{\mathrm{x}} + P_s b_s \quad \text{and} \quad \mathrm{g} \approx \bar{\mathrm{g}} + P_g b_g \tag{5.2}$$

where $\bar{\mathrm{g}}$ and $\bar{\mathrm{x}}$ represent the average texture and shape vectors, P_g and P_s the texture and shape eigenvector matrices, and b_g and b_s the texture and shape parameters characterizing each training sample.

From the shape and texture models, an AAM is created by concatenating the shape and texture parameter vectors:

$$b = \begin{pmatrix} W b_s \\ b_g \end{pmatrix} = \begin{pmatrix} W P_s^T \left(\mathrm{x} - \bar{\mathrm{x}}\right) \\ P_g^T \left(\mathrm{g} - \bar{\mathrm{g}}\right) \end{pmatrix} \tag{5.3}$$

W denotes a weight factor coupling the shape and texture coefficients.

After a final PCA over the set of appearance vectors b the resulting AAM can be written as:

$$b = Qc \tag{5.4}$$

in which Q is the matrix containing the combined shape/texture eigenvectors and c denotes the appearance parameters for the combined model.

5.2.2 Using AAMs for Segmentation

Matching the model to an unseen image involves minimizing the sum of squared pixel differences between the model gray-value patch and the normalized target image, within the boundaries of statistically plausible model limits. To drive the model matching iterations, the parameter update steps are computed from the residual images $\delta g_0 = g_s - g_m$, where g_s denotes the normalized target image, and g_m the model synthesized image. From the current estimate of the model parameters c_0 and the parameter derivatives for the model and pose parameters, captured in the pre-computed gradient matrices R_c (for the model parameters) and R_p (for the pose parameters), Cootes describes an iterative matching algorithm, consisting of the following steps [12,14]:

1) Normalize the target image patch to zero mean and unit variance

2) Calculate the residual between target image and model patch $\delta g_0 = g_s - g_m$

3) Calculate the error from the difference vector $E_0 = |\delta g_0|^2$

4) Using the pre-computed gradient matrices, determine the model parameter update $\delta c = R_c \delta g_0$ and pose update $\delta p = R_p \delta g_0$

5) Set $k = 1$

6) Determine new estimates for the model parameters $c_1 = c_0 - k\delta c$ and pose parameters $p_1 = p_0 - k\delta p$

7) Calculate a new model based on c_1 and p_1

8) Determine a new difference vector and calculate a new error E_1

9) If $E_1 < E_0$, select c_1 and p_1 as the new parameter vectors, else try $k = 1.5$, $k = 0.5$, $k = 0.25$ etc. and go to step 6

Repeat until convergence, either using a fixed number of iterations, or until no improvement is achieved.

As mentioned in Section 5.1, we propose a different matching strategy, which differs substantially from this approach. This novel approach will be discussed in Section 5.3.

5.3 Segmentation Method

The proposed method consists of three novel components: the Multi-View AAM, in which different views of the same object are modeled simultaneously, a parameter updating strategy that isolates the modes of variation yielding the largest criterion decrease, and a locally selective Dynamic Programming algorithm as post-processing to relax potential over-constraining model priors, increasing border localization accuracy.

5.3.1 Multi-View AAM

In many medical image segmentation problems one deals with multiple viewpoints, multiple cross sections or multiple time instances. Because all these views describe one single object, correlations in pixel intensities and contour shapes between views are present and can be exploited. This is particularly useful for X-ray LV angiography.

The Multi-View Active Appearance Model introduced here is specifically constructed to exploit the existing correlation between different views of the same object. The concept is derived from Cootes' work on coupled-view AAMs [15], where a frontal and a side view of a face are segmented simultaneously by building separate models for each view and a combined model for both views. During matching, segmentation is performed using the single view models, while shape constraints are applied from the combined model. Our method differs from this concept in that it models both organ shape and organ texture simultaneously for all views. Both during model training as during automatic segmentation, ED and ES scale, orientation and position are independent.

The key novelty in this approach is the direct modeling of existing correlations in image intensities, which is used to drive the segmentation of both images simultaneously. Contrary to Cootes' coupled-view AAM, the Multi-View AAM segments all views simultaneously using only one model. Because this model is constructed by concatenating, for every training sample, the shape and intensity vectors for all views, it directly exploits existing correlations, both in shape and in intensities, between the views.

The Multi-View model is constructed by aligning the training shapes for different views separately, and concatenating the aligned shape vectors x_i (see equation 5.1) for each of the N views. A Multi-View shape vector, x_{mv}, for N frames is defined as:

$$\mathrm{x}_{\mathrm{mv}} = \left({x_1}^T, {x_2}^T, \ldots {x_N}^T \right)^T \tag{5.5}$$

By applying a Principal Component Analysis on the sample covariance matrix of the combined shapes, a shape model is computed for all frames simultaneously.

The principal model components represent shape variations, which are intrinsically coupled for all views.

For the intensity model, the same applies: an image patch is warped on the average shape for view *i* and sampled into an intensity vector g_i, the intensity vectors for each single frame are normalized to zero mean and unit variance, and concatenated:

$$g_{mv} = \left(g_1^T, g_2^T, \ldots, g_N^T\right)^T \tag{5.6}$$

Analogous to the single frame AAM, a PCA is applied to the sample covariance matrices of the concatenated intensity sample vectors, and subsequently each training sample is expressed as a set of shape- and appearance coefficients. A combined model is computed from the combined shape/intensity sample vectors. Figure 5.1 demonstrates that in the combined model, the shape and appearance of both views are strongly interrelated.

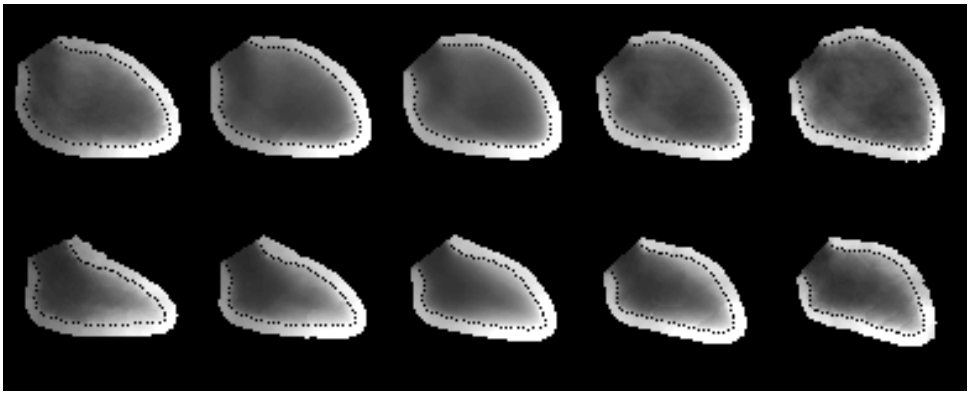

Figure 5.1: First mode of variation for a left ventricle Multi-View AAM, constructed from 70 ED-ES X-ray LV angiograms. Upper row = ED, lower row = ES. From left to right the columns represent a standard deviation of minus two, minus one, zero, plus one and plus two sigma. The black dotted line represents the ventricle border. Correlation in shape between ED and ES is clearly visible. Also the texture variation, describing mainly the local contrast between the LV and its embedding around the mitral valve, shows clear similarities between ED and ES.

Estimation of the gradient matrices for computing parameter updates during image matching is performed by applying perturbations on the model and pose parameters, and measuring their effect on the residual images [12,14]. Because of the correlations between views in the model, a disturbance in an individual model parameter yields residual images in all views simultaneously.

Although full 2D + time and 3D + time ASMs an AAMs have been reported [16-18], this work only reports a coupling of the ED and the ES frame in X-ray LV angiography, since they are the most clinically relevant frames. The ES image frame

in which much of the injected contrast agent has been ejected is especially difficult to interpret. ED images generally exhibit a better contrast. The existing correlations between both frames can be exploited by Multi-View AAMs to achieve better boundary delineation especially in the ES image. In practice, this will give the opportunity to exchange, for example, information about overlapping structures between the several views. When, for example in ED segmentation, such an overlapping structure is 'recognized', this information can be used in the simultaneous segmentation of the ES frame. This kind of image intensity information exchange between both views is crucial, in particular for difficult to interpret images like LV angiograms.
Stegmann and Pedersen [19] proposed a similar AAM for cardiac MRI, in which pose information was captured in the shape vector by concatenating the shapes of different views before Procrustes Alignment was carried out. This approach might also be useful for exploiting pose correlations between the ED and ES frames in LV angiography. It is however an extra factor that can over-constrain the model.

5.3.2 Controlled Gradient Descent

LV angiograms may exhibit many acquisition artifacts, such as overlapping anatomical structures (ribs, diaphragm) or strong shadows. In these cases, the regular AAM matching strategy described above, occasionally shows difficulties in converging to the true contour positions. A typical example of a diverging model is displayed in Figure 5.2. To cope with these situations during segmentation, images like this have to be included in the training data set, resulting in large allowed texture variations incorporated in the model.

Also the gradient matrix R_c which is used for updating the model parameters, is constructed during training by measuring the effect of disturbances on the isolated model parameters, while the pose parameters remain undisturbed. Therefore, fitting the model to the image using this matrix therefore will function optimally when the pose initialization is (nearly) correct. However, when the model is initialized far from the object of interest, or has a strongly deviating scale or orientation, the matrix R_c may loose its validity. This explains why a regular AAM initialized far from the correct position may converge to a local minimum, since the algorithm tries to reduce the difference between model and underlying image based on inaccurate gradient approximations.

Several methods have been described on constraining the energy function for improved convergence robustness; a review of such methods can be found in [20]. A common way to increase robustness is by limiting the number of simultaneous degrees of freedom during optimization; this parameter scheduling has been described mainly applied for minimizing physics-based energy functions, e.g. [21]; In the context of AAM fitting, we developed a Controlled Gradient Descent, updating a limited number of parameters at a time, where the free parameters are selected dynamically as follows. First all parameter updates, corresponding to the specific modes of variation, are sorted to descending magnitude and the largest

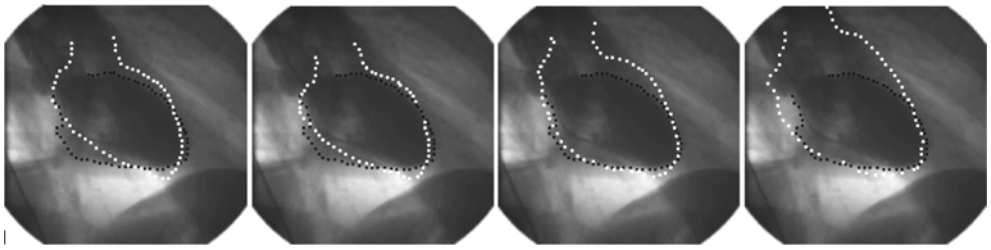

Figure 5.2: Example of spurious error criterion behavior. Black dotted lines represent correct LV borders, white dotted lines represent model results. From left to right the error criterion decreases.

single parameter update is executed. If this results in a lower error criterion, the proposed update is accepted, new model and pose parameters are calculated and a new vector of parameter updates is determined and ordered again in the next iteration. In case an update proposal does not lower the error criterion, the number of updated model parameters is incremented in the next attempt. If a new update proposal is successful, the next iteration will start again with only one model parameter.

5.3.3 Motion-Based Dynamic Programming

The power of the AAM algorithm is that it is able to still come to an acceptable global segmentation in an environment with partly invisible, or only vaguely perceptible features. AAM segmentation is based on minimizing the sum of squared pixel errors between a global model patch and the normalized underlying image and due to the global nature of this criterion it does not focus on local borders. Moreover, statistical models such as AAMs generally are over-constrained: the model freedom to deform is limited by the modes of variation derived from the training data set. Therefore, a shape that slightly deviates from characteristic shapes in the training set should also be considered as valid and a refinement of the contour is desirable. In previous work [8] an AAM contour refinement was done by applying a second AAM, in which only image intensities close to the contour were incorporated. This approach had a positive effect on the segmentation, but being model-based, it still intrinsically over-constrained the contours towards the training data. The same holds for a hybrid ASM/AAM segmentation approach, which has been reported for cardiac MR [22]. To allow for more shape flexibility a shape relaxation is required.

We developed a Dynamic Programming algorithm, in which the cost function is constructed from image and motion features, to mimic the experts' routine of including knowledge of contraction dynamics. A generalized Dynamic Programming algorithm that is used in X-ray angiography, for example for extracting coronary contours [23], searches for an optimal contour path through a cost matrix, based on first and second order derivatives, describing the edges of the object to be segmented. The cost function is generally defined by:

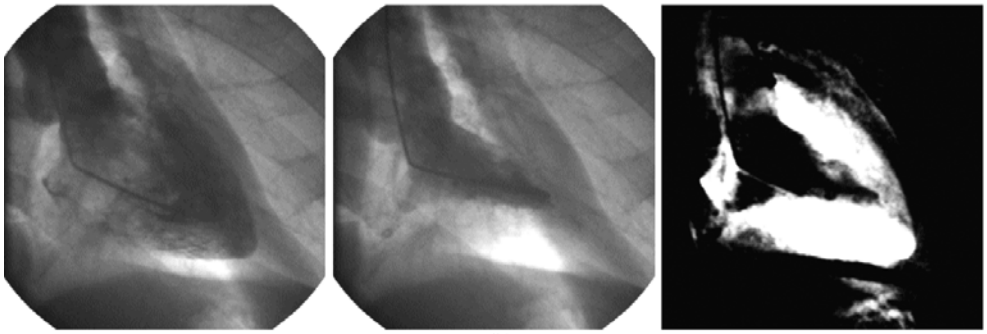

Figure 5.3: Additional information on true LV border position is available in the subtraction image (c): ES (b) minus ED (a). This specific example shows that the subtraction image results in a better definition of the mitral valve area in both the ED and ES frame. In addition it diminishes the influence of a diagonal shadow in the true image data.

$$C(i,j) = \alpha G(i,j) + (1-\alpha)T(i,j) \tag{5.7}$$

in which $C(i,j)$ is the cost of element in row *i* and column *j*, $G(i,j)$ represents the gradient, $T(i,j)$ is the second order derivatives and α denotes the weighing factor between the first and second order derivatives.

In this work we have integrated features from a subtraction image (ES image minus ED image, see Figure 5.3) into the cost function. The cost function is constructed such that it searches a minimal cost path based on directional edges, while integrating both information of true image data and the subtraction image. The polarity of edges in the subtraction image is defined differently for ED and ES, making the cost function locally selective for each phase. In ED the area outside the contour should be dark and the area inside the contour should be light. For ES this edge polarity is opposite. The use of these directional edges is only possible, because the Multi-View AAM already produces a reliable global segmentation in each frame, close to the desired solution. This enables Dynamic Programming in a limited search space. The cost function used in our algorithm is similar to equation 5.7:

$$C(i,j) = \beta(\alpha_1 G_1(i,j) + (1-\alpha_1)T_1(i,j)) + (1-\beta)(\alpha_2 G_2(i,j) + (1-\alpha_2)T_2(i,j)) \tag{5.8}$$

in which $C(i,j)$ is the cost of element in row *i* and column *j*, β denotes the weighing factor between the cost matrix constructed from the true image data and the cost matrix constructed from the subtraction image, $G_1(i,j)$ and $G_2(i,j)$ are the gradients of both images, $T_1(i,j)$ and $T_2(i,j)$ are the second order derivatives and α_1 and α_2 are weighing factors between the first and second order derivatives for the true image data and the subtraction image data respectively.

5.4 Clinical Evaluation

The purpose of this study is to determine the clinical utility of our approach and more specifically, whether Multi-View AAM segmentation results are of a comparable quality as manual segmentation results produced by clinicians. We evaluate the automatically generated contours by relating them to contours of three experts. Furthermore we determine the state of automation that can be achieved, by comparing a fully automatic method with a semi-automatic approach in which for both ED and ES the endpoints of the aortic valve and the apex are predefined by a user. In addition we compare the proposed techniques with conventional Active Appearance Models and with conventional Dynamic Programming.

5.4.1 Data Material

To examine the effectiveness of our methodology we have tested it on 70 single-plane ED-ES pairs. All angiograms were acquired in the 30^0 right anterior oblique view, using standard contrast agent (Iopamiro© 350). Average acquisition time was about 8 to 10 seconds, covering 7 to 9 cardiac cycles. All data stemmed from adult patients, suffering from one, two or diffuse coronary diseases. There was no pathology-based selection of the data set. Two exclusion criteria were applied: ventricles being not fully imaged and ventricles showing only extra-systolic contraction. As Figure 5.4 illustrates, many different acquisition artifacts were encountered. The situations displayed in Figures 5.4d and 5.4e were especially frequently occurring (20 out of 70 cases and 15 out of 70 cases respectively).

5.4.2 AAM Training

For all 70 paired ED-ES images a clinician has drawn manual contours which have been used to train the Active Appearance Model. Point correspondence was achieved by resampling every contour to 60 equidistant points, based on three specific landmark points: the upper aortic valve point, the lower aortic valve point and the apex. This resulted in a training sample description of 120 points, combining the ED and the ES shapes. 14 leave-five-out models were trained, on 65 out of the 70 ED-ES image pairs, leaving out 5 pairs for testing purposes. Using leave-five-out instead of leave-one-out was opted mainly for efficiency reasons, whereas a model trained on 65 data sets does not differ very much from a model trained on 69 data sets.

All models were constructed retaining 100% shape variance and 95% intensity variance. This corresponded with 64 shape modes and 27 intensity modes and resulted in 64 appearance modes of variation.
To speed up both AAM training and AAM matching, all training and matching experiments were executed after subsampling the images by a factor 4.

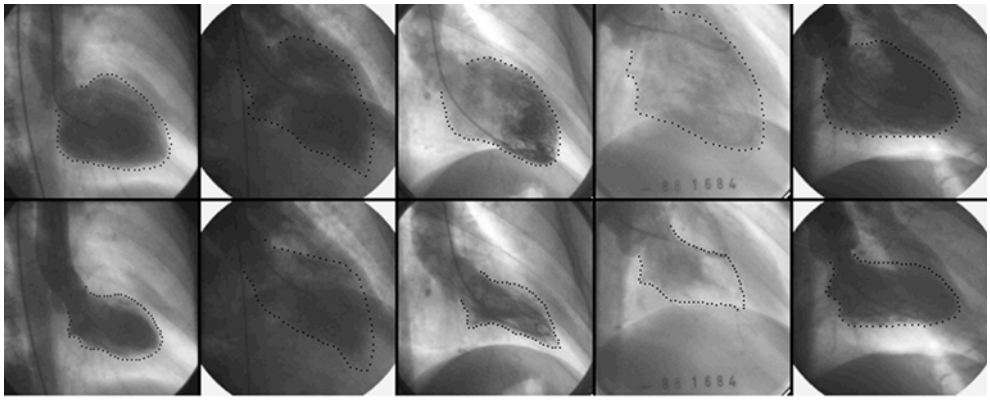

Figure 5.4: Typical examples of LV angiograms (upper row = ED; bottom row = ES): good contrast (a), poor contrast (b), uneven contrast agent distribution (c), partial overlap with the diaphragm (d) and substantial shadows caused by the shutter (e), expressed in this example as a diagonal dark band. The black dotted lines represent the LV boundaries as determined manually by an expert. Particular difficulty can be expected in the ES frame of image (d). In a normal situation the texture knowledge within the model consists of a relative dark ventricle in an embedding with higher pixel intensities. Locally in this image it is opposite, while the true LV contour apparently coincides more or less with the strong edge of the diaphragm.

5.4.3 Semi-Automatic Segmentation

In the semi-automatic segmentation, the model was initialized using three landmark points: upper aortic valve point, lower aortic valve point and apex. Initial model scale, orientation and position were estimated from these three points. Initial scale, orientation and position were furthermore used to constrain the pose parameters, which were allowed to differ 10% from the initial pose.
Model parameters were ordered and initially updated separately while the number of model parameters was incremented when a proposed model update was rejected. To ignore the influence of trivial model parameters, a maximum of 50% of the most pronounced modes of variation was employed. Possible local minima were evaded by following Cootes' forced update approach [12,14] twice after the model could not improve any further. The best values for model and pose parameters were stored and, if not improved in a subsequent attempt, were considered to be the final result.

5.4.4 Fully Automatic Segmentation

The fully automatic segmentation consisted of two stages. The first stage globally positioned the model, after initialization in the image center. The second stage was similar to the semi-automatic segmentation. However, without user interaction no knowledge about approximate scale, orientation and position was available and therefore pose constraints were not applied.
When large changes in pose parameters occur, it is likely that previous updates of

model parameters have been inaccurate, since the overlap between the model and the ventricle probably was limited. Therefore, it is better to discard these model parameter updates. In the global positioning of the model, model parameters were reset when the scaling or orientation deformation exceeded 10% or when the shift in x or y direction exceeded 5% of image width or height respectively.

5.4.5 Comparison with Conventional Methods

To determine the effect of all proposed contributions, the following comparisons were executed:

- A comparison between Single-View and Multi-View AAMs.
- A comparison between the Controlled Gradient Descent and a conventional AAM.
- A comparison between the hybrid AAM / Dynamic Programming algorithm and standalone AAM / Dynamic Programming.
- A comparison between conventional Dynamic Programming and Dynamic Programming in which subtraction image information is included.

5.4.6 Dynamic Programming Parameters

Table 5.1 summarizes the relevant Dynamic Programming parameters, used for all experiments. The parameters were selected after a pilot study on part of the data set. The allowed search area for ED is 16 mm on both sides of the AAM contour, for ES this area is set to 6 mm inside and 12 mm outside the AAM contour. Due to lack of visible contrast agent in ES and the resulting tendency of the AAM to produce an LV ES segmentation with a slightly too small surface area, the Dynamic Programming search area for ES is restricted more. The weighting factor β during Dynamic Programming is 0.5 for ED and 0.7 for ES. Due to a better definition of the ES contour in the subtraction image, information in the subtraction image is

	ED	ES
α	0.5	0.5
β	0.5	0.7
area outside [mm]	16	12
area inside [mm]	16	6

Table 5.1: Dynamic Programming parameters.

graded higher than the information from the true image data. For the Dynamic Programming in the ED frame and in the ES frame, edge convolution filters with opposite signs are used. This way the correct edge polarity is created.

5.4.7 Evaluation Indices

Experiments were carried out using the data set of 70 ED-ES image pairs. None of the test images was included in the model that was used for AAM segmentation. Calculated ED volume, calculated ES volume and calculated EF were compared with the manually defined independent standard. Volumes were calculated by using the area-length equation introduced by Sandler and Dodge [1]:

$$V = \frac{8A^2}{3\pi L_A} \tag{5.9}$$

in which A denotes the projected surface area and L_A is the distance from upper aortic valve point to apex. Linear regression was used to determine relationships between manually traced and computer determined values. A two-tailed paired samples t-test was applied to volume measurements from manual and automatic contours to investigate systematic errors. A p-value smaller than 0.05 was considered significant.
In addition, the point-to-curve errors of the contours and the percentage of the automatic contour requiring manual correction by an expert were determined. When a contour part of at least 3 successive points had a point-to-curve error larger than 2 mm, it was considered necessary to redraw this contour part. This parameter for contour editing was not selected to discriminate between proper segmentation and failure, but to distinguish between drawing preferences of different experts in practice. A quantitative evaluation method from recently published work [6] has been adopted for comparison:

$$E_C = \frac{\sum_{x,y\in R_E} \{a_P(x,y) \otimes a_D(x,y)\}}{\sum_{x,y\in R_E} a_D(x,y)} \tag{5.10}$$

$$E_A = \frac{\left|\sum_{x,y\in R_E} a_D(x,y) - \sum_{x,y\in R_E} a_P(x,y)\right|}{\sum_{x,y\in R_E} a_D(x,y)} \tag{5.11}$$

with

$$a_P(x,y) = \begin{cases} 1, (x,y) \in R_P \\ 0, \quad otherwise \end{cases} \tag{5.12}$$

$$a_D(x,y) = \begin{cases} 1, (x,y) \in R_D \\ 0, \quad otherwise \end{cases} \tag{5.13}$$

in which R_P is the region within the automatically drawn contour, R_D is the region within the manually drawn contour, R_E is the region of evaluation and $\otimes$ denotes the logical exclusive OR operator. Equation 5.10 represents a contour error defined as the summation of pixels that are exclusively located within the boundaries of either one of the two compared contours, divided by the total sum of pixels of the evaluation area (in this case the surface area of the manual contour). Equation 5.11 denotes the difference in surface area between automatic and manual contour, in respect to the surface area of the manual contour.

It is well known that the difficulty in interpreting LV angiograms results in a large inter- (and intra-) observer variability. When comparing, for example, the contours of the three experts contributing to this project, differences in estimated ES volumes up to a factor 2.6 were observed. The highest observed average unsigned point-to-curve differences amounted to 5 mm. Therefore it is difficult to define a gold standard or to define the notion of success of an automatic LV segmentation algorithm. To this end, we first investigated inter-observer variability for the ejection fraction, ED volume calculation, ES volume calculation, ED point-to-curve values and ES point-to-curve values. The cut-off parameter thresholds for outliers were defined as the average of the three maximum differences in the parameters between the three experts. These obvious segmentation failures were noted and excluded in further contour evaluation indices.

The performance of our algorithms was tested by comparing obtained results with the manual contours, that were used to train the 14 AAMs (expert #1 contours). Because the leave-five-out setup was used, none of the tested image pairs was included in the specific model that was used for segmentation. To assess the clinical relevance of the method, calculated contours were compared with manually drawn contours of three experts. In addition, to establish the accuracy of the manually defined standard, different experts were compared to each other.

5.5 Results

5.5.1 Semi-Automatic Segmentation

The semi automatic algorithm yielded borders that agreed closely to the manual expert contours. The success rate of the algorithm is 100% for ED and 99% (1 outlier) for ES. After removal of the image pair with this partial failure, both ED and ES contour errors, calculated areas and calculated volumes were, to our knowledge, better than any previously reported method [2-6]. Figure 5.5 displays representative examples of obtained contours, proving that accurate segmentation is also feasible in images with acquisition artifacts.

Border positioning errors were generally small. Average unsigned point-to-curve errors were 0.68 ± 0.37 mm for ED and 1.45 ± 0.76 mm for ES. All quantitative results (model vs. expert #1) are summarized in Figure 5.6, together with a

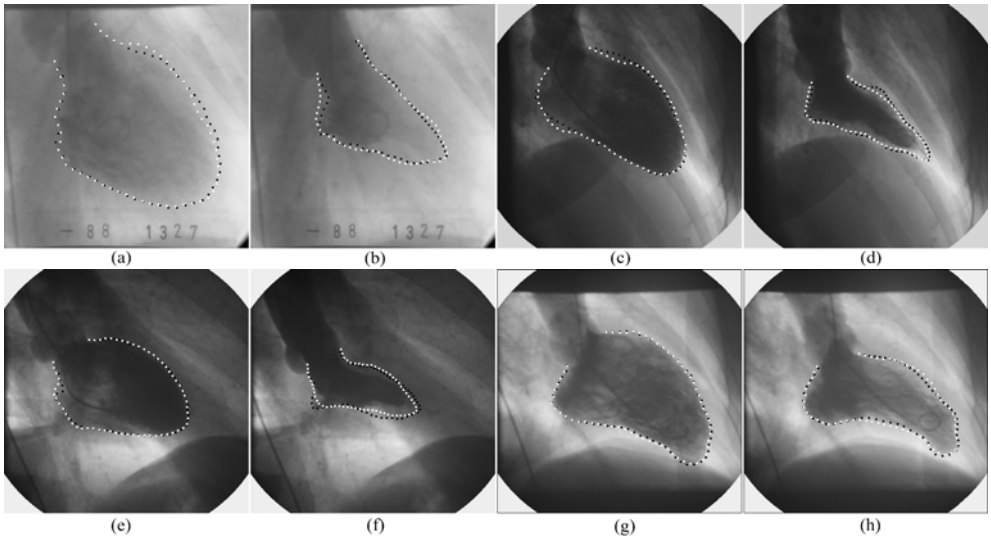

Figure 5.5: Successful matches for ED and ES generated with the semi-automatic algorithm. Black dotted lines denote the manual contour, white dotted lines represent the semi-automatic contours. Semi-automatic contours correspond closely with manual contours, also in images with acquisition artifacts such as low contrast (a & b), overlapping diaphragm (c & d), strong shadows (e & f). Contours are particularly good in images without acquisition artifacts (g & h).

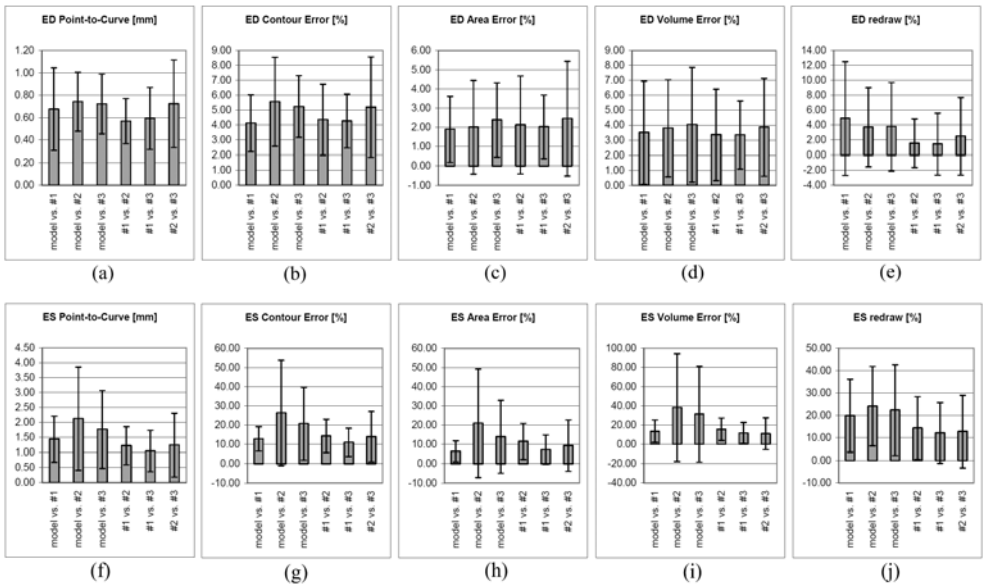

Figure 5.6: Point-to-curve distances (a & f), contour errors (see equation 5.10) (b & g), area errors (see equation 5.11) (c & h), volume errors (d & i) and the percentage of contour that needs to be redrawn (e & j) for ED (a-e) and ES (f-j). All bars in the graphs denote average values, error ranges span 1 standard deviation in both directions. Six comparisons are displayed: model vs. expert #1, model vs. expert #2, model vs. expert #3, expert #1 vs. expert #2, expert #1 vs. expert #3 and expert #2 vs. expert #3.

comparison of semi-automatically generated contours with contours drawn by expert #2 and expert #3 and a mutual comparison of all three experts. For the mutual comparison of experts, only 43 samples of the original 70 paired ED-ES data were available.

Excellent correlation between volumes based on manual and semi-automatic contours was achieved, as shown in Figure 5.7. In a paired samples t-test differences between manually and semi-automatically calculated ED volume, ES volume and ejection fraction were found statistically insignificant (p=0.13, p=0.76 and p=0.15 respectively). Table 5.2 provides an overview of errors in ED volume, ES volume and ejection fraction. The semi-automatic algorithm compared to expert #1 has the overall best results. In particular, the differences in calculated ES volume and EF are remarkably good, better than any of the inter-expert differences.

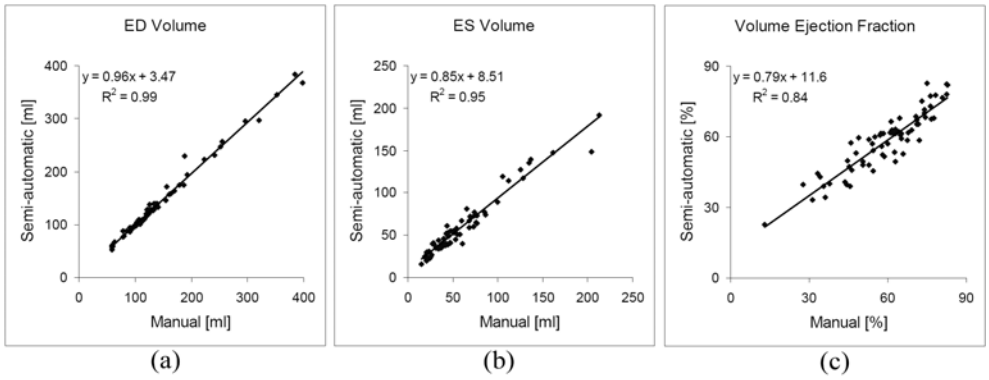

Figure 5.7: Volume regression plots for ED (a), ES (b) and ejection fraction (c) for the semi-automatic algorithm.

	samples	ED error [%]	ES error [%]	EF error [%]
model vs exp 1	69	-1.56	-0.88	-1.20
model vs exp 2	42	-0.86	12.79	-6.20
model vs exp 3	42	0.30	9.54	-4.26
exp 1 vs exp 2	43	0.70	12.11	-4.95
exp 1 vs exp 3	43	1.85	9.45	-2.98
exp 2 vs exp 3	43	1.15	-3.03	1.96

Table 5.2: Comparison of semi-automatic contours with 3 experts and comparing the experts mutually: relative ED volume and ES volume errors and the absolute ejection fraction error.

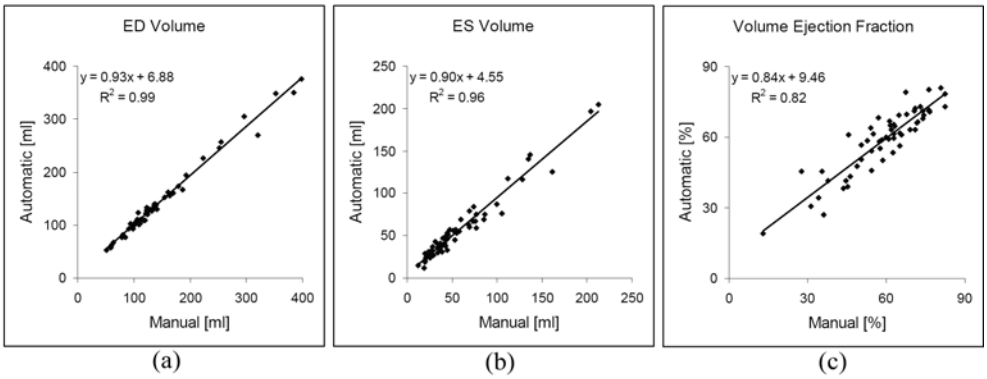

Figure 5.8: Volume regression plots for ED (a), ES (b) and ejection fraction (c) for the automatic algorithm.

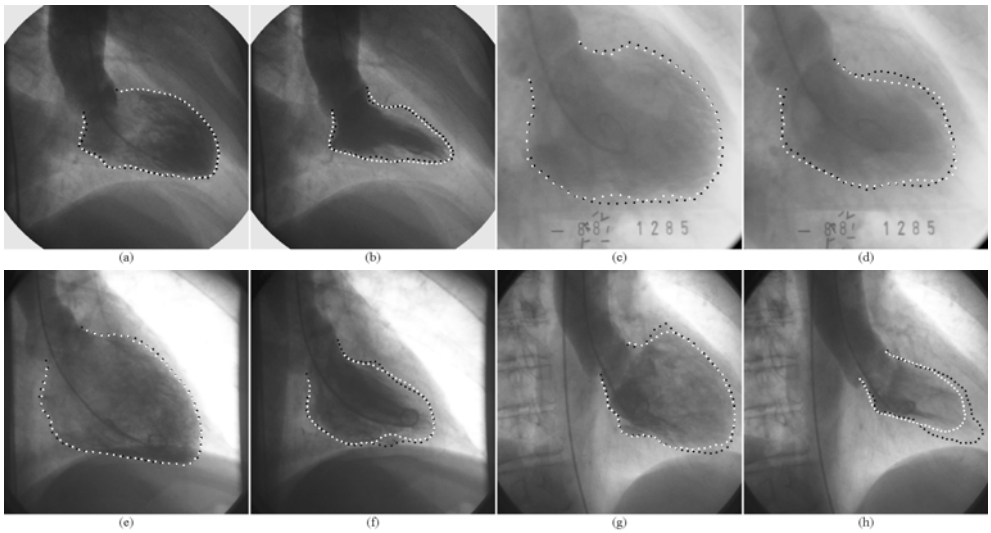

Figure 5.9: Successful matches for ED and ES generated with the automatic algorithm. Black dotted lines denote the manual contour, white dotted lines represent the automatic contours. Acceptable results can be achieved for good quality images (a & b) as well for images with artifacts such as low contrast (c & d), overlapping diaphragm (e & f) and poor contrast distribution (g & h). Also when the LV scaling is extremely large (c & d) or when the LV is relatively far from the image center (g & h), where the model is initialized, acceptable segmentation is feasible. Note that in image (h) user information on the apex location is indispensable for correct segmentation in the apex area.

5.5.2 Fully Automatic Segmentation

The success rate of the fully automatic algorithm is 91% for ED and 83% for ES. 6 complete failures were observed, in which both ED and ES segmentation diverged, and 6 partial failures in which only ES segmentation failed. After the removal of these outliers, unsigned point-to-curve errors were 0.79 ± 0.43 for ED and 1.55 ± 0.66 for ES, comparable to the semi-automatic results.

Linear regression plots are presented in Figure 5.8, showing acceptable results. Only ED volume comparison between manual and automatic contours was statistically significant (p=0.03). Errors in ES volume and ejection fraction were found statistically insignificant (p=0.33 and p=0.72 respectively). Examples of successful fully automatic segmentations are shown in Figure 5.9.

5.5.3 Comparison with Conventional Methods

The three proposed technical contributions (Multi-View AAM, Controlled Gradient Descent and the hybrid AAM / Dynamic Programming) have been compared with conventional AAMs and with conventional Dynamic Programming. Table 5.3 gives an overview of the experiments. All results in this table are based on the entire data set, without removal of obvious segmentation failures. The values denote averages ± standard deviation. ED_Ec and ES_Ec denote contour errors for ED and ES, as defined by equation 5.10. ED_Ev and ES_Ev denote relative volume errors for ED and ES.

The first two lines in Table 5.3 show the difference between Multi-View AAMs and Single-View AAMs for the semi-automatic algorithm, when no Controlled Gradient Descent and no post-processing by means of Dynamic Programming is applied. When initialization is done manually (first 2 lines), the results for Multi-View and

	ED_EC [%]	ED_EV [%]	ES_EC [%]	ES_EV [%]
Multi-View (semi)	13.2 ± 6.2	15.7 ± 13.5	22.6 ± 14.8	25.8 ± 37.3
Single-View (semi)	12.8 ± 6.7	15.3 ± 13.3	22.2 ± 13.9	24.7 ± 29.4
Multi-View (fully)	20.4 ± 15.8	18.7 ± 20.4	34.7 ± 24.2	33.1 ± 40.3
Single-View (fully)	26.6 ± 21.6	26.7 ± 32.8	48.5 ± 37.2	51.4 ± 63.9
CGD	13.4 ± 8.1	14.3 ± 12.7	25.6 ± 16.4	25.3 ± 23.8
no CGD	20.4 ± 15.8	18.7 ± 20.4	34.7 ± 24.2	33.1 ± 40.3
AAM + DP	4.1 ± 1.9	3.6 ± 3.5	14.1 ± 12.1	17.4 ± 34.7
only AAM	13.7 ± 6.0	15.7 ± 13.4	23.3 ± 14.2	26.0 ± 32.8
only DP	4.8 ± 3.1	4.5 ± 5.5	19.2 ± 17.1	28.7 ± 52.0
AAM + 1 img DP	5.8 ± 3.9	6.2 ± 7.6	15.5 ± 15.1	21.6 ± 42.2

Table 5.3: Comparison with regular AAMs and Dynamic Programming.

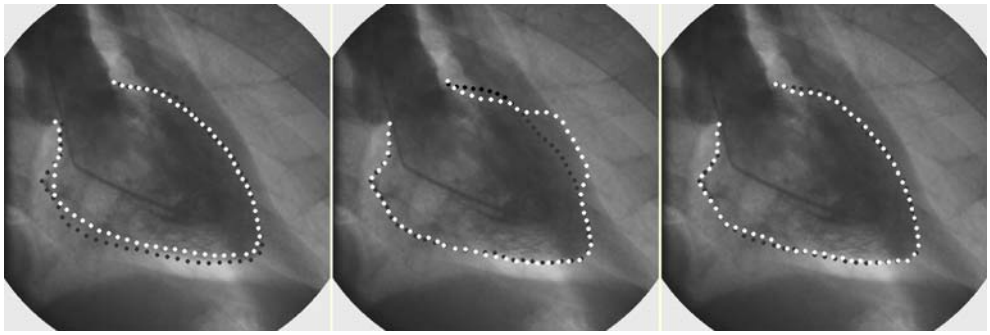

Figure 5.10: The benefit of integrating both true image information and subtraction image information in Dynamic Programming. Black dotted lines denote the manual contour, white dotted lines represent the computed contours. Results after AAM segmentation (left) show a proper segmentation of the anterior wall, while the posterior wall is delineated poorly. With regular Dynamic Programming as post-processing tool (middle) using only the true image information, the segmentation of the posterior wall is corrected. However, due to the strong shadow in the image, the contour near the anterior wall is attracted to the wrong edge. Including also subtraction image information (right) results in a proper segmentation of both anterior and posterior wall (The subtraction image information for this example can be found in Figure 5.3c).

Single-View are comparable, although the standard deviation for ES_Ev is significantly smaller for the Single-View Model. The added value of the Multi-View model becomes obvious when comparing results for fully automatic segmentation (lines 3 and 4). For all 4 parameters the Multi-View Model clearly outperforms the Single-View models.

To determine the effect of the Controlled Gradient Descent, experiments were repeated while using a regular Multi-View AAM instead of the proposed algorithm. When applying a regular Multi-View AAM in semi-automatic segmentation, performance and accuracy remained similar. However, a significant difference in performance occurred when applying a regular Multi-View AAM in fully automatic segmentation (lines 5 and 6).

The lines 7-9 in Table 5.3 show the need for a hybrid algorithm, combining AAMs and Dynamic Programming. When providing the model with the correct positions of the upper valve point, lower valve point and apex point, for both ED and ES, the hybrid algorithm obviously outperforms both methods, when applied separately. Furthermore, when the subtraction image information is not incorporated in Dynamic Programming (last line of the table), results deteriorate. Figure 5.10 shows a typical example.

5.6 Discussion

The method proposed in this chapter introduces three novel elements: a Multi-View AAM is developed to exploit the coherence between different image frames, a

locally selective Dynamic Programming is introduced to relax over-constraining inherent to statistical shape models and a Controlled Gradient Descent strategy is proposed to improve convergence and lock-in range. The Multi-View AAM robustly detects the initial models for the Dynamic Programming, enabling the integration of locally selective motion features in the cost function. The proposed method proved to be a robust and accurate tool for automatic segmentation of the left ventricle in angiographic images. It uses knowledge about shape, texture and motion from a large variety of training images and inherently mimics the drawing behavior of the clinical expert. Even in images that are difficult to interpret the algorithm produces reliable results.

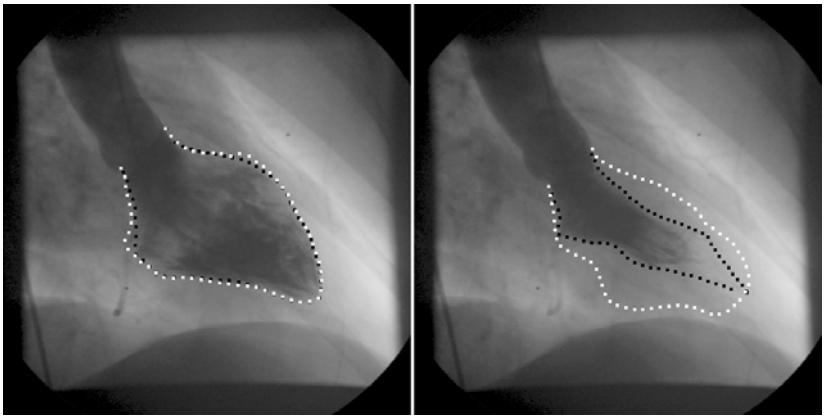

Figure 5.11: The only, partial, segmentation failure when using the semi-automatic algorithm. Black dotted lines denote the manual contour, white dotted lines represent the semi-automatic contours.

5.6.1 Automatic versus Semi-Automatic Segmentation

The semi-automatic algorithm shows a high success rate of 100% for ED and 99% for ES. The only failure occurred when the ES image showed an extremely slim and elongated shape (see Figure 5.11). Because of the elongated shape, the model is initialized with a relatively large scale. This, in combination with the object's shape extremity and the applied pose constrains, resulted in a failure. In general, pose constraints are a useful guarantee to prevent the model from diverging, but this example shows that in extreme cases it restricted the model too much. The less restricted fully automatic algorithm actually performs better in this example.
Correlation between manually determined LV volumes and semi-automatically calculated LV volumes was excellent. In particular, the ES results were very good compared to previously reported segmentation methods for this modality [2,3] which can be attributed to the large amount of knowledge, incorporated in the model. The correlation values shown in Figure 5.7 are, to our knowledge, the best values reported until now. However, correlation values (R^2 = {0.99; 0.95; 0.84}) do not match inter-observer correlations (R^2 = {0.99; 0.98; 0.93}). Due to a lack of image information, ES volumes are generally slightly underestimated.

Quantitative evaluation results of the semi-automatic algorithm, displayed in Figure 5.6 and Table 5.2, proved to be within boundaries of inter-observer variability. The average difference and standard deviation in comparing the semi-automatic method with expert #1 contours (the expert who produced the training contours) were comparable to values obtained when comparing different experts. The ability to mimic expert drawing behavior is most particularly pronounced in Table 5.2. Differences between the semi-automatic algorithm and expert #1 are generally smaller than differences between the three experts. Furthermore, comparing line 2 with line 4 of Table 5.2 and comparing line 3 with line 5, indicates that the model has comparable behavior as expert #1. The proposed method produces results that are within limits of inter-observer variability and therefore is considered to be clinically relevant.

Also, our method outperforms other recently published methods. Suzuki's neural edge detector [6], trained on 12 ED and 12 ES images, achieved average contour errors E_C of 6.2% and 17.1% for ED and ES respectively and average area errors E_A of 4.2% and 11.6% for ED and ES respectively. The semi-automatic approach presented in this chapter needs a similar amount of user interaction and produces (after removal of the single ES segmentation failure) E_C values of 4.1% and 12.8% and E_A values of 1.9% and 6.4%, comparing favorably to Suzuki's results on all indices. Moreover, more than five times as much data was used in our evaluation.

Both the success rate and the quantitative results for the fully automatic algorithm were not as good as the semi-automatic approach. The major difficulty in fully automatic segmentation is the location of the three landmark points; upper aortic valve point, lower aortic valve point and apex. Errors for these landmarks are 3.8 mm, 4.1 mm and 3.0 mm respectively for ED and 4.4 mm, 3.8 mm and 6.2 mm for ES. Errors in these landmarks strongly influence the volume estimates using the area-length method (Equation 5.9).

In terms of accuracy, the fully automatic algorithm provided very good segmentation results, as Figure 5.9 points out. However, the rate of matching failures is significantly higher than for the semi-automatic algorithm. After removal of these failures, quantitative results are comparable to the results obtained with the semi-automatic algorithm. Although fully automatic segmentation results are promising, the semi-automatic algorithm is more robust, while the amount of user interaction remains limited.

5.6.2 Behavior of the Proposed Algorithm

Multi-View versus Single-View

Given optimal initialization, the Multi-View algorithm displays comparable results as Single-View models, as Table 5.3 points out. For ES segmentation, the Single-View model even appears to be marginally better. The benefit of the Multi-View AAM becomes evident when the initialization is not perfect. Table 5.3 clearly shows that the average contour error and the average volume error are significantly higher for the Single-View models, than for the Multi-View model. More pronounced is the difference in the standard deviations of the errors. This all corresponds with the higher amount of obvious segmentation failures, observed for the Single-View

models. One can conclude that a model that is dedicated to a specific view is only slightly better than a model dealing with multiple views, *only* when the initialization is perfect. When the initialization is less good, Multi-View AAMs are much more robust than Single-View AAMs. Segmentation of the ES frame is improved in particular, due to the coupling of shape and intensity information from both the ED phase and the ES phase.
In LV angiography strong correlation in the ventricle's pose between the ED image and the ES image is apparent. However, strict coupling of the ED and ES pose parameters seemed to excessively tie the pose parameters of the two views, hampering a correct convergence.

Controlled Gradient Descent

Using the Controlled Gradient Descent further constrains model convergence: The model adapts only one or a few model parameters, while pose parameters remain unaffected. The constraint, introduced by the Controlled Gradient Descent, results in a gradual updating of the model parameters, preventing the model from locking in on the direct underlying image features.
As expected, the Controlled Gradient Descent clearly outperforms a regular AAM, as Table 5.3 points out. It is more robust than a regular AAM and it is a proper instrument to cope with texture ambiguities and structures that are in some cases present in the image, and in some cases not.
Other solutions to this problem may be possible, such as the one proposed in [19], in which the regions in short-axis MR images where papillary muscles could possibly be visible were excluded from the model. Since in X-ray LV angiography the entire posterior wall can be obstructed by the diaphragm and the entire anterior wall can be obstructed by either a rib or a shutter-induced shadow, such a pruning technique is not suitable for automatic segmentation of X-ray angiograms. A parameter update strategy, comparable to the Controlled Gradient Descent, is presented in [21], for fitting blended 3D deformable models. First global parameters of one model are adapted, followed by parameters that blend different 3D models, and subsequently parameters that change the model's topology. In the final stages of fitting the model all parameters are released simultaneously. In this updating scheme the parameters are updated in a fixed order. The Controlled Gradient Descent, however, first decides in every iteration which parameter(s) should be regarded most significant, based on the features found in the underlying image. These parameters are updated first, resulting in a tailor-made parameter updating strategy.

Hybrid AAM and Dynamic Programming

The proposed AAM is a robust tool for global segmentation. However, because of its global nature, it lacks sufficient accuracy for correct border delineation. The result contour computed by the AAM on the other hand, creates a solid base for subsequent local segmentation by means of Dynamic Programming. Since the AAM segmentation result is already close to the desired solution (see for example the left image in Figure 5.10), the Dynamic Programming can be constrained to a small

specific area. Therefore, the proposed hybrid algorithm outperforms both an AAM and Dynamic Programming, when applied separately, as Table 5.3 indicates.
Including the subtraction image into the Dynamic Programming cost function is a way of capturing cardiac motion dynamics. The hyper-intensity area in this image strongly correlates with the area in which the ventricle boundary progresses during contraction and release. This information is essential to make Dynamic Programming a proper post-processing tool for contour refinement, as shown in Figure 5.10.

5.6.3 Clinical Applicability

The presented results prove that the semi-automatic algorithm is a highly robust and accurate method for segmentation of the left ventricle in angiograms. Both end-diastolic and end-systolic segmentation results were within boundaries of inter-observer variability. Accurate results were obtained, even when acquisition artifacts were present, such as poor contrast, overlapping diaphragm or strong shadows in the image.
A predominant feature of our algorithm is that it is trained on a large data set of clinical images and manually drawn expert contours. Therefore it inherently mimics the drawing behavior of the clinical expert. Because the model is trained on patient data the majority of pathologies can be recognized and matched during segmentation.
The method is fast (1-2 seconds per case) and needs minimal user input. After setting 6 seed points, the model produces the ED and ES contours. Subsequent manual editing of the contours should be possible in clinical practice, but little need for editing is expected.
Estimations based on experiments are that on average less than 5% of editing is needed for an automatically generated ED contour and approximately 20% editing is needed for an automatically generated ES contour. To put these numbers in perspective, based on the same conditions, expert #1 on average would redraw 2% of an ED contour drawn by expert #2, 1% of an ED contour drawn by expert #3, 14% of an ES contour drawn by expert #2 and 12% of an ES contour drawn by expert #3.
In conclusion, the semi-automatic algorithm can be a helpful and reliable tool in automated segmentation of LV angiograms in daily clinical practice. As Table 5.2 points out, a further refinement of the algorithm can be achieved by training the model on expert data from several different experts. This will result in a more solid base for creating a quality standard in segmenting LV angiograms.

5.7 Conclusions

A new algorithm for semi-automatic segmentation of the left ventricle in X-ray LV angiograms is presented. The method is a combination of a Multi-View Active Appearance Model and a locally selective Dynamic Programming approach and

exploits knowledge about LV shape, image texture and contraction dynamics. The algorithm is capable of mimicking the drawing behavior of a clinical expert and therefore provides excellent results. ES segmentation results have especially improved significantly with respect to previously reported methods, due to the coupling of statistical data for both frames. Local AAM border positioning is refined by a Dynamic Programming step in which both image information and knowledge of contraction dynamics was integrated in the cost function. Furthermore, the robustness in fully automatic segmentation has improved significantly by introducing a Controlled Gradient Descent approach in updating the model parameters, evading local minima.

The algorithm has been tested on 70 paired ED-ES images from patient studies, showing high robustness and accuracy, when compared to expert contours. Results were within boundaries of inter-observer variability and derived volume calculations were accurate and unbiased.

Although less robust than the semi-automatic algorithm, the proposed fully automatic method has shown high potential. The proposed Controlled Gradient Descent has especially shown its benefit in fully automatic segmentation.

The semi-automatic method has proven to have high relevance for daily clinical practice, in segmenting the left ventricle angiograms for the quantitative assessment of cardiac function.

References

[1] H. Sandler and H.T. Dodge, "The use of single plane angiocardiograms for the calculation of left ventricular volume in man," *American Heart Journal*, vol. 75, no. 3, pp. 325-334, 1968.

[2] S. Tehrani, T. E. Weymouth, and G. B. J. Mancini, "Model generation and partial matching of left ventricular boundaries," *Proceedings of SPIE Medical Imaging*, vol. 1445, pp. 434-445, 1991.

[3] P. Lilly, J. Jenkins, and P. Bourdillon, "Automatic contour definition on left ventriculograms by image evidence and a multiple template-based model," *IEEE Transactions on Medical Imaging*, vol. 8, no. 2, pp. 173-185, 1989.

[4] M. A. T. de Figueiredo and J. M. N. Leitão, "Bayesian estimation of ventricular contours in angiographic images," *IEEE Transactions on Medical Imaging*, vol. 11, no. 3, pp. 416-429, 1992.

[5] J. A. McDonald and F. H. Sheehan, "Ventriculogram segmentation using boosted decision trees," *Proceedings of SPIE Medical Imaging*, vol. 5370, pp. 1804-1814, 2004.

[6] K. Suzuki, I. Horiba, N. Sugie, and M. Nanki, "Extraction of left ventricular contours from left ventriculograms by means of a neural edge detector," *IEEE Transactions on Medical Imaging*, vol. 23, no. 3, pp. 330-339, 2004.

[7] C. R. Oost, B. P. F. Lelieveldt, M. Üzümcü, H. Lamb, J. H. C. Reiber, and M. Sonka, "Multi-view active appearance models: application to x-ray LV angiography and cardiac MRI," *Proceedings of Information Processing in Medical Imaging*, C. J. Taylor and J. A. Noble Eds., vol. 2732, pp. 234-245, 2004.

[8] E. Oost, B. P. F. Lelieveldt, G. Koning, M. Sonka, and J. H. C. Reiber, "Left ventricle contour detection in x-ray angiograms using multi-view active appearance models," *Proceedings of SPIE Medical Imaging*, vol. 5032, pp. 394-404, 2003.

[9] G. J. Edwards, C. J. Taylor, and T. F. Cootes, "Interpreting Face Images using Active Appearance Models," *Proceedings of the 3rd International Conference on Automatic Face and Gesture Recognition*, pp. 300-305, 1998.

[10] T. F. Cootes, G. J. Edwards, and C. J. Taylor, "Active appearance models," *Proceedings of the European Conference on Computer Vision*, H. Burkhardt and B. Neumann, Eds., vol. 2, Berlin: Springer Verlag, 1998, pp. 484-498.

[11] M. B. Stegmann, "Generative interpretation of medical images," *Kgs. Lyngby: PhD thesis Informatics and Mathematical Modelling*, Technical University of Denmark. 232 p., 2004.

[12] T. F. Cootes and C. J. Taylor, "Statistical models of appearance for computer vision," Online available: *http://personalpages.manchester.ac.uk/staff/timothy.f.cootes/Models/app_models.pdf*

[13] J. C. Gower, "Generalized procrustes analysis," *Psychometrika*, vol. 40, no. 1, pp. 33-51, 1975.

[14] T.F.Cootes, P.Kittipanya-ngam, "Comparing Variations on the Active Appearance Model Algorithm," *Proceedings of British Machine Vision Confererence*, vol.2, pp. 837-846, 2002.

[15] T.F. Cootes, G.V. Wheeler, K.N. Walker, C.J. Taylor, "View-based active appearance models," *Image and Vision Computing*, vol. 20, no. 9-10, pp. 657-664, 2002.

[16] J. G. Bosch, S. C. Mitchell, B. P. F. Lelieveldt, F. Nijland, O. Kamp, M. Sonka, and J. H. C. Reiber, "Automatic segmentation of echocardiographic sequences by active appearance motion models," *IEEE Transactions on Medical Imaging*, vol. 21, no. 11, pp. 1374-1383, 2002.

[17] R. J. van der Geest, B. P. F. Lelieveldt, E. Angelié, M. Danilouchkine, C. Swingen, M. Sonka, and J. H. C. Reiber, "Evaluation of a new method for automated detection of left ventricular boundaries in time serie of magnetic resonance images using active appearance motion model," *Journal of Cardiovascular Magnetic Resonance*, vol. 6, no. 3, pp. 609-617, 2004.

[18] G. Hamarneh and T. Gustavsson, "Deformable spatio-temporal shape models: extending active shape models to 2D+time," *Image and Vision Computing*, vol. 22, no. 6, pp. 461-470, 2004.

[19] M. B. Stegmann and D. Pedersen, "Bi-temporal 3D Active Appearance Models with Applications to Unsupervised Ejection Fraction Estimation," *Proceedings SPIE Medical Imaging*, vol. 5747 pp. 336-350, 2005.

[20] J. Montagnat, H. Delingette, N. Ayache, "A review of deformable surfaces: topology, geometry and deformation," *Image and Vision Computing*, vol. 19, no. 14, pp. 1023-1040, 2001.

[21] D. DeCarlo and D. Metaxas**, "**Blended deformable models," *IEEE Transactions on Pattern Analysis and Machine Intelligence*, vol. 18, no. 4, pp. 443-448, 1996.

[22] S. C. Mitchell, B. P. F. Lelieveldt, R. J. Van der Geest, H. G. Bosch, J. H. C. Reiber, and M. Sonka, "Multistage hybrid active appearance model matching: segmentation of left and right ventricles in cardiac MR images," *IEEE Transactions on Medical Imaging*, vol. 20, no. 5, pp. 415-423, 2001.

[23] J. H. C. Reiber, L. R. Schiemanck, P. M. J. van der Zwet, B. Goedhart, G. Koning, M. Lammertsma, M. Danse, J. J. Gerbrands, M. J. Schalij, and A. V. G. Bruschke, "State of the Art in Quantitative Coronary Arteriography as of 1996," In: J. H. C. Reiber and E. E. van der Wall editors. *Cardiovascular Imaging*, Dordrecht: Kluwer Academic Publishers, pp. 39-56, 1996.

細心の
'careful'

Chapter 6

Automated Left Ventricular Delineation in X-Ray Angiograms: A Validation Study

This chapter was adapted from:
Automated Left Ventricular Delineation in X-ray Angiograms: A Validation Study
E. Oost, P.V. Oemrawsingh, J.H.C. Reiber, and B.P.F. Lelieveldt
Accepted for publication in Catheterization and Cardiovascular Interventions

Abstract

Recently an automated analysis approach for X-ray left ventricular (LV) angiographic studies was proposed. This particular study aims to assess the clinical potential of this approach. Over the past 30 years much research has been carried out to develop a technique with automated contour detection of the left ventricular outline in the end-diastolic (ED) and end-systolic (ES) phases. Very few have made it into clinical practice. Our latest approach is based on innovative model-based image processing techniques. Two expert cardiologists analyzed 30 patient studies both by contouring the LV manually and by using the proposed automated methodology. In the latter procedure the experts were allowed to edit the automatically generated contours manually. The manual, automatic and edited automatic contours were compared, focusing on accuracy, workflow efficiency and inter- and intra-observer variabilities. No significant differences between the automatically derived and manual LV volumes were observed. The average patient study analysis time was reduced by 26%, from 4.2 to 3.1 minutes. When editing was required, 19% of the ED and 25% of the ES contour length needed manual correction. Furthermore, a reduction in inter-observer variability of 12.4% was observed. Employing the proposed automated methodology for X-ray LV angiographic study analysis, a considerable reduction in required analysis time and manual effort is achieved. Since the acquired results are of clinically acceptable quality and the inter- and intra-observer variabilities are reduced, this automated approach has the potential to optimize the analysis workflow for X-ray LV angiography in clinical practice.

6.1 Introduction

A quick and reliable assessment of cardiac function is essential in the diagnosis of patients with ischemic heart disease and possible heart failure. Various imaging modalities are available in clinical routine. Echocardiography is used for quick assessment of global cardiac function and valvular dysfunction. Both MRI and CT are evolving towards reliable standards for cardiac imaging based on the fact that the heart anatomy is available in three dimensions. Nonetheless, X-ray left ventricular (LV) angiography still is a widely used technique, due to it's high spatial resolution and widespread clinical availability. The left ventricular angiogram is acquired during each cardiac catheterization procedure and provides essential information for the (interventional) cardiologist and cardiac surgeon.

An objective and reproducible assessment of the cardiac ejection fraction requires the delineation of the left ventricular outline in the end-diastolic and end-systolic frames, and the subsequent calculation of the corresponding volumes, from which the ejection fraction can be derived [1]. Once the outlines are available other regional parameters can be derived as well.

Despite a higher resolution in comparison with MR or CT images, the general image quality in LV angiography is relatively low. Since it is a projection image, other anatomical structures, such as ribs or the diaphragm (when a patient cannot

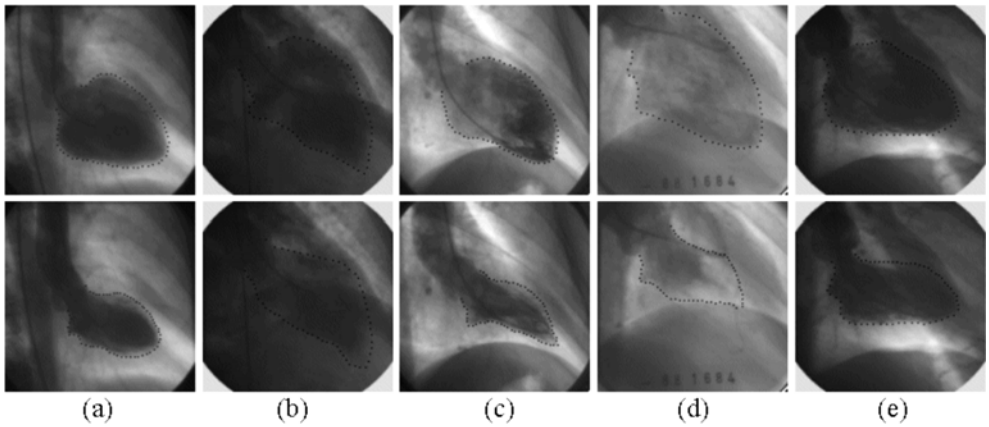

Figure 6.1: Typical examples of LV angiograms (upper row = ED; bottom row = ES): good contrast (a), poor contrast (b), uneven contrast agent distribution (c), partial overlap with the diaphragm (d) and substantial shadows caused by the shutter (e), expressed in this example as a diagonal dark band. The black dotted lines represent the LV boundaries as determined manually by an expert.

comply with the requirement of breath holding), can occlude the left ventricle in an X-ray projection. Additionally, shadows induced by the shutter of the imaging device may overlap with the LV, making the LV border harder to delineate. The biggest problem with LV angiography border detection however, is the presence of the trabeculations and the papillary muscles. Depending on the amount of contrast still visible between these trabeculations, it is difficult to decide where the actual boundary lies. All these challenging aspects make the analysis of LV angiograms difficult, time consuming and prone to inter- and intra-observer variability (Figure 6.1).

Over the past 30 years various approaches have been developed for the automated delineation of the left ventricular contours [2-16]. The fact that so many researchers have attempted to solve this problem over such a long period underlines that it is a difficult image recognition problem. One of the main recurrent conclusions in recent literature is that this challenge of achieving a sufficiently high degree of robustness, that is acceptable in clinical practice, cannot be solved without a priori knowledge about the ventricular shape. One such method with a limited amount of a priori information was developed towards a commercial application [8]. However, our approach represents a next generation in automated LV analysis [16]. The method, based on Active Appearance Models [17,18], has been described and technically validated in [16]. This paper illustrated excellent results and, as the main conclusion, showed the algorithm's capacity of mimicking the drawing behavior of expert cardiologists. However, it did not investigate any improvements in analysis speed and workflow in a clinical setting.

The goal of this chapter is to investigate the clinical efficacy of this novel methodology. To this end the algorithm was incorporated in a clinical software package to evaluate three performance aspects:

- Speed and efficiency of the workflow.
- Accuracy with respect to manual analysis.
- Inter- and intra-observer variability.

On all these points a quantitative comparison between the automated system and the manual analyses has been carried out. The software package that has been used in these experiments is the QAngio® XA package by Medis medical imaging systems B.V., which until recently only provided manual contour drawing facilities.

6.2 Materials and Methods

6.2.1 Image Data Acquisition and Processing

Thirty randomly selected patient studies, all acquired at the department of cardiology at the Leiden University Medical Center (LUMC) for diagnostic purposes, were evaluated. These cases were selected from the data base of the department, and served only for validation purposes in this study; as a result, informed patient consent was not necessary. All studies were single-plane 30° right anterior oblique view acquisitions. Each study was a full image run consisting of approximately seven to nine cardiac cycles, covering the arrival and washout of the contrast fluid. Two eligibility criteria were pursued in the data selection and analysis procedure: within an angiographic image sequence there should be at least one pair of an ED frame and subsequent ES frame available in which, according to the cardiologist, the ventricle was acceptably filled with contrast medium. Furthermore the upper valve point, lower valve point and apical point should be visible in and around the two frames that were to be evaluated.
Two expert cardiologists examined the data set in two ways: first by drawing the ED and ES contours manually on a LV workstation, and second by using the automatic method presented in [16]. In the latter situation, the cardiologists were allowed to edit the contours when the delineation was not fully satisfactory. To prevent possible influence of the automatically generated contour on the drawing behavior of the expert, the experts were asked to perform the manual contouring first.

6.2.2 Automatic Contour Detection

Automating the process of delineating the left ventricle in X-ray angiograms cannot be achieved without the integration of a priori information. Knowledge about the expected shape and image intensity characteristics of the LV is essential. This knowledge can be captured and described by an Active Appearance Model (AAM), which is a statistical model trained on information from a large data set of manually delineated example images. When applying such a model to

automatically detect, for example, an anatomical structure in a medical image, the model deforms its shape and image intensity representation to optimally fit the underlying image. By maintaining these deformations within the statistical boundaries of the training data set, only plausible shapes are found.

AAMs have been widely applied in segmenting medical images, as summarized in [19]. As mentioned previously, in X-ray angiography the left ventricle is notoriously difficult to segment in the ES image frame and in general AAMs will perform poorly in these images. To improve the automatic delineation results, Multi-View AAMs have been created, in which the shape and intensity of the LV in both the ED and the ES frame have been modeled in a combined fashion [14-16]. As Oost *et al.* described, this combined modeling improves the overall segmentation results significantly [16].
It is generally known that AAMs are a very strong tool for fitting the model globally to the object of interest. However, when no clear edges are available, or the overall contrast of the image is not optimal, the local border delineation results are not satisfactory. In the method described by Oost *et al.* and used in this study, local border detection is improved dramatically by using a dedicated Dynamic Programming algorithm as a post-processing step, in which both image information and LV motion characteristics are incorporated [16]. A general and elaborate description of AAM training and matching can be found in [18].

The AAM used in this validation study was constructed from 65 ED example images and 65 ES example images in which the LV contours were drawn manually by an expert cardiologist.

6.2.3 Analysis Workflow

Manual Workflow
In manual patient study analysis, the expert cardiologists were asked to first calibrate the image data by means of catheter calibration, then select a properly displayed ED frame, draw a contour curve delineating the LV using the workstation's mouse, select the subsequent ES frame, and once again delineate the LV. After these actions the mitral valve position could be adjusted along the drawn contour and a pane, containing the calculated ejection fraction and the results of a set of wall motion models (Slager model, centerline model and Stanford model), was presented to the user for evaluation purposes. After inspection of this pane the study was saved and closed.

Automated Workflow
When analyzing the image sequences automatically, the workflow was similar, apart from the drawing activities: after selecting the ED frame, the upper valve point, lower valve point and apical point had to be localized by mouse-clicks. This could be done in arbitrary order. Subsequently the ES frame was selected. After again identifying the upper valve point, lower valve point and apical point, the program automatically started the automatic delineation of both ED and ES

frames. Generated contours could be edited by redrawing unsatisfactory contour regions manually with the mouse. Further handling was identical to the fully manual investigation of a patient study.

Time Recording
During all analyses, the software package created a log file in which the timing of activities was recorded. This data was used to evaluate differences in time requirements between the manual and automatic segmentation of the LV. Hence, experts were asked to perform all examinations in a fluent fashion, without other activities intervening.

6.2.4 Comparison Metrics and Statistical Analysis

In terms of generated ED and ES contours, the output of this study is threefold: manually drawn contours, automatically generated contours and edited automatic contours. Differences in accuracy and required time are presented by comparing these contours interdependently, in terms of the following quantified metrics.

Time Requirement
Two measures were used to assess differences in time requirements between manual and automated analysis of patient studies. First, a comparison was performed of the time interval from the start of the drawing (manual analysis) or landmark identification (automated analysis) in the ED frame until acceptance of both ED and ES contours. Second, the entire time required from opening a study until closing the study was evaluated. Because a different approach in contour generation might lead to different evaluation of the quantified clinical data by the expert cardiologists, the total study duration can provide additional insight. From hereon these two time periods will be referred to as 'LV function analysis duration' and 'total study duration'.

Volumetric Comparison
Estimating LV volumes from drawn contours was done by means of Sandler and Dodge's area-length method [1], formulated as:

$$V = \frac{8A^2}{3\pi L_A} \tag{6.1}$$

in which A denotes the projected surface area and L_A is the distance from the upper aortic valve point to the apex. To correct for shape irregularities and the presence of papillary muscles and trabeculations, a regression equation was applied [20]. Linear regression and Bland-Altman analysis were used to determine volume and ejection fraction relationships between manually traced, computer determined and edited automatic LV outlines. A two-tailed paired samples t-test was applied to investigate systematic errors, where a p-value smaller than 0.05 was considered statistically significant.

Contour Comparison
All drawn or calculated contours are defined as a discrete set of points. When comparing two differently generated contours with each other, point-to-curve differences were measured mutually and averaged. A point-to-curve distance is herein defined as the geometrical distance from a single discrete point of contour A to the closest interpolated position on contour B.
An additional measure is the percentage of the contour length that was edited manually. This percentage represents the amount of effort required to achieve clinical quality contours in cases where the automatic contours are sub-optimal. When comparing an edited automatic contour with an automatically generated contour, the percentage of required editing can be simply derived. However, when comparing the manually drawn contours with the edited automatic contours, both could be regarded as gold standard, because both contours have been approved by the expert. The same holds when comparing a contour approved by expert cardiologist #1 with a contour ratified by expert cardiologist #2. To evaluate this, a comparison was made of the amount of editing when for example expert cardiologist #1 would evaluate a contour generated by expert cardiologist #2. A point-to-curve distance exceeding 8 pixels (i.e. approximately 2 mm.), persisting over at least 3 percent of the total contour length, was defined as the threshold for editing requirement. This definition is designed to include significant local detail differences, while longer contour parts with insignificantly low point-to-curve differences are excluded.

6.3 Results

Evaluation of the results was carried out on 29 of the 30 initial data sets. After inspection one outlier was detected in which the apical area of the LV moved out of the image frame. All experiments related to automatic or edited automatic contours of MD #1 comprise of 28 data sets, due to an error in saving one of the studies.
Although all studies were calibrated 4 times (before manual analysis and before automated analysis, by 2 MDs), the average calibration factor of 0.273 mm/pixel was used for comparison purposes.

6.3.1 Ejection Fraction and Volumetric Accuracy

To asses the clinical validity of the proposed automated method, the calculated ED and ES volumes and the calculated ejection fractions were compared with the manual contour analysis results.
Excellent correlation was found when comparing the manual and edited automatic results, with all correlation coefficients larger than $R^2 = 0.95$ (Table 6.1). All comparisons were found statistically insignificant: $p = 0.19$ (ED) and $p = 0.08$ (ES) when analyzed by expert cardiologist #1 and $p = 0.57$ (ED) and $p = 0.05$ (ES) for expert cardiologist #2. Bland-Altman plots showed a slight but statistically non-significant overestimation of ES volumes, when using the automated method. For

ED no clear over- or underestimation could be observed (Figure 6.2). Bland Altman analysis did not show dependence of the error on LV volume.

Also for the ejection fractions good correlation was achieved, with correlation coefficients $R^2 = 0.92$ for expert cardiologist #1 and $R^2 = 0.94$ for expert cardiologist #2 (Table 6.1, Figure 6.3). In a paired samples t-test, differences were found to be statistically insignificant ($p = 0.06$) for expert #1 and significant ($p = 0.02$) for expert #2. The good correlation is supported by the small difference in the derived ejection fraction between manual and edited contours, which is approximately 2% ejection fraction for both experts (Table 6.2).

6.3.2 Workflow Speed

In 23 out of 29 cases, MD #1 was able to analyze a patient in a shorter time period with the presented automated algorithm than by drawing contours by hand. For MD #2 this figure was 23 out of 28 cases, since the audit trail showed discontinuity in the workflow in one case. The speed gain in terms of LV function analysis duration was 15.7%. The average total study duration even decreased with 26.1% when using the automated method (Table 6.3).

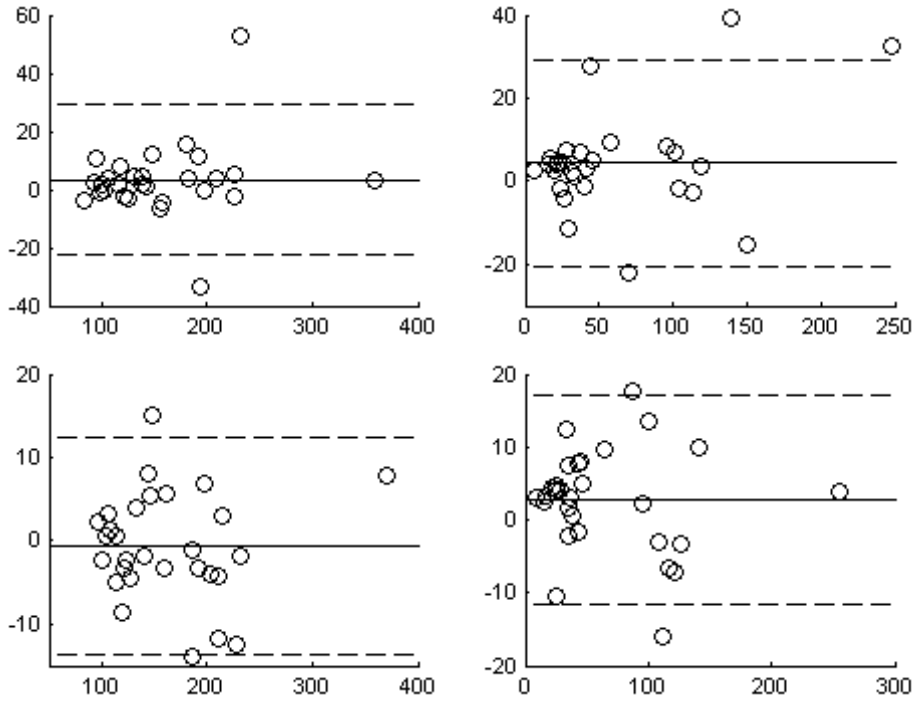

Figure 6.2: Bland-Altman analysis of manual and edited automatic volumes. The top row shows the results for expert #1, the bottom row shows expert #2 results. The ED results are shown on the left-hand side, the ES results are shown on the right. y-axes denote edited minus manual, x-axes denote averages.

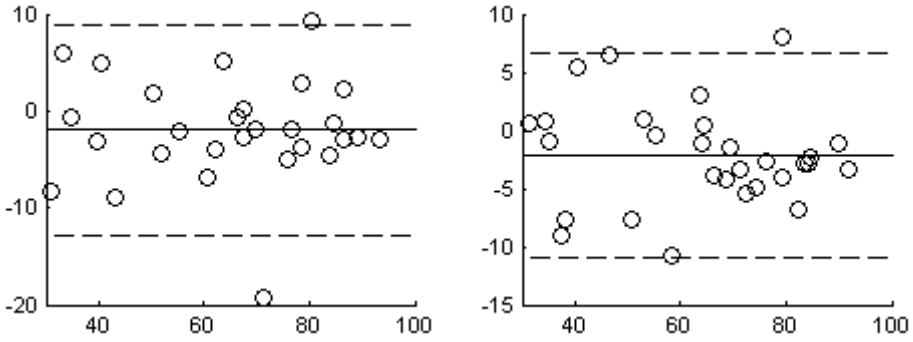

Figure 6.3: Bland-Altman analysis of manual and edited automatic ejection fractions, for expert #1 (left) and expert #2 (right). y-axes denote edited minus manual, x-axes denote averages.

	MD	Regression Equation	R^2	p
Edit vs. Man ED	1	y = 1.01x + 1.38 [ml]	0.96	0.19
Edit vs. Man ES	1	y = 1.06x + 0.99 [ml]	0.96	0.08
Edit vs. Man EF	1	y = 0.96x + 0.74 [%]	0.92	0.06
Edit vs. Man ED	2	y = 0.99x + 0.57 [ml]	0.99	0.57
Edit vs. Man ES	2	y = 0.98x + 4.21 [ml]	0.98	0.05
Edit vs. Man EF	2	y = 0.95x + 1.13 [%]	0.94	0.02
Auto vs. Edit ED	1	y = 0.99x + 4.13 [ml]	0.98	0.12
Auto vs. Edit ES	1	y = 0.97x + 6.59 [ml]	0.98	0.01
Auto vs. Edit ED	2	y = 1.05x – 7.34 [ml]	0.98	0.47
Auto vs. Edit ES	2	y = 0.93x + 4.73 [ml]	0.98	0.94
Auto vs. Man ED	1	y = 1.01x + 3.99 [ml]	0.96	0.03
Auto vs. Man ES	1	y = 0.98x + 9.70 [ml]	0.93	0.01
Auto vs. Man ED	2	y = 1.04x – 5.48 [ml]	0.95	0.80
Auto vs. Man ES	2	y = 0.91x + 9.13 [ml]	0.98	0.06

Table 6.1: Correlation statistics.

6.3.3 Manual Correction Effort

The majority of the automatically generated ED contours was accepted without further manual editing. Expert #1 accepted 15 out of 28 contours directly, expert #2 accepted 19 out of 29 contours. For the ES contours these numbers were 2 and 4 for expert #1 and expert #2 respectively.
When editing was required, on average 18.7% of the total ED contour length was corrected manually (14.6% for MD #1 and 22.9% for MD #2). For ES on average 25.3% of the total contour length was adjusted (26.0% for MD #1 and 24.6% for MD #2).

6.3.4 Inter- and Intra-Observer Variability

For both ED and ES the difference between edited automatic and automatic contours on average is smaller than the difference between manual and automatic

	Auto vs. Edit [%]	Man vs. Auto [%]	Man vs. Edit [%]
MD #1	-4.6 ± 11.8	6.6 ± 12.2	2.0 ± 5.4*
MD #2	-0.7 ± 7.8*	2.8 ± 7.9*	2.1 ± 4.4

Table 6.2: Signed differences in ejection fraction in comparing manual, automatic and edited automatic results. Numbers denote average ± standard deviation, asterix marks statistical significance.

	LV function analysis duration			Total study duration		
	Man [s]	Auto [s]	Gain [%]	Man [s]	Auto [s]	Gain [%]
MD #1	146.7	135.3	7.7	251.2	201.9	19.6
MD #2	166.1	127.9	23.0	254.6	171.3	32.7
Average	156.2	131.7	15.7	252.9	186.9	26.1

Table 6.3: Average LV function analysis duration and average total study duration.

	Inter-Obs, Man	Inter-Obs, Edit	Intra-Obs, Expert #1	Intra-Obs, Expert #2	Auto vs. Edit
ED	0.74 ± 0.21	0.64 ± 0.45	0.80 ± 0.23	0.84 ± 0.32	0.46 ± 0.83
ES	1.48 ± 0.60	1.33 ± 0.95	0.93 ± 0.21	1.24 ± 0.46	1.06 ± 0.85

Table 6.4: Point-to-curve differences [mm].

contours (Table 6.2). Hence, this indicates that the automatic method introduces a bias on the (ratified) edited automatic contours, which reduces the inter-observer variability. Furthermore, the average point-to-curve differences between expert cardiologists #1 and #2, for the manual contours and the edited automatic contours were evaluated (Table 6.4, first two columns). For both ED and ES the inter-observer variability is lower for the edited automatic contours. For ED the variability is 0.64 mm (vs. 0.75 mm for the manual contours), for ES it is 1.33 mm (vs. 1.48 mm for the manual contours).
When comparing the manually drawn contours with the edited automatic contours for both experts, the average intra-observer variability is 0.82 mm for ED and 1.08 mm for ES (Table 6.4, columns three and four).
All results for inter- and intra-observer variability are based only on comparisons of studies in which exactly the same ED or ES frame was selected for analysis.

6.3.5 Accuracy of the Automatic Contours

The fully automatic contours for ED and ES LV delineation, generated by the presented algorithm, are the base for the clinically approved edited automatic contours. As the previous section suggests, these automatic contours introduce a

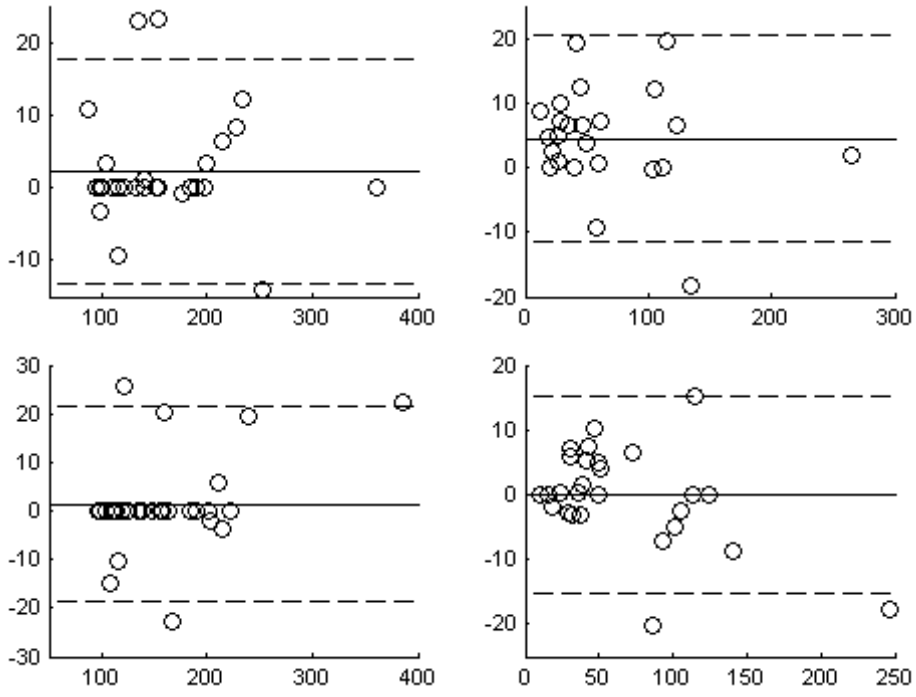

Figure 6.4: Bland-Altman analysis of automatic and edited automatic volumes. The top row shows the results for expert #1, the bottom row shows expert #2 results. The ED results are shown on the left-hand side, the ES results on the right. y-axes denote automatic minus edited, x-axes denote averages.

bias. It is therefore essential that the quality of the contours presented by the algorithm approximate the level of clinical acceptance.
The success rate for automatic segmentation was 100% for ED for both experts and 86% (expert #1, 4 failures) and 93% (expert #2, 2 failures) for ES. A segmentation failure was defined as when the volume difference was above 30% and the point-to-curve difference was more than 3 mm.
Corresponding volumetric differences between the automatically generated contours and both ratified contours were low (Table 6.1, Figure 6.4, Figure 6.5). Overall correlation coefficients between automatic and edited automatic results were high (R^2 = 0.98 for all results), with p-values of 0.12 (ED MD #1), 0.01 (ES MD #1), 0.47 (ED MD #2) and 0.94 (ES MD #2). Bland-Altman plots showed a slight overestimation of the automatic volumes of approximately 2 ml for both ED and ES, with respect to the edited volumes (Figure 6.4).
When comparing the automatic results with the manual contours, the correlation coefficients dropped somewhat (R^2 = {0.98; 0.93; 0.95; 0.98} for ED MD #1, ES MD #1, ED MD #2, ES MD #2 respectively), yet the correspondence still was good, with p-values of 0.03 (ED MD #1), 0.01 (ES MD #1), 0.80 (ED MD #2) and 0.06 (ES MD #2). A slight overestimation of the automatic volumes of approximately 3 ml (ED) and 6 ml (ES) could be derived from the Bland-Altman analysis (Figure 6.5).

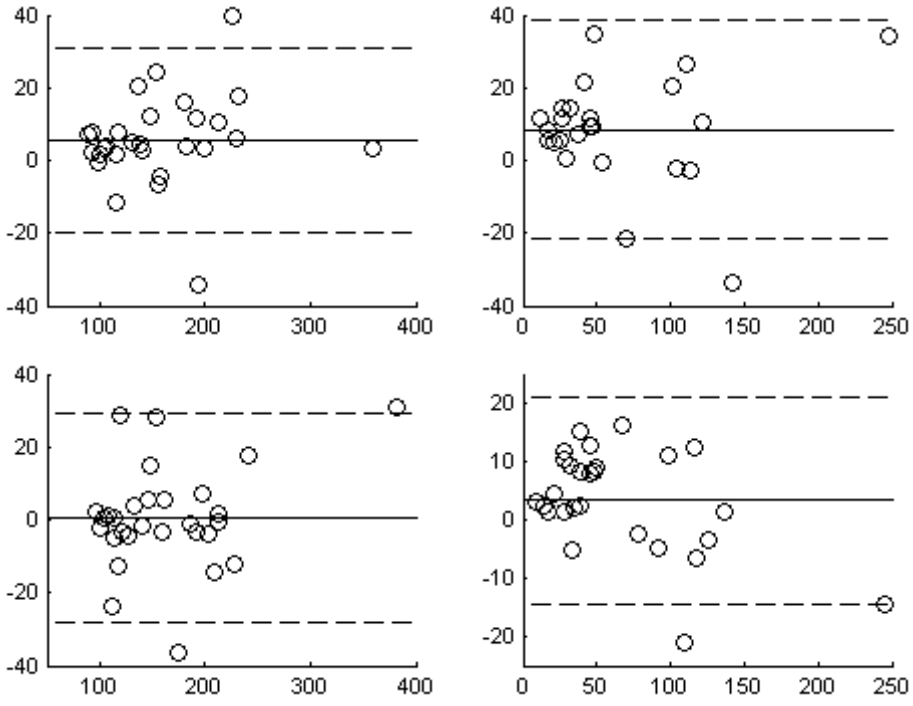

Figure 6.5: Bland-Altman analysis of automatic and manual volumes. The top row shows the results for expert #1, the bottom row shows expert #2 results. The ED results are shown on the left-hand side, the ES results are shown on the right. y-axes denote automatic minus manual, x-axes denote averages.

The average point-to-curve differences between the automatic and the edited automatic contours, combined for both expert cardiologists is an additional measure to determine the accuracy of the automated method. These differences (0.46 mm for ED and 1.06 mm for ES) are generally equal to or smaller than the reported inter- and intra-observer variability results (Table 6.4, right column).

6.4 Discussion

6.4.1 Accuracy of the Volumetric Measurements

The experiments presented in this chapter provide two reference standards for delineation of the left ventricle in X-ray angiograms. First, the manually drawn contours by the expert cardiologists and second, the edited automatic contours. Both types of contours were approved by the expert cardiologists as valid LV delineation.
For the most relevant clinical parameter, the ejection fraction, there is an excellent correlation between the manual results and the results based on the approved edited automatic contours (Table 6.1, Figure 6.3). This holds for the calculated ejection fractions by both cardiologists. For cardiologist #1, there was no statistically significant difference between the two approaches, meaning that the edited automatic contours could be regarded as an equally reliable gold standard as the manual contours. The p-value of 0.02 for expert cardiologist #2 does not directly support this conclusion.
Nonetheless, when concentrating on the correspondence between the calculated ED and ES volumes, from which the ejection fractions are derived, the correlation coefficients were even higher than the ones found for the ejection fraction (Table 6.1, Figure 6.2). Specifically the results for cardiologist #2 (R^2 = 0.99 for ED and R^2 = 0.98 for ES) were excellent. Since in the paired samples t-test differences between manually and semi-automatically calculated ED and ES volumes were found statistically insignificant for both expert cardiologists, the edited automatic contours can be regarded as an equally reliable gold standard as the manual contours.

6.4.2 Workflow Optimization

The previous section shows that the presented method provides robust, accurate and clinically acceptable performance. However, aspects such as the speed of the workflow and the amount of manual effort are equally important for clinical acceptance.
The proposed method dramatically reduces the amount of manual contouring. 60% of all automatically generated ED contours and 11% of all automatically generated ES contours did not need any further manual editing. Furthermore, when editing was required, the average amount of manual editing was 18.7% of the total contour length for ED and 25.3% of the total contour length for ES.

When using the proposed method, the average speed gain in LV function analysis duration was recorded at 15.7%. The speed gain in total study duration even amounted to 26.1%, reducing the total amount of time spent on analyzing one patient from, on average, 253 seconds (= 4 minutes and 13 seconds) to 187 seconds (3 minutes and 7 seconds). The additional gain in total study analysis is difficult to explain. Possibly the initially generated automatic contours influence the interpretation of the experts such that it results in a faster analysis: because they are immediately dealing with a set of contours, they are converging towards an image interpretation in an earlier stage of the workflow.
Given the fact that both expert cardiologists were fully familiar with the manual workflow, while the automated workflow was new to them, it is likely to expect an even further decrease in patient analysis time in routine clinical practice.

6.4.3 Inter- and Intra-Observer Variability Decrease

Compared to manual analysis, introducing an automated method that is dedicatedly trained on delineating anatomical structures in medical images should theoretically reduce the inter- and intra-observer variability in patient analysis.
Regarding the inter-observer variability, the average point-to-curve difference between both expert cardiologists dropped from 0.75 ± 0.23 mm to 0.64 ± 0.45 mm for ED and from 1.48 ± 0.60 mm to 1.33 ± 0.95 mm for ES.
Furthermore, the introduction of a bias can evidently be derived: the differences between automatic contours and edited automatic contours generally are smaller than differences between automatic contours and manual contours (Table 6.2). This bias supports the suggestion that the presented automated algorithm does reduce the inter-and intra-observer variability.
Finally, one can argue that the introduction of a bias is not necessarily a good development. Nevertheless, the generated contours are edited and/or ratified by an expert and the resulting clinical parameters are not significantly affected.
The intra-observer variability was measured by comparing the manual results with the edited automatic results, but this could only be used to assess the quality of the automatically generated contours. Nonetheless, given the fact that the inter-observer variability did decrease when using the automated algorithm, a similar trend can be expected for the intra-observer variability.

6.4.4 Accuracy of the Automatic Contours

The previous sections show that the results of the presented automated algorithm are of clinically acceptable quality, can be generated faster in comparison with manual contour drawing and have the capacity to reduce the inter- and intra-observer variability. These results are a combination of automatically generated contours and, possibly, additional manual editing. Since there is a large automatic component in the presented method that evidently influences the expert cardiologists, a more thorough investigation of the accuracy of the automatically generated contours is desired.

The described method is incorporated in the QAngio® XA package marketed by Medis medical imaging systems B.V. and has been subject to a thorough technical validation by Oost *et al.* [16]. Another available commercial package for automated contouring of ventriculograms, the CAAS LVA package, is marketed by Pie Medical Imaging B.V. The methodology used in the CAAS LVA package is mainly based on Dynamic Programming [8]. The methodology described by Oost *et al.* is a hybrid algorithm in which statistical modeling and Dynamic Programming are combined. It has been proven that this hybrid approach outperforms the individual application of Dynamic Programming alone [16]. The high degree of accuracy of the hybrid approach by Oost *et al.* is corroborated by the results in this clinical validation study. Good agreement was found between the automatically derived ED and ES volumes and both reference standards (Table 6.1, Figure 6.4, Figure 6.5).
Looking at the point-to-curve difference between automatic contours and edited automatic contours, the quality of the automatic contours is even more apparent. Both the ED and the ES results (0.46 mm and 1.06 mm) are well within the measured ranges for inter-observer variability (0.64 - 0.74 mm for ED and 1.33 - 1.48 mm for ES) and within the ranges of the averaged intra-observer variability for expert #1 and expert #2 (0.82 mm for ED and 1.09 mm for ES).
Furthermore, the presented results for inter-observer variability are based on study comparisons in which the frame selection was identical. However, in clinical practice different MDs will select different frames to be analyzed, either because they have a different judgment on the exact time point for ED or ES, or because they consider a different cardiac cycle to be optimal for patient analysis. Hence, numbers on inter- and intra-observer variability will be higher in practice than those reported in this study.

6.5 Conclusions

An automated methodology was presented to delineate the left ventricular contours in the ED and ES phases in X-ray LV angiograms. The method proved to be accurate and the results were highly similar to the manually traced outlines, which were regarded to be the gold standard. The method significantly reduced the analysis workload by diminishing the necessary amount of manual contouring and by considerably reducing the average time required for a patient analysis. Moreover, the algorithm reduced the inter- and intra-observer variability. The presented results indicate that this automated approach has the potential to optimize the analysis workflow for X-ray LV angiography in clinical practice.

References

[1] H. Sandler and H. T. Dodge, “The use of single plane angiocardiograms for the calculation of left ventricular volume in man,” *American Heart Journal*, vol. 75, no. 3, pp. 325-334, 1968.

[2] C. K. Chow and T. Kaneko, “Automatic boundary detection of left ventricle from cineangiograms,” *Computers and Biomedical Research*, vol. 5, no. 4, pp. 388-410, 1972.

[3] P. D. Clayton, L. D. Harris, S. R. Rumel, and H. R. Warner, “Left ventricular videometry,” *Computers and Biomedical Research*, vol. 7, no. 4, pp. 369-379, 1974.

[4] C. J. Slager, J. H. C. Reiber, J. C. H. Schuurbiers, and G. T. Meester, “Automated detection of left ventricular contour. Concept and application,” in Heintzen, P. H. and Bursch, J. H. (eds.) *Roentgen-Video-Techniques for dynamic studies of structure and function of the heart and circulation.* Stuttgart: Georg Thieme Publishers, 1978, pp. 158-167.

[5] C. J. Slager, J. H. C. Reiber, J. C. H. Schuurbiers, and G. T. Meester, “Contouromat – A hard-wired left ventricular angio processing system. I. Design and application,” *Computers and Biomedical Research*, vol. 11, no. 5, pp. 491-502, 1978.

[6] J. H. C. Reiber, C. J. Slager, J. C. H. Schuurbiers, and G. T. Meester, “Contouromat – A hard-wired left ventricular angio processing system. II. Performance evaluation,” *Computers and Biomedical Research*, vol. 11, no. 5, pp. 503-523, 1978.

[7] D. L. Pope, D. L. Parker, P. D. Clayton, and D. E. Gustafson, “Left ventricular border recognition using a dynamic search algorithm,” *Radiology*, vol. 155, no. 2, pp. 513-518, 1985.

[8] P. N. J. van der Zwet, G. Koning, and J. H. C. Reiber, “Left ventricular contour detection: a fully automated approach,” *Computers in Cardiology*, pp. 359-362, 1992.

[9] S. Tehrani, T. E. Weymouth, and G. B. J. Mancini, “Model generation and partial matching of left ventricular boundaries,” *Proceedings of SPIE Medical Imaging*, vol. 1445, pp. 434-445, 1991.

[10] P. Lilly, J. Jenkins, and P. Bourdillon, “Automatic contour definition on left ventriculograms by image evidence and a multiple template-based model,” *IEEE Transactions on Medical Imaging*, vol. 8, no. 2, pp. 173-185, 1989.

[11] M. A. T. de Figueiredo and J. M. N. Leitão, "Bayesian estimation of ventricular contours in angiographic images," *IEEE Transactions on Medical Imaging*, vol. 11, no. 3, pp. 416-429, 1992.

[12] J. A. McDonald and F. H. Sheehan, "Ventriculogram segmentation using boosted decision trees," *Proceedings of SPIE Medical Imaging*, vol. 5370, pp. 1804-1814, 2004.

[13] K. Suzuki, I. Horiba, N. Sugie, and M. Nanki, "Extraction of left ventricular contours from left ventriculograms by means of a neural edge detector," *IEEE Transactions on Medical Imaging*, vol. 23, no. 3, pp. 330-339, 2004.

[14] E. Oost, B. P. F. Lelieveldt, G. Koning, M. Sonka, and J. H. C. Reiber, "Left ventricle contour detection in x-ray angiograms using multi-view active appearance models," *Proceedings of SPIE Medical Imaging*, vol. 5032, pp. 394-404, 2003.

[15] C. R. Oost, B. P. F. Lelieveldt, M. Üzümcü, H. Lamb, J. H. C. Reiber, and M. Sonka, "Multi-view active appearance models: application to x-ray LV angiography and cardiac MRI," *Proceedings of Information Processing in Medical Imaging*, C. J. Taylor and J. A. Noble Eds., vol. 2732, pp. 234-245, 2004.

[16] E. Oost, G. Koning, M. Sonka, P. V. Oemrawsingh, J. H. C. Reiber, and B. P. F. Lelieveldt, "Automated contour detection in x-ray left ventricular angiograms using multiview active appearance models and dynamic programming," *IEEE Transactions on Medical Imaging*, vol. 25, no. 9, pp. 1158-1171, 2006.

[17] T. F. Cootes, G. J. Edwards, and C. J. Taylor, "Active appearance models," *Proceedings of the European Conference on Computer Vision*, H. Burkhardt and B. Neumann, Eds., vol. 2, Berlin: Springer Verlag, 1998, pp. 484-498.

[18] T. F. Cootes and C. J. Taylor, "Statistical models of appearance for computer vision," Online available: *http://personalpages.manchester.ac.uk/staff/timothy.f.cootes/Models/app_models.pdf*

[19] M. B. Stegmann, "Generative interpretation of medical images," *Kgs. Lyngby: PhD thesis Informatics and Mathematical Modelling*, Technical University of Denmark. 232 p., 2004.

[20] J. H. C. Reiber, A. R. Viddeleer, G. Koning, M. J. Schalij, and P. E. Lange, "Left ventricular regression equations from single plane cine and digital x-ray ventriculograms revisited," *International Journal of Cardiac Imaging*, vol. 12, no. 2, pp. 69-78, 1996.

会心
‘satisfaction’

Chapter 7

Summary and Conclusions

7.1 Summary

The high prevalence of cardiovascular diseases worldwide underlines the importance of cardiac imaging based diagnostics. In assessing cardiac function, X-ray left ventricular angiography has been an important clinical standard for years and, despite the rapid development of both MRI- and MSCT-based techniques, it is expected to retain high value in daily clinical practice. As long as X-ray coronary angiography is employed during cardiac catheterization procedures, X-ray LV angiograms will be acquired most often in the same session as well. However, the manner in which LV angiograms are currently analyzed leaves room for improvement. The expert cardiologist either visually inspects the patient image data, estimates the cardiac ejection fraction and observes possible wall motion defects. Alternatively, patient analysis requires the manual delineation of the endocardial boundary in both the end diastolic and end systolic image frames. The latter method obviously is preferable, because it introduces a certain diagnostic standard and it enables patient follow-up studies. However, manual contouring is characterized by a high workload for the cardiologist or technician, it is time consuming and prone to inter- and intra-observer variabilities. The need for an automated technique for the analysis of X-ray LV angiograms therefore has been apparent for a long time.

The main goal of the work presented in this thesis was to develop an automated algorithm for the delineation of the cardiac left ventricle in the ED and ES phase in X-ray LV angiography, that would be robust enough so that it can be used in routine clinical practice. The general approach to achieve a higher degree of automation in the interpretation of X-ray LV angiographic images is based on the application of Active Appearance Models. With these statistical models of shape and appearance, an automatic delineation of the left ventricle can be realized. This thesis has identified both the challenges of automatic interpretation of X-ray LV angiograms, and the limitations of Active Appearance Models in general and in their application to segment the left ventricle in angiographic images. In exploring possible ways of solving this medical image processing problem, the following sub-goals were formulated in Chapter 1:

- The observed redundancies and similarities between the ED and ES frames should be exploited by a combined modeling of the shape and image intensity characteristics of both frames in the AAM framework.

- The sensitivity of AAM segmentation with respect to the unstable behavior of the error criterion should be decreased.

- Optimal settings regarding the size and composition of the model training data set must be investigated to increase AAM segmentation performance.

- The effect of model over-constraining towards the training data should be neutralized to improve local LV border delineation.

- The clinical relevance of the developed methodology should be demonstrated.

Chapters 2 through 6 provide a detailed description of the construction, benefits and clinical relevance of an automated methodology for the delineation of the left ventricle in X-ray angiograms.

In Chapter 2 the Multi-View Active Appearance Model was introduced, in which the desired combined modeling of the ED and ES image frame of an X-ray LV angiographic image sequence was realized. In this new extension on the general AAM framework, the shape statistics of both frames were correlated by concatenating the ED and ES shape vectors for every training sample and applying a Principal Component Analysis on the concatenated vectors. An identical method was applied to the image intensity vectors of the ED and ES training data. By further concatenation of the resulting shape model and intensity model, and applying PCA on the data, the Multi-View Active Appearance Model was constructed. The ED and ES scale, orientation and position were modeled separately, to accommodate for trivial pose differences. Another novelty introduced in Chapter 2 was the sequential application of two Multi-View AAMs in the segmentation of the left ventricle in the target ED and ES images. The first model was the proposed 'general' Multi-View AAM, the second was a dedicated model that was employed to improve local LV boundary delineation. In this latter model, only the image intensity characteristics in the direct vicinity of the LV border were modeled, discarding the majority of image information of the LV blood pool.
The benefit of these methodological innovations of the AAM framework were tested by applying the models on a patient data set of 70 subjects, describing a variety of pathologies and image acquisition artifacts. Without manual initialization a performance of 81% was achieved. The remaining 13 failure cases were subsequently initialized manually, by which the robustness of the algorithm was improved to 87%. Good correlation was observed between the projected areas and derived volumes of the manually drawn reference contours and the automatically generated contours. However, the automated algorithm showed a minor underestimation of the projected areas and derived volumes. Also the border positioning differences between the manual and automated approach were generally small and the calculated ejection fractions did not show a systematic error.
The negligible differences in robustness between ED and ES convergence and the similarity in the linear regression trends and correlation coefficients, demonstrated the advantageous effect of the Multi-View AAM. However, the benefit of the boundary AAM seemed arguable. Although a possible positive effect could be observed occasionally, systematic improvement could not be proven.

Chapter 3 described the application of the Multi-View AAM approach in two different modalities. First in X-ray LV angiograms, similar to the work presented in Chapter 2, and second in cardiac MRI images. With respect to Chapter 2, an optimization was made of the percentages of shape and image intensity information that were incorporated in the model, during the training of the AAM.

Applying the Multi-View AAM in cardiac MRI resulted in a model that was capable of combining shape and image intensity information of three views of one anatomical object, showing three substantially different geometrical shapes.
For X-ray LV angiography the same data set as in Chapter 2 was used. Without manual interaction, convergence was achieved in 87% of the cases. A small but statistically significant underestimation of the automatically defined projected LV areas was observed, while the automatically derived area ejection fraction showed a slight statistically significant overestimation.
For cardiac MRI the methodology was tested on a data set of 29 patients, providing short-axis views, two chamber views and four chamber views. The Multi-View AAM successfully segmented all three views in 27 cases. In the other two data sets only one contour did not converge properly, resulting in an overall success rate of 98%. Good correlation was observed between manually and automatically derived surface areas for all three views. Differences between manual and automatic area calculations proved to be statistically insignificant. No volumetric reconstruction was intended in this experiment. Hence, no registration between the three different views was performed. In future experiments more views (a stack of short-axis views, combined with the two chamber and four chamber views) could be modeled simultaneously, from which a 3D reconstruction could be made by registering all views.
The results presented in Chapter 3 proved that poor left ventricle definition in one view could be overcome by utilizing image information from a corresponding view. Furthermore, the generic potential of the Multi-View was underlined by the excellent performance in the cardiac MRI study, segmenting substantially different geometrical shapes simultaneously.

Chapter 4 presented a study into the optimal characteristics of a data set in training Active Appearance Models for medical image segmentation purposes. Three issues in construction a training data set were addressed, focusing on the application of AAMs in segmenting the left ventricle endo- and epicardial ED and ES contours in short-axis cardiac MRI images. First the optimal size of the data set was assessed. Second, the influence of the data composition in terms of healthy subjects versus patients was investigated and third, the effect of the data composition in terms of image material from different MRI scanners was explored.
When the training of the AAM and the model fitting were performed on short-axis cardiac MRI image data from healthy subjects, an optimal data set size was found to be approximately 200 to 250 images. No experiments on pathological data were executed, but numbers for such data sets were expected to be higher. In general, when increasing the number of training samples, the AAM segmentation performance trend showed asymptotic behavior, rather than a deterioration of accuracy when a surplus of training data was used.
Three different compositions of training data were constructed to assess the influence of healthy subject examples and patient data examples. For one model the data consisted of 80% healthy subjects and 20% patients, for another model healthy subjects and patients were equally represented and a third model was constructed for 20% on healthy subjects data and for 80% on patient data. In a cross validation study the Active Appearance Model that was composed of 80%

healthy subjects data and 20% patient data, showed the best overall performance.
In the studies performed and discussed in Chapter 4, data material of three different MRI vendors was available. This data was used to assess whether an AAM constructed from images from multiple scanner brands would outperform a model that was trained on vendor specific image data. The obtained results proved the contrary; vendor specific Active Appearance Models showed a higher accuracy in automatic left ventricular contour delineation and ejection fraction calculation.

In Chapter 5 the Multi-View Active Appearance Model, first explored in Chapters 2 and 3, was further optimized for automated segmentation of the ED and ES frames in X-ray LV angiography. A novel model matching scheme, the Controlled Gradient Descent, was developed, in which the updates of the model parameters were evaluated and only the most significant updates were processed. Furthermore, a dedicated Dynamic Programming algorithm was employed to improve local border delineation. The search area of the Dynamic Programming scheme was restricted to the direct vicinity of the final AAM segmentation result. Another novelty was the incorporation of information on the contraction dynamics of the left ventricle by constructing the cost function from both image features and from features of a subtraction image (ES minus ED). The described approach was validated both as a semi-automatic method, in which the upper and lower valve points and the apex position were specified, and as a fully automatic method.
The semi-automatic algorithm attained a performance of 100% for ED segmentation and 99% for ES segmentation, in which only one failure was observed. Border positioning errors were generally low, also in examples with a poor LV definition. Although a slight underestimation was perceived, excellent correlation was observed between the manually and semi-automatically derived volumes and the resulting ejection fractions (R^2 = {0.99; 0.95; 0.84} for ED, ES and EF respectively). Differences between manual and semi-automatic results were found statistically insignificant.
The accuracy of the fully automatic algorithm was comparable to the accuracy of the semi-automatic method. The correlation with the manual reference was similarly good (R^2 = {0.99; 0.96; 0.82}) and besides the ED calculation, all differences were found statistically insignificant. However, the robustness of the fully automatic approach proved to be inferior, converging in 91% of the ED and 83% of the ES cases.
The efficacy of the four novel elements of our approach (Multi-View AAM, Controlled Gradient Descent, dedicated Dynamic Programming as post-processing step and the incorporation of cardiac contraction dynamics in Dynamic Programming) was validated by comparison with baseline AAM and Dynamic Programming techniques. The Multi-View AAM resulted in a tremendous improvement of the segmentation results for ES, while the initial high quality results for ED remained unaffected. Both the ED and ES segmentation results were significantly improved by the Controlled Gradient Descent algorithm. This effect was mainly observed in the fully automatic approach. The hybrid application of the Multi-View Active Appearance Model and Dynamic Programming outperformed the separate utilization of both methods. Furthermore, the benefit of the incorporation of cardiac contraction dynamics in Dynamic Programming was

clearly shown.
The semi-automatic algorithm showed better results than previously reported approaches. It was clearly proven that, due to the wide range of information that was incorporated in the algorithm, it had the capacity to mimic the drawing characteristics of a clinical expert. The resulting algorithm satisfied the first, second and fourth requirements as formulated in Chapter 1. Because the errors in the volume calculations were within the limits of inter-observer variability, the fifth goal, clinical relevance, was also suggested.

Chapter 6 investigated whether the proposed algorithm could be viable in daily clinical practice. For this clinical validation study, two expert cardiologists were asked to analyze a set of 30 patient studies. This was done in two ways; first by drawing the left ventricular contours manually, and second by using the proposed automated method. In the latter situation, the two experts had to manually localize the upper and lower aortic valve point and the apex for initialization. Furthermore, the cardiologists were allowed to correct the automatically generated contours by hand. The focus of the experiments was to gain insight in the accuracy, workflow efficiency and inter- and intra-observer variabilities when using the automated methodology.
In comparing the automated and manual LV outlines, no statistically significant differences were observed. For both the ED and ES image frames an excellent correlation was found between the volumes, calculated by the two approaches: R^2 = {0.96; 0.99} for ED (for the two cardiologists) and R^2 = {0.96; 0.98} for ES. Also the derived ejection fraction showed good correlation: R^2 = {0.92; 0.94}. Only a small systematic difference of 2% ejection fraction was observed when comparing the automated results with the manual results.
The overall reduction in the analysis time required for a patient study was 26%, from 4.2 minutes to 3.1 minutes. In addition, according to the expert cardiologists, 60% of the automatically generated ED contours did not need any manual modification. Obviously for ES this number was lower: 11%. However, when editing was required, only 19% of the ED contour length and 25% of the ES contour length was manually corrected.
The inter-observer variability was reduced when the automated methodology was used. The point-to-curve difference between both experts dropped from 0.75 mm to 0.64 mm for ED and from 1.48 mm to 1.33 mm for ES. Also the obtained intra-observer variability was low: 0.82 mm for ED and 1.08 mm for ES.
The results presented in Chapter 6 showed that by utilizing the proposed automated methodology a considerable reduction could be achieved in patient analysis time, manual contouring effort and inter- and intra-observer variabilities, while the calculated ED and ES volumes were equally accurate as manually derived volumes. Hence, these results proved the applicability of the method in daily clinical practice to optimize the analysis workflow for X-ray left ventricular angiography.

7.2 Conclusions and Future Work

Based on the results presented in Chapters 2 to 6 it can be concluded that all formulated goals have been achieved to a large extent. The coupling of different views of one single object significantly improved the AAM segmentation, the robustness of the model has been improved and the accuracy in local LV border delineation has been increased. When utilizing the created algorithm in clinical practice, it proved to decrease the analysis time, the manual effort and the inter-observer variability, while providing ED and ES volumes that did not show any statistical difference from manually derived volumes.

Given the satisfactory results of the presented methodology, the algorithm presented in Chapters 5 and 6 has been recently incorporated in a clinical software package (QAngio® XA, by Medis medical imaging systems bv, The Netherlands), which is sold worldwide.

Though the overall performance of the proposed methodology was satisfactory, some further improvements can still be made. In Chapter 4 insight was gained in the optimal composition of the model training set. However, this knowledge was not yet integrated in the proposed algorithm.

Furthermore, the resulting Multi-View AAM was trained only on manually drawn LV contours from one clinical expert. As a result, Chapter 5 proved the remarkable mimicking behavior of the algorithm, showing a clear bias towards the preferred contour drawing characteristics of the expert cardiologist. Although the clinical validation of the model, performed in Chapter 6, showed no statistical difference between manually and automatically derived ED and ES volumes, a model based on contours from a variety of different clinical experts is expected to improve the standardization of the analysis of X-ray LV angiograms even further.

Due to the availability of clinical data, all the experiments described in this thesis concerning X-ray LV angiography were based on single-plane angiograms. Hence, the applied Multi-View Active Appearance Model was constructed on only two images; the ED and ES projections in the 30° right anterior oblique view. A more comprehensive model description and possibly better segmentation results could be obtained when the Multi-View AAM is constructed from bi-plane acquisitions.

Zhang *et al.* [1] showed the additional value of statistical shape models of the heart, in distinguishing between normal subjects and pathological cases. The two strongest modes of variation of a 3D or 4D statistical model of the left and right cardiac ventricle proved to be good classifiers to separate normals from Tetralogy of Fallot patients. Similarly, Suinesiaputra *et al.* showed that the strongest principal component of a statistical model of short-axes MR images could discriminate between normal subjects and infarct patients [2]. Furthermore, when the statistical shape model was constructed using independent component analysis, the infarcted region could be localized more precisely [3]. Future work in employing the proposed methodology as described in this thesis could include a similar approach in recognizing various pathologies. However, because the proposed method is a hybrid algorithm combining the Multi-View Active Appearance Model and Dynamic Programming, the contours provided by the Multi-View AAM are not the final result. Hence, using Dynamic Programming as a

post-processing tool to refine the AAM contours, a discrepancy between the resulting model parameters and the final endocardial contours is created. This might reduce the efficacy in distinguishing between normal and pathological cases.
In addition, improvements in model initialization could be considered. The results in Chapter 2 pointed out that the accuracy in local border detection was considerably lower in the vicinity of the upper and lower aortic valve points and the apex, when compared to overall border delineation accuracy. Because of the sensitivity of the area-length method to sub-optimal placement of these three points, the implemented clinical version of the algorithm required the manual localization of these landmarks. To establish a fully automatic delineation algorithm, dedicated Active Appearance Models describing only the valve plane or the apex could be considered. This could be either employed to provide image coordinates of the desired landmarks, or it could be implemented similarly to the method proposed by Roberts *et al.* [4].
A final modification to come to a fully automated methodology is the design of an algorithm to automatically extract the optimal ED and ES frame from a full X-ray left ventricular angiographic image sequence.

References

[1] H. Zhang, N. Walker, S. C. Mitchell, M. Thomas, A. Wahle, T. Scholz, and M. Sonka, "Analysis of four-dimensional cardiac ventricular magnetic resonance images using statistical models of ventricular shape and cardiac motion," *Proceedings of SPIE Medical Imaging*, vol. 6143, 614307, 2006.

[2] A. Suinesiaputra, A. F. Frangi, M. Üzümcü, J. H. C. Reiber, and B. P. F. Lelieveldt, "Extraction of myocardial contractility patterns from short-axes MR images using independent component analysis," *Proceedings of CVAMIA-MMBIA*, vol. 3117, Berlin: Springer Verlag, 2004, pp. 75-86.

[3] A. Suinesiaputra, M. Üzümcü, A. F. Frangi, T. A. M. Kaandorp, J. H. C. Reiber, and B. P. F. Lelieveldt, "Detecting regional abnormal cardiac contraction in short-axis MR images using independent component analysis," *Proceedings of Medical Image Computing and Computer-Assisted Intervention*, vol. 3216, Berlin: Springer Verlag, 2004, pp. 737-744.

[4] M. G. Roberts, T. F. Cootes, and J. E. Adams, "Linking sequences of active appearance sub-models via constraints: an application in automated vertebral morphometry," *Proceedings of the British Machine Vision Conference*, Berlin: Springer Verlag, 2003, pp. 349-358.

やれやれ、これで一安心だ
‘Well, we don’t have to worry about that for a while...’

Chapter 8

Samenvatting en Conclusies

8.1 Samenvatting

Het hoge aantal gevallen van cardiovasculaire aandoeningen wereldwijd onderstreept het belang van cardiale beeldacquisitie en diagnostiek. Röntgen linkerventrikel angiografie is al geruime tijd een belangrijke klinische standaard in het beoordelen van de hartfunctie. De snelle opkomst van zowel op MRI (Magnetic Resonance Imaging) en MSCT (Multi Slice Computed Tomography) gebaseerde technieken ten spijt, zal röntgen linkerventrikel angiografie haar waarde in de klinische praktijk blijven behouden. Zolang röntgen angiografie wordt ingezet om de coronaire vaten af te beelden tijdens katheterisatieprocedures, zullen linkerventrikel angiogrammen in het meerendeel van de procedures gelijktijdig worden geacquireerd. De manier waarop het linkerventrikel angiogram wordt geanalyseerd kan echter nog verbeterd worden. In sommige gevallen zal de expert cardioloog door middel van visuele interpretatie van de beeldsequentie de globale ejectiefractie en mogelijke wandbewegingsdefecten kunnen bepalen. In de meeste gevallen zal de arts handmatig een contourlijn moeten tekenen rondom de endocardiale wand in zowel het eind diastolische (ED) als in het eind systolische (ES) beeld. Deze laatste methode verdient de voorkeur, aangezien het een bepaalde diagnostische standaardisatie introduceert en aangezien het vervolgstudies bij patiënten mogelijk maakt. Echter, het handmatig tekenen van contouren is arbeidsintensief, tijdrovend en onderhevig aan inter- en intraobserver variabiliteiten. De noodzaak van een geautomatiseerde techniek voor de analyse van linkerventrikel angiogrammen is daarom evident.

Het voornaamste doel van het in dit proefschrift gepresenteerde werk was de ontwikkeling van een algoritme voor de geautomatiseerde contourbepaling van het cardiale linkerventrikel in de ED en ES fase in röntgen linkerventrikel angiografie, dat voldoende robuust is om toegepast te kunnen worden in de klinische praktijk. Om dit te bereiken is gebruik gemaakt van Active Appearance Modellen (AAM). Met behulp van deze statistische modellen, waarin tegelijkertijd de vorm en grijswaardes van een afgebeeld object worden gemodelleerd, kan een automatische omlijning van het linkerventrikel worden gerealiseerd. In dit proefschrift zijn zowel de uitdagingen van het automatisch interpreteren van linkerventrikel angiogrammen belicht, alsmede de beperkingen van Active Appearance Modellen in het algemeen en de beperkingen bij de toepassing van deze modellen op het segmenteren van het linkerventrikel in röntgen angiografische beelden. Om dit medische beeldverwerkingsvraagstuk op te lossen werden in hoofdstuk 1 de onderstaande doelstellingen geformuleerd:

- De geobserveerde overeenkomsten tussen het ED en het ES beeld dienen benut te worden door het gelijktijdig modelleren van vormkennis en grijswaardekennis van beide beelden met behulp van AAM technologie.

- De gevoeligheid van de op AAM gebaseerde segmentatie methode, ten opzichte van het instabiele karakter van het fout-criterium, dient beperkt te worden.

- Om de prestaties van AAM segmentatie te verbeteren moet onderzoek gedaan worden naar de optimale omvang en samenstelling van de dataset waarop het model getraind wordt.

- Om de locale omlijning van het linkerventrikel te verbeteren dient het effect van statistische, model-intrinsieke beperkingen te worden geneutraliseerd.

- De klinische relevantie van de ontwikkelde methode dient te worden gedemonstreerd.

De hoofdstukken 2 tot en met 6 geven een uitgebreide beschrijving van de methodologie, de voordelen en de klinische relevantie van het ontwikkelde algoritme voor de geautomatiseerde contourbepaling van het linkerventrikel in röntgen linkerventrikel angiografie.

In hoofdstuk 2 werd het Multi-View Active Appearance Model geïntroduceerd, waarmee de gewenste gecombineerde modellering van het ED en ES beeld van een röntgen linkerventrikel angiografie beeldsequentie werd gerealiseerd. Met deze uitbreiding van het gangbare AAM werd de statistische vormkennis van beide beelden gecorreleerd door voor elk trainingsvoorbeeld de vormvectoren aaneen te schakelen en vervolgens een Principal Component Analysis (PCA) uit te voeren op de gekoppelde vectoren. Een identieke methode werd toegepast om de statistische intensiteitskennis van het ED en ES beeld te koppelen. Door vervolgens de verkregen vorm- en intensiteitsmodellen aaneen te schakelen en wederom een PCA uit te voeren, werd uiteindelijk het Multi-View Active Appearance Model geconstrueerd. Om triviale verschillen in pose tussen beide beelden te kunnen modelleren, werden de schaling, orientatie en locatie afzonderlijk gemodeleerd voor ED en ES. Een andere innovatie die in hoofdstuk 2 werd geïntroduceerd was de opeenvolgende toepassing van twee Multi-View AAMs, met als doel de segmentatie van het linkerventrikel in ED en ES beelden. Het eerste model was het voorgestelde ‘generieke’ Multi-View AAM, het tweede was een model dat zich specifiek richtte op het verbeteren van de locale detectie van de rand van het linkerventrikel. In dit laatste model waren enkel de karakteristieken van de beeldintensiteit in de directe omgeving van de rand van het ventrikel gemodelleerd en werd de overgebleven beeldinformatie genegeerd.
De mogelijk effecten van deze innovaties van het AAM werden getest door het model toe te passen op de detectie van het linkerventrikel in een dataset van 70 patiënten, waarin een veelheid aan ziektebeelden en beeldacquisitie-artefacten gerepresenteed was. Zonder handmatige initialisatie werd 81% van de beelden globaal goed geïnterpreteerd. Na handmatige initialisatie in de 13 overgebleven gevallen werd de robuustheid van het algoritme verhoogd tot 87%. Een goede correlatie in geprojecteerde oppervlakten en berekende volumes tussen de automatisch gegenereerde contouren en de handmatig getekende contouren kon worden aangetoond. Desalniettemin liet het automatische algoritme een lichte onderschatting van de oppervlakten en volumes zien. De verschillen tussen de automatische en handmatige analyse met betrekking tot het positioneren van de

rand van het ventrikel waren over het algemeen klein en de berekende ejectiefracties vertoonden geen systematische fout.
De verwaarloosbare verschillen in robuustheid tussen het vinden van het linkerventrikel in ED en in ES, de vergelijkbare trends in lineaire regressie en de vergelijkbare correlatie coëfficiënten, tonen het voordelig effect van het Multi-View AAM aan. De toegevoegde waarde van het model waarin enkel de intensiteiten rond de rand van het ventrikel werden gemodeleerd kon niet aangetoond worden. Hoewel er regelmatig voorbeelden waren waarin een positief effect kon worden geobserveerd, kon er geen systematische verbetering worden bewezen.

Hoofdstuk 3 beschreef de toepassing van het Multi-View Active Appearance Model op twee verschillende modaliteiten. Ten eerste in röntgen linkerventrikel angiografie, zoals ook beschreven in hoofdstuk 2, en ten tweede in cardiale MRI beelden. Ten opzichte van hoofdstuk 2 werd een optimalisering bereikt in de percentages van vormkennis en grijswaardekennis die tijdens het trainen in het model opgenomen dienden te worden. Bij het toepassen van het Multi-View AAM in de cardiale MRI beelden, werd een model gecreëerd waarin de vorm- en beeldintensiteitskennis werden gekoppeld van drie verschillende aanzichten van één anatomisch object, met drie aanmerkelijk verschillende geometrische vormen.
Voor de experimenten in röntgen linkerventrikel angiografie werd dezelfde dataset gebruikt als bij de experimenten beschreven in hoofdstuk 2. Zonder handmatige interactie werd 87% van de beelden globaal goed geïnterpreteerd. De automatisch bepaalde projectie oppervlakten lieten een lichte maar statistisch significante onderschatting zien. De automatisch bepaalde oppervlakte ejectiefracties vertoonden een lichte maar statistisch significante overschatting ten opzichte van de handmatig bepaalde oppervlakte ejectiefracties.
Voor de experimenten in cardiale MRI was een dataset met korte-as, twee-kamer en vier-kamer opnamen van 29 patiënten beschikbaar. Toepassing van het Multi-View AAM op deze dataset resulteerde in 27 gevallen in een succesvolle segmentatie van alle drie de aanzichten. In de twee andere gevallen werd slechts één van de drie aanzichten verkeerd geïnterpreteerd, waardoor de algehele score van het algoritme 98% bedroeg. Voor alle drie de aanzichten werd een goede correlatie gevonden tussen de handmatig en automatisch bepaalde projectie oppervlakten van het linkerventrikel. Verschillen tussen handmatige en automatische methode bleken statistisch insignificant. Aangezien het binnen de uitgevoerde experimenten niet beoogd was om volumes te bepalen is er geen aandacht besteed aan het registreren van de drie aanzichten tot een 3D reconstructie van het hart. In toekomstig onderzoek zouden meer aanzichten gelijktijdig gemodeleerd kunnen worden (bijvoorbeeld de gehele verzameling van korte-as slices, gecombineerd met de twee-kamer en vier-kamer aanzichten), waaruit een 3D reconstructie zou kunnen worden afgeleid.
De in hoofdstuk 3 gepresenteerde resultaten toonden aan dat het mogelijk is om een beeld van het linkerventrikel waarin weinig contrast aanwezig is, automatisch goed te kunnen interpreteren op basis van informatie van een gerelateerd beeld. Daarnaast werd de generieke kracht van het Multi-View AAM aangetoond door de excellente prestaties in de cardiale MRI studie, waarin totaal verschillende geometrische vormen tegelijkertijd werden gesegmenteerd.

De in hoofdstuk 4 beschreven studie was gericht op het vinden van de optimale omvang en samenstelling van een dataset die gebruikt wordt voor het trainen van een Active Appearance Model dat wordt ingezet voor het interpreteren van medische beelddata. Met het segmenteren van de endo- en epicardiale rand van het linkerventrikel in korte-as slices MRI beelden als toepassing, werden drie parameters geoptimaliseerd. Ten eerste de omvang van de dataset. Ten tweede de ratio tussen patiëntendata en data van gezonde personen. Ten derde werd het effect gemeten van de verhouding waarin data van drie verschillende MRI scanners in de training dataset aanwezig was.
Voor het trainen van een AAM op basis van korte-as cardiale MRI data van gezonde personen, bleek een dataset van rond de 200 tot 250 beelden een optimaal segmentatieresultaat op te leveren. Vergelijkbare experimenten met patiëntendata werden niet uitgevoerd, maar de optimale omvang voor het trainen van een dergelijk model werd groter ingeschat. Op basis van de experimenten viel op te maken dat bij een verhoging van de hoeveelheid trainingsdata er een asymptotische trend ontstaat in het segmentatieresultaat. Een verslechtering van de resultaten vanwege een overvloed aan trainingsdata kon niet worden vastgesteld.
Om de invloed van de hoeveelheid patiëntendata versus de hoeveelheid data van gezonde personen in te schatten, werden drie verschillende samenstellingen van trainingsdata getest. Bij één model was 80% van de trainingsdata van gezonde personen en 20% betrof patiëntendata. In een ander model waren beide groepen evenredig verdeeld en bij een derde model werd een verhouding gemaakt van 20% data van gezonde personen en 80% van patiënten. Alle drie de getrainde modellen werden getest op drie test-datasets, die vergelijkbare ratios hadden als in de drie getrainde modellen gebruikt was. Hieruit volgde dat met het model met 80% data van gezonde personen en 20% data van patiënten over de gehele breedte de beste resulaten werden behaald.
Daarnaast werden in hoofdstuk 4 experimenten beschreven met beelddata van drie verschillende merken MRI scanners. Het doel van deze experimenten was om te testen of een AAM waarin beelddata van verschillende scanners verwerkt was, beter zou werken dan merk-specifieke AAMs. De resultaten bewezen het tegenovergestelde; merk-specifieke Active Appearance Modellen vertoonden een hogere nauwkeurigheid, zowel in de automatische contourbepalingen als in de resulterende ejectiefracties.

In hoofdstuk 5 werd het Multi-View Active Appearance Model verder geoptimaliseerd voor de geautomatiseerde segmentatie van het ED en het ES beeld in röntgen linkerventrikel angiografie. Een nieuwe manier om het model te sturen naar de correcte oplossing werd ontwikkeld, de zogeheten Controlled Gradient Descent. Met deze methode werd voorafgaand aan elke model-iteratie een analyse gemaakt van de updates van de model parameters en werden vervolgens enkel de meest significante updates voor de parameters van het AAM uitgevoerd. Verder werd een gespecialiseerd minimale kosten algoritme (ook wel Dynamic Programming genoemd) ontwikkeld om de lokale contourbepaling te verbeteren. De zoekruimte van dit minimale kosten algoritme werd beperkt tot de directe omgeving van de door het AAM berekende omlijning van het linkerventrikel. Verder werd gepoogd om in het minimale kosten algoritme de dynamiek van de

samentrekking van de hartspier op te nemen, door de kostenmatrix te baseren op zowel de grijswaarden van het ED en het ES beeld, alsook op de grijswaardekarakteristieken van een subtractiebeeld (ES beeld minus ED beeld). Het algoritme, bestaand uit alle hierboven benoemde componenten, werd getest voor een volledig automatische toepassing en voor een semi-automatische oplossing waarin de uiteinden van het aortaklepvlak en de locatie van de apex waren gespecificeerd.

Het semi-automatische algoritme presteerde goed in 100% van de ED beelden en in 99% van de ES beelden, waarvan slechts één verkeerd werd geïnterpreteerd. De foutmarge in de contourbepaling was laag, zelfs in gevallen waar de rand van het linkerventrikel moeilijk was te onderscheiden. Ondanks een lichte onderschatting door de semi-automatische methode, was een uitstekende correlatie te zien tussen de handmatig en de semi-automatisch bepaalde volumes en ejectiefracties (R^2 = {0.99; 0.95; 0.84} voor ED, ES en EF, respectievelijk). De verschillen tussen de handmatige en de semi-automatische methode bleken statistisch insignificant.

De nauwkeurigheid van de volledig automatische methode bleek vergelijkbaar met de nauwkeurigheid van de semi-automatische methode, met vergelijkbaar goede correlatie-coëfficiënten (R^2 = {0.99; 0.96; 0.82} voor ED, ES en EF, respectievelijk). Afgezien van de berekende ED volumes, bleken de verschillen tussen de handmatige en de volledig automatische methode statistisch insignificant. Echter, de robuustheid van de volledig automatische methode bleek beduidend minder. In 91% van de ED beelden en 83% van de ES beelden werd de omlijning van het linkerventrikel correct geïnterpreteerd.

De doeltreffendheid van de vier innovatieve elementen van onze aanpak (Multi-View AAM, Controlled Gradient Descent, specialistische Dynamic Programming als verfijningsmethode en de toevoeging van informatie over de dynamiek van de hartspier in Dynamic Programming) werd getest door ze te vergelijken met de standaard AAM en Dynamic Programming technieken. Ten opzichte van een AAM dat enkel getraind was op ES beelden, zorgde het Multi-View AAM voor een geweldige verbetering van de ES segmentatie, terwijl de goede kwaliteit van de segmentatie van de ED beelden gewaarborgd bleef. Zowel voor ED als voor ES beelden was een duidelijke verbetering in segmentatie te zien wanneer de Controlled Gradient Descent methodiek werd toegepast. Deze methode bleek vooral effectief in het geval van volledig automatische segmentatie. De sequentiele toepassing van het Multi-View AAM en Dynamic Programming bleek betere resultaten op te leveren dan de gevallen waarin beide methodieken afzonderlijk werden toegepast. Daarnaast werd duidelijk aangetoond dat het toevoegen in Dynamic Programming van informatie over de dynamiek van de hartspier, de verfijning van de segmentatieresultaten positief beïnvloed.

Het semi-automatische algoritme liet beduidend betere resultaten zien dan eerder gerapporteerde methoden. Bewezen werd dat, vanwege de grote hoeveelheid informatie die in het algoritme was verwerkt, het algoritme de capaciteit had om de manier van tekenen van een klinisch expert te imiteren. De behaalde resultaten realiseerden de eerste, tweede en vierde doelstelling, zoals geformuleerd in hoofdstuk 1. Aangezien de foutmarges in de berekende volumes binnen de grenzen van de inter-observer variabiliteit vielen, leek het vijfde doel, klinische relevantie, eveneens gehaald.

Hoofdstuk 6 was gericht op het inschatten van de klinische relevantie van het voorgestelde algoritme. Voor deze klinische validatie studie werd twee expert cardiologen gevraagd om een dataset van 30 patiëntenstudies te analyseren. In eerste instantie door middel van het handmatig tekenen van de contourlijnen rondom het linkerventrikel in ED en ES, en vervolgens door middel van de ontwikkelde geautomatiseerde methode. In het laatste geval dienden de experts de uiteinden van het aortaklepvlak en de locatie van de aorta handmatig aan te geven. Daarnaast was het de cardiologen toegestaan om de automatisch gegenereerde contouren zo nodig handmatig aan te passen. Het doel van de experimenten was om inzicht te krijgen in de nauwkeurigheid, de efficiëntie van de werkzaamheden en de inter- en intra-observer variabiliteiten, wanneer het geautomatiseerde algoritme werd gebruikt.
De verschillen tussen de geautomatiseerde en de handmatige methode bleken statistisch insignificant. Voor zowel ED volumes als voor ES volumes werd een uitstekende correlatie waargenomen tussen beide methoden: R^2 = {0.96; 0.99} voor ED (voor de twee cardiologen) and R^2 = {0.96; 0.98} voor ES. Ook de bepaalde ejectiefracties vertoonden een goede correlatie: R^2 = {0.92; 0.94}. Slechts een klein systematisch verschil van 2% ejectiefractie werd waargenomen bij het vergelijken van de geautomatiseerde resultaten met de handmatige resultaten.
De gemiddeld benodigde tijd voor het analyseren van een patiëntenstudie werd met 26% gereduceerd, van 4.2 minuten tot 3.1 minuten. Daarnaast was er volgens beide expert cardiologen voor 60% van de automatisch gegenereerde ED contouren geen noodzaak voor handmatige aanpassingen. Vanzelfsprekend was dit getal lager voor ES: 11%. Echter, wanneer handmatige aanpassingen nodig bleken, behoefde gemiddeld slechts 19% van de ED contourlengte en 25% van de ES contourlengte handmatig te worden verbeterd.
Met het toepassen van de geautomatiseerde methode werd de inter-observer variabiliteit verlaagd. De point-to-curve verschillen tussen beide experts daalden van 0.75 mm tot 0.64 mm voor ED en van 1.48 mm tot 1.33 mm voor ES. Daarnaast was de intra-observer variabiliteit laag: 0.82 mm voor ED en 1.08 mm voor ES.
De in hoofdstuk 6 gepresenteerde resultaten toonden aan dat, met het toepassen van het algoritme voor het geautomatiseerd analyseren van linkerventrikel angiogrammen, er een aanzienlijke vermindering kan worden bereikt van de benodigde analysetijd, van de hoeveelheid handmatig werk en van de inter- en intra-observer variabiliteiten, terwijl de berekende ED en ES volumes even nauwkeurig waren als handmatig bepaalde volumes. Deze resultaten bewezen daarmee dat de methode toegepast kan worden om de analyse van röntgen linkerventrikel angiogrammen in de dagelijkse klinische praktijk te optimaliseren.

8.2 Conclusies en Aanbevelingen

Op basis van de in de hoofdstukken 2 tot en met 6 gepresenteerde resultaten kan worden geconcludeerd dat alle geformuleerde doelstellingen grotendeels zijn behaald. Het gelijktijdig modelleren van meerdere aanzichten van één object resulteerde in een duidelijke verbetering van met AAMs behaalde

segmentatieresultaten. Verder werd door het toepassen van de ontwikkelde methodiek de robuustheid en de nauwkeurigheid van de geautomatiseerde contourbepaling van het linkerventrikel in röntgen angiogrammen verbeterd. In een klinische validatiestudie bleek dat het algoritme in staat was om zowel de analysetijd, als de noodzaak tot handmatig tekenen van (delen van) contourlijnen, als de inter-observer variabiliteit te reduceren. Tevens bleken de geautomatiseerd bepaalde ED en ES volumes geen statistisch significante verschillen met handmatig bepaalde volumes te vertonen.

Vanwege de bevredigende resultaten is het in hoofdstuk 5 en 6 gepresenteerde algoritme recent geïntegreerd in een klinisch software pakket (QAngio® XA, van Medis medical imaging systems bv, Nederland), dat wereldwijd wordt verkocht.

Ondanks de goede resultaten zijn er nog enkele verbeteringen op het algoritme denkbaar. In hoofdstuk 4 werd inzicht verkregen met betrekking tot de optimale omvang en samenstelling van de training dataset voor het AAM. Deze kennis is nog niet opgenomen in het huidige algoritme.

Het Multi-View Active Appearance Model werd getraind op de handmatig getekende linkerventrikel contouren van slechts één klinisch expert. Hierdoor kon in hoofdstuk 5 het uitzonderlijke kopieergedrag van het algoritme worden aangetoond. Hoewel de klinische validatie van dit model, uitgevoerd in hoofdstuk 6, geen statistisch significante verschillen liet zien tussen handmatig en automatisch gegenereerde ED en ES volumes, is de verwachting dat een model dat gebaseerd is op de handmatig getekende contourlijnen van meerdere klinische experts de standaardisatie in het analyseren van linkerventrikel angiogrammen nog sterker zal bevorderen.

Vanwege het gebrek aan beschikbare data zijn alle beschreven experimenten, die betrekking hebben op linkerventrikel angiografie, uitgevoerd op single-plane angiogrammen. Zodoende is het ontwikkelde Multi-View Active Appearance Model slechts gebaseerd op twee beelden; de ED en ES projecties in het zogeheten 30° right anterior oblique view. Een uitgebreider model van het linkerventrikel, met mogelijk verbeterde segmentatieresultaten als gevolg, zou gerealiseerd kunnen worden wanneer het AAM op bi-plane data gebaseerd zou zijn.

Zhang *et al.* [1] toonden de toegevoegde waarde van vorm-beschrijvende statistische modellen van het hart aan door ze in te zetten voor het onderscheiden van gezonde personen en pathologische gevallen. De twee sterkste variaties van een 3D of 4D statistisch model van het linker- en rechterventrikel bleken goede parameters voor het onderscheiden van gezonde personen van patiënten met Tetralogie van Fallot. Op vergelijkbare wijze lieten Suinesiaputra *et al.* zien dat gezonde personen en patiënten met een infarct van elkaar onderscheiden konden worden met behulp van de sterkste principal component van een statistisch korte-as MRI model [2]. Tevens kon de regio waarin het infarct zich bevond nauwkeuriger worden bepaald, wanneer er tijdens de constructie van het model gebruik werd gemaakt van independent component analysis in plaats van principal component analysis [3]. Mogelijk zou het in dit proefschrift beschreven algoritme voor de segmentatie van linkerventrikel angiogrammen op een vergelijkbare wijze bepaalde ziektebeelden kunnen herkennen. Echter, aangezien het ontwikkelde algoritme een combinatie van een statistische model en Dynamic Programming is, corresponderen de uiteindelijke contourlijnen niet volledig met de geregistreerde

model parameters. Dit zou het onderscheidend vermogen van het algoritme kunnen aantasten.
Eveneens zouden verbeteringen in het initialiseren van het model overwogen kunnen worden. De resultaten in hoofdstuk 2 toonden aan dat de nauwkeurigheid van het algoritme aanzienlijk lager was in de directe omgeving van het aortaklepvlak en rondom de apex. Vanwege de gevoeligheid van de area-length methode voor de sub-optimale plaatsing, vereist de commerciele versie van het algoritme een handmatige aanduiding van deze punten. Om een volledig automatisch algoritme te realiseren zou gebruik gemaakt kunnen worden van gespecialiseerde AAMs die zich richten op het detecteren van het aortaklepvlak of de apex. Deze modellen zouden de coördinaten voor de initialisatie van het linkerventrikel model kunnen genereren, of een vergelijkbare methode zoals ontwikkeld door Roberts *et al.* zou kunnen worden gebruikt [4].
Een laatste verbetering zou de automatische selectie van de geschikte ED en ES beelden uit een volledige linkerventrikel beeldsequentie zijn. Hiermee zou een volledig automatisch algoritme kunnen worden gerealiseerd.

Bibliografie

[1] H. Zhang, N. Walker, S. C. Mitchell, M. Thomas, A. Wahle, T. Scholz, and M. Sonka, “Analysis of four-dimensional cardiac ventricular magnetic resonance images using statistical models of ventricular shape and cardiac motion,” *Proceedings of SPIE Medical Imaging*, vol. 6143, 614307, 2006.

[2] A. Suinesiaputra, A. F. Frangi, M. Üzümcü, J. H. C. Reiber, and B. P. F. Lelieveldt, “Extraction of myocardial contractility patterns from short-axes MR images using independent component analysis,” *Proceedings of CVAMIA-MMBIA*, vol. 3117, Berlin: Springer Verlag, 2004, pp. 75-86.

[3] A. Suinesiaputra, M. Üzümcü, A. F. Frangi, T. A. M. Kaandorp, J. H. C. Reiber, and B. P. F. Lelieveldt, “Detecting regional abnormal cardiac contraction in short-axis MR images using independent component analysis,” *Proceedings of Medical Image Computing and Computer-Assisted Intervention*, vol. 3216, Berlin: Springer Verlag, 2004, pp. 737-744.

[4] M. G. Roberts, T. F. Cootes, and J. E. Adams, “Linking sequences of active appearance sub-models via constraints: an application in automated vertebral morphometry,” *Proceedings of the British Machine Vision Conference*, Berlin: Springer Verlag, 2003, pp. 349-358.

Publications

Peer reviewed papers in international journals

E. Oost, P.V. Oemrawsingh, J.H.C. Reiber, and B.P.F. Lelieveldt, "Automated Left Ventricular Delineation in X-ray Angiograms: A Validation Study", Accepted for publication in *Catheterization and Cardiovascular Interventions*, 2008.

E. Angelié, **E.R. Oost**, D. Hendriksen, B.P.F. Lelieveldt, R.J. van der Geest, and J.H.C. Reiber, "Automated Contour Detection in Cardiac MRI Using Active Appearance Models: The Effect of the Composition of the Training Set", *Investigative Radiology*, vol. 42, no. 10, pp. 697-703, 2007.

E. Oost, G. Koning, M. Sonka, P.V. Oemrawsingh, J.H.C. Reiber, and B.P.F. Lelieveldt, "Automated Contour Detection in X-Ray Left Ventricular Angiograms Using Multi-View Active Appearance Models and Dynamic Programming", *IEEE Transactions on Medical Imaging*, vol. 25, no. 9, pp. 1158-1171, 2006.

Peer reviewed papers in conference proceedings

E. Oost, G. Koning, M. Sonka, J.H.C. Reiber and B.P.F. Lelieveldt, "Automated Segmentation of X-Ray Left Ventricular Angiograms Using Multi-View Active Appearance Models and Dynamic Programming", *In: Proceedings of FIMH 2005*, A.F. Frangi et al. Eds., vol. 3504, pp. 23-32, 2005.

C.R. Oost, B.P.F. Lelieveldt, M. Üzümcü, H. Lamb, J.H.C. Reiber, and M. Sonka, "Multi-View Active Appearance Models: Application to X-Ray LV Angiography and Cardiac MRI", *In: Proceedings of IPMI 2003*, C.J. Taylor and J.A. Noble Eds., vol. 2732, pp. 234-245, 2003.

E. Oost, B.P.F. Lelieveldt, G. Koning, M. Sonka, and J.H.C. Reiber, "Left Ventricle Contour Detection in X-Ray Angiograms using Multi-View Active Appearance Models", *In: Proceedings of SPIE Medical Imaging*, M. Sonka and J.M. Fitzpatrick Eds., vol. 5032, pp.394-404, 2003.

Acknowledgements

This thesis describes the results of research that was performed in the Knowledge Guided Image Processing section (in Dutch abbreviated to KGB) of the Division of Image Processing (in Dutch abbreviated to LKEB), Department of Radiology, Leiden University Medical Center, under the supervision of Prof. dr. ir. J.H.C. Reiber and Dr. ir. B.P.F. Lelieveldt.

During my quest for a Ph.D. degree I have received a lot of support, both scientifically and morally. It has been a tremendous privilege and pleasure to be a member of KGB. First of all, I would like to thank Hans van Assen, Mehmet Üzümcü and Mike Danilouchkine for welcoming me as a new member of KGB, 7 years ago. You all have contributed in transforming me from an agricultural engineer into a 'medical image processor'. Hansa and Mehmet, thank you for the incredible fun we had at the KGB headquarters and during several domestic and international seminars. Mr. Mike, thank you for always having a moment to discuss matters, whether they were scientific, reflecting or just fun. Furthermore, I would like to thank Julien Milles, Avan Suinesiaputra, Maribel Adame, Martin Baiker and Meng Ma for being supporting and enjoyable KGB-colleagues. Julien, we must be twin brothers, for we share a brain. Thank you for throwing ducks, playing squash and assisting me as a paranymph. Avan, thank you for also assisting me as a paranymph and thank you for your tranquil presence; it resets me when I need it.

I would like to thank Jasper Janssen and Patrick de Koning for their open-door policy. Thanks for allowing me to ask programming-related questions and for playing 'office-ball'. I would like to thank Gerhard Koning for answering my clinical questions.

Regarding 'life after KGB', I would like to thank Henk Marquering, Michel Frenay and Pieter Kitslaar for adopting me as a new CTA-group member and for the enjoyable time in the CTA-room. In general, I would like to thank all current and former LKEB colleagues for the fun conversations and for listening to my attemptedly funny nonsense.

I am grateful to my father (may his God have his soul) for showing the ultimate perseverance in obtaining a Ph.D., in your case a Ph.D. degree in Theology. In the same light, I would like to thank my mother and brothers for understanding and supporting me during my work as a Ph.D. student.

Elly, thank you for your reflectance, your occasional kick-in-the-butt that I need, your solidarity in simultaneously pursuing a Ph.D. degree and for your love. Koen, I admire you for being the first in the family to obtain a Ph.D. and I thank you (and your younger brother/sister) for the entertaining distraction that you provide.

To all my friends, family and colleagues. As my twelfth proposition states, I am the weighted average of all of you. You have made me. Hence, you all have contributed to this work and I am very grateful for that.

Elco Oost
July 2008

Curriculum Vitae

Cornelis Roel (Elco) Oost was born in Rutten, the Netherlands, in 1976. In 1994 he graduated from the VWO at the Emelwerda College in Emmeloord, after which he started a study in Agricultural Engineering at the Wageningen University. Within the Systems and Control Group he completed a graduation project on adaptive control in greenhouse climate and a graduation project on automatic in-row mechanical weeding. After also fulfilling a traineeship at the Bio-oriented Technology Research Advancement Institution of the Institute of Agricultural Machinery in Omiya, Japan, he received his MSc. degree in November 2000.

After a short extension of his stay at Wageningen University, he started working at the Laboratory for Clinical and Experimental Image Processing (LKEB) of the Leiden University Medical Center in October 2001. His main topic of research was the application of statistical models to the automatic delineation of the cardiac left ventricle in X-ray left ventricular angiography, of which this thesis mainly reports. Other research topics included the coupling of diagnostic image information between the function scan, perfusion scan and delayed contrast enhancement scan in short-axis cardiac MRI. Currently he is working on the automatic detection and quantification of atherosclerotic plaque in CT images of the coronary arteries.